Aalto University
School of Chemical
Technology

School of Chemical Technology

Degree Programme of Chemical Technology

Christian Frilund

CO_2 HYDROGENATION TO METHANOL

Master's thesis for the degree of Master of Science in Technology submitted for inspection, Espoo, 31 January, 2016.

Supervisor **Professor Juha Lehtonen**

Instructor **M.Sc. (Tech) Francisco de Sáles Vidal Vázquez**

Aalto University
School of Chemical
Technology

Aalto University, P.O. BOX 11000, 00076 AALTO
www.aalto.fi

Abstract of master's thesis

Author Christian Frilund

Title of thesis CO_2 hydrogenation to methanol

Department Department of Biotechnology and Chemical Technology

Professorship Industrial Chemistry **Code of professorship** KE-40

Thesis supervisor Professor Juha Lehtonen

Thesis advisor(s) / Thesis examiner(s) M. Sc. (Tech) Francisco de Sáles Vidal Vázquez

Date 31.01.2016 **Number of pages** 121+13 **Language** English

Abstract

The literature survey discusses the recent developments in heterogeneous catalytic hydrogenation of CO_2 to methanol. Special focus was given to new coated catalysts and reactors. Methanol is an important chemical that is currently produced from synthesis gas. Methanol can also be produced from CO_2, but the reaction is less thermodynamically favoured. The main reaction is the exothermic CO_2 hydrogenation, and there is a competing fast reaction, the reverse water-gas shift, which converts CO_2 to CO. The catalysts for CO_2 hydrogenation are usually Cu/ZnO-based, and experiments have indicated that the methanol yield increases linearly with the active copper surface area. The catalysts have proven to be surface sensitive, which can be affected by preparation techniques and the addition of special modifiers. The reactant gas composition has also shown to modify the active state of the catalyst, and therefore special catalysts developed for the CO_2 hydrogenation reaction need to be used. The reactions are generally recognized to occur at the Cu/oxide interfaces, but the exact reaction steps are still under debate. Coated catalysts are thin layers of catalyst deposited on a structure like a reactor wall in monolith or microchannel reactors. These reactors have milli- or micro-scale coated channels which enable high catalyst surface areas and improved mass- and heat transfer properties compared to packed bed reactors. However, due to the challenges with the performance and the coating techniques, these solutions are still very experimental.

In the experimental part of the thesis new formulations of Cu-based particulate catalysts and coated catalysts for CO_2 hydrogenation were tested in a 0.2 dm^3 CSTR at fixed conditions. Moreover, new nanocoating formulations for particulate catalysts were screened. Particulate catalysts in varying reaction conditions were also tested. Finally, the experimental results were compared to simulated results calculated with two commonly used kinetic models for methanol synthesis. The performance test at fixed conditions revealed that the best performing catalysts were the commercial catalysts and catalysts developed at the University of Porto. With the best performing catalysts the CO_2 conversions were about 23 % and methanol selectivities about 55 %, which was similar to the latest studies found in literature. The nanocoating screening for the particulate catalysts showed that the best nanocoating formulations can improve the catalyst performance. The in-house manufactured coated catalyst formulations experienced quality problems, and were partly discarded. The coated catalysts that were tested exhibited very low activity. The condition testing results indicated noticeable mass transfer limitations in the system within the tested range. The reactor ideality was also experimentally determined applying a step change experiment, which indicated that the reactor was working close to an ideal CSTR. The simulation study with the Graaf model and the vanden Bussche model showed that the Graaf model failed to simulate similar CO reaction rates as in the experiments, but the predicted MeOH yields were more accurate than with the vanden Bussche model.

Keywords CO_2 hydrogenation, methanol, copper, catalysis, CSTR, autoclave, nanocoating, simulation

Aalto-yliopisto
Kemian tekniikan korkeakoulu

Aalto-yliopisto, PL 11000, 00076 AALTO
www.aalto.fi

Diplomityön tiivistelmä

Tekijä Christian Frilund

Työn nimi CO_2:n hydraus metanoliksi

Laitos Kemian tekniikan korkeakoulu

Professuuri Teknillinen kemia **Professuurikoodi** KE-40

Työn valvoja Professori Juha Lehtonen

Työn ohjaaja(t)/Työn tarkastaja(t) DI Francisco de Sáles Vidal Vázquez

Päivämäärä 31.01.2016 **Sivumäärä** 121+13 **Kieli** Englanti

Tiivistelmä

Diplomityön kirjallisuusosassa tarkastellaan heterogeenistä katalyyttistä CO_2:n hydrausta metanoliksi. Lisäksi tutkimuksen kohteena oli uudet pinnoitetut katalyytit ja reaktorit. Metanoli on tärkeä kemikaali, jota valmistetaan synteesikaasusta. Metanolia voi myös valmistaa hiilidioksidista, mutta reaktio ei ole termodynaamisesti yhtä suotuisa. CO_2:n hydrausreaktio on eksoterminen ja samalla kilpaileva nopea reaktio, endoterminen käänteinen vesikaasun siirtoreaktio, konvertoi hiilidioksidia hiilimonoksidiksi. Hiilidioksidin vedytyskatalyytit ovat yleensä Cu/ZnO-pohjaisia ja tutkimukset ovat osoittaneet, että metanolin saanto lisääntyy lineaarisesti aktiivisen kuparin pinta-alan kasvaessa. Katalyytit ovat osoittautuneet katalyyttipinnan suhteen herkiksi. Pintaa voi muokata lisäaineilla tai katalyytin valmistusmenetelmien avulla. Reaktiokaasun koostumuksen on myös todettu muokkaavan katalyytin aktiivista pintaa ja siksi on suositeltavaa käyttää erityisiä CO_2 hydrausta varten kehiteltyjä katalyyttejä. Reaktioiden on todettu yleisesti tapahtuvan Cu/oksidi-rajapinnalla, mutta reaktiomekanismeista väitellään edelleen. Mikrokanavareaktoreissa tai monoliittireaktoreissa on tyypillisesti halkaisijaltaan milli- tai mikrometriluokan virtauskanavia. Nämä kanavat voidaan päällystää ohuella katalyyttikerroksella, mikä mahdollistaa suuren katalyytin pinta-alan. Pinnoitettuihin katalyytteihin perustuvissa reaktoreissa on näin ollen parempi aineen- ja lämmönsiirto verrattuna perinteisiin kiintopatjareaktoreihin. Suorituskykyongelmat sekä ongelmat päällystystekniikoiden kanssa tekevät pinnoitetuista reaktoreista kuitenkin vielä hyvin kokeellisia.

Diplomityön kokeellisessa osassa testattiin määrätyissä olosuhteissa uusia Cu-pohjaisia partikkeli- sekä pinnoitettuja katalyyttejä CO_2 hydrausreaktiota varten. Kokeet suoritettiin 0.2 dm^3 jatkuvatoimisessa sekoitussäiliöreaktorissa (CSTR). Lisäksi testattiin uusia partikkelikatalyyttien nanopinnoituksia. Partikkelikatalyyttiä testattiin myös erilaisissa olosuhteissa. Lopuksi kokeellisia tuloksia vertailtiin simuloituihin tuloksiin, jotka laskettiin kahden yleisesti metanolin synteesin simuloinnissa käytetyn kineettisen mallin avulla. Kokeiden aktiivisimmat partikkelikatalyytit olivat Porton yliopistossa kehitetyt katalyytit sekä kaupalliset katalyytit. Parhaimpien katalyyttien testeissä CO_2-konversiot olivat noin 23 %, ja MeOH-selektiivisyydet noin 55%. Nanopinnoitusten kokeissa selvisi, että parhaat nanopinnoitukset parantavat katalyytin suorituskykyä. Osa metalliverkkoon pinnoitutetuista katalyyteistä oli laadullisesti heikkoja, ja ne päätettiin hylätä. Testatut pinnoitetut katalyytit olivat suorituskyvyltään hyvin vaatimattomia. Erilaisissa olosuhteissa suoritetut kokeet partikkelikatalyyteille indikoivat aineensiirtorajoitteista koejärjestelyssä. Myös reaktorin toiminnan ideaalisuus tarkistettiin kokeellisesti. Tulosten perusteella reaktori toimi lähes ideaalisen CSTR-reaktorin tavoin. Graafin- sekä vanden Busschen-kinetiikkamalleilla laskettuja simulointituloksia vertailtiin tämän työn partikkelikatalyyttien tuloksiin. Vertailu havainnollisti, että Graafin-mallilla CO-saannot eivät vastanneet kokeellisia arvoja. Graafin-mallilla simuloidut MeOH-saannot kuitenkin seurasivat kokeellisia MeOH-saantoja tarkemmin kuin vanden Busschen-mallilla lasketut saannot.

Avainsanat CO_2 hydraus, metanoli, kupari, katalyytti, CSTR, autoklaavi, nanopinnoitus, simulointi

Foreword

This master's thesis has been conducted at the Catalysis & Synfuels team of VTT Technical Research Centre of Finland for the Neo-Carbon Energy project between June 2015 and December 2015.

I thank Pekka Simell for offering me the possibility of making this master's thesis. I especially thank my instructor Francisco Vidal Vázquez for the valuable advice and help that I received throughout the course of the project. I am also grateful for the feedback and comments from Professor Juha Lehtonen, Pekka Simell and Matti Reinikainen.

I would also like to thank Mari-Leena Koskinen-Soivi and the personnel working in the lab for the guidance during the experimental part of this work.

Espoo, 31 January, 2016

Christian Frilund

Contents

Nomenclature

Abbreviations

BET	Brunauer–Emmett–Teller isotherm
BtL	Biomass-to-Liquids
CAMERE	Carbon dioxide hydrogenation to form methanol via a reverse water-gas shift reaction
CFD	Computational fluid dynamics
CRI	Carbon Recycling International Inc.
CSTR	Continuous stirred tank reactor
DFT	Density functional theory
DP	Deposition precipitation
DMFC	Direct methanol fuel cells
FBR	Fixed bed reactor
FEUP	Faculdade de Engenharia da Universidade do Porto
FFV	Flexible fuel vehicle
FID	Flame ionization detector
GC	Gas chromatograph
GSA	Geometric surface area
ICE	Internal combustion engine
LHHW	Langmuir-Hinschelwood-Hougen-Watson
MS	Methanol synthesis
MTG	Methanol-to-Gasoline process
MTBE	Methyl *tert*-butyl ether
MWCNT	Multi-walled carbon nanotubes
NC	Nanocoating
OFA	Open front area
PBR	Packed bed reactor
PFR	Plug flow reactor
PtL	Power-to-Liquids
RKS-MHV2	Redlich-Kwong-Soave with modified Huron-Vidal-2 mixing rule
RTD	Residence time distribution
rWGS	Reverse water-gas shift
S-C	Süd Chemie

STP	Standard temperature and pressure, 273 K and 1.01325 bar
STR	Stirred tank reactor
TAME	*tert*-Amyl methyl ether
TCD	Thermal conductivity detector
WGS	Water-gas shift
VTT	Technical research center of Finland

Symbols

a	Catalyst activity
A	Average GC peak area
A_c	Cross sectional area (m^2)
a_v	Specific surface area ($\frac{m^2}{m^3}$)
c	Concentration ($\frac{mol}{m^3}$)
Cp	Specific heat at constant pressure ($\frac{J}{molK}$)
D_e	Effective diffusion coefficient ($\frac{m}{s}$)
d	Catalyst particle diameter (m)
E_a	Activation energy ($\frac{kJ}{mol}$ or $\frac{J}{mol}$)
f	Fugacity (bar or atm)
f_f	Fanning friction factor
ΔG	Gibbs free energy ($\frac{kJ}{mol}$)
G	Superficial mass velocity ($\frac{m}{s}$)
GHSV	Gas hourly space velocity ($\frac{1}{h}$)
ΔH	Enthalpy ($\frac{kJ}{mol}$)
ΔH_f	Enthalpy of formation ($\frac{kJ}{mol}$)
h	heat transfer coefficient ($\frac{W}{m^2K}$)
K^{eq}	Equilibrium constant
k	Rate constant
k^*	Pseudo-first-order rate constant
K^{eq*}	Pseudo-equilibrium constant
K_g	Mass transfer coefficient ($\frac{m}{s}$)

$\dot{m}$	Mass flow ($\frac{g}{min}$)
m	Mass (g)
$\dot{n}$	Molar flow ($\frac{mmol}{min}$)
n	Moles (mol or mmol)
P	Pressure (bar or bar(g))
p	Partial pressure (bar or bar(g))
$\dot{Q}$	Heat stream (W)
r'	Reaction rate ($\frac{mmol}{g_{cat}h}$)
RF	Response factor
r	Particle or pellet radius (m)
ΔS	Entropy ($\frac{kJ}{mol}$)
S	Selectivity (%)
STY	Space time yield of product ($\frac{mmol}{g_{cat}h}$)
T	Temperature (^{o}C or K)
T.o.S.	Time on stream (min)
U	Overall heat transfer coefficient ($\frac{W}{m^2K}$)
V	Volume (dm^3)
V%	Volume percentage (vol-%)
W/F	Contact time ($\frac{kg_{cat}s}{mol}$ or $\frac{g_{cat}ms}{cm^3}$)
WHSV	Weight hourly space velocity ($\frac{1}{h}$)
V_m	Molar volume ($\frac{dm^3}{mmol}$)
$\dot{v}$	Volumetric flow ($\frac{dm^3}{min}$)
X	Conversion (%)
Y	Yield (%)
y	Mol fraction
Z	Compressibility factor

Greek letters

μ	Dynamic viscosity ($\frac{kg}{m*s}$)
ε	Void fraction

η	Catalyst effectiveness factor
ρ	Density ($\frac{kg}{m^3}$)
τ	Mean residence time (min)
ϕ	Thiele modulus

Subscripts

0	Inlet conditions
i	Component or reaction index
j	Component index
meas	Measured conditions
p	Catalyst particle or pellet
R	Reaction conditions
s	At catalyst surface
t	Total

1 Introduction

In the 20th century humanity experienced explosive growth in energy consumption and a rapid increase in population. New technologies and man-made products started a new era of which one of the most revolutionizing was that of transport, namely the invention engine powered cars, planes, trains and ships. This has made the world totally dependent on the combustion of hydrocarbon fossil fuels, such as diesel and gasoline. Also the invention of electrical power plants and electric appliances has made us increasingly dependent on fossil fuels such as coal and natural gas. [1] Currently 85% of the world's energy comes from fossil sources [2]. This unprecedented era of development fuelled by fossil based carbon has led to environmental problems that mankind has started to become consciously aware of in the last few decades. Moreover, fossil fuels are not renewed on a human time scale, and thus are rapidly depleting. The so called Hubbert's peak, when the demand for oil and gas outpaces the global production capacity, thus sharply increasing their prices, is estimated to occur in the coming decades [3]. Greenhouse gases from the combustion of fossil fuels, mainly carbon dioxide (CO_2) and methane (CH_4), pose a major threat in the form of increase in global temperatures and climate changes due to the "greenhouse effect" [4]. Reducing anthropogenic CO_2 emissions is a difficult and long-term task. Three paths exist for solving the problem: 1) Reducing the amount of CO_2 produced. 2) Storage of CO_2. 3) Usage of CO_2.

This master's thesis is part of the Neo-Carbon Energy project, which focuses on creating new emission-free and reliable energy systems, based mainly on solar and wind power. Solar and wind power are practically infinite renewable sources of energy, and they are expected to be the cheapest form of energy in the near future in large parts of the world. However, they are inflexible and variable in their production, which poses challenges. [5] Electricity is a good means to transport energy over short distances, however it is difficult to store on a large scale, because of for example capacity limitations of current batteries. Therefore, electricity production has to closely follow demand. Consequently, storing energy in the form of chemical compounds such as hydrogen and hydrocarbons is interesting. [3]

A "Hydrogen Economy" concept has been proposed, where hydrogen acts as an energy carrier, by for example producing hydrogen by water electrolysis with renewable energy. Though, it has serious drawbacks, such as hydrogen being very volatile, highly flammable and explosive. Moreover, there is currently no infrastructure for it. [3] The "neocarbonization" concept suggests that we do not need to think in terms of "zero-carbon" or "low-carbon" economy as a solution for a sustainable future. Instead, carbon could be used sustainably, and continued use of carbon as a fundamental building block and energy carrier is possible. [5] Therefore, Olah et al. [3] proposed the concept of a "Methanol Economy", where methanol is used instead of hydrogen, because it is easier to handle, transport and store, and would cause only minor modifications to the existing fossil fuel infrastructure. In the concept CO_2 would be captured from any natural or industrial source, and chemically converted into methanol and other hydrocarbons. The use of carbon dioxide for methanol production has several advantages because it is the usage of non-fossil fuel sources (instead of syngas), avoidance of CO_2 sequestration (which is expensive), and it mitigates the greenhouse effect by recycling of CO_2 to essential fuels and materials. [6]

Carbon dioxide is in fact an attractive C_1 building block that is abundant, safe and renewable. Its use is currently limited to only a few industrial processes, such as synthesis of urea, salicylic acid and carbonates. This is because CO_2 is thermodynamically very stable, which causes significant energy demands and requires the application of extremely good catalysts, capable of driving its selective conversion into targeted chemicals. Therefore, the toxic carbon monoxide (CO) is currently more used as a C_1 building unit. [7] Carbon dioxide chemical usage is a challenge, but efficient reactions using CO_2 as a reagent would have great impact on efforts towards carbon management. If mankind wants to continue consuming carbon-based products in a similar fashion as at present, CO_2 needs to be recycled in an anthropogenic version of nature's own carbon cycle.

1.1 Aim of the thesis

The aim of the literature survey is to present and give a comprehensive overview of the recent developments in catalytic hydrogenation of CO_2 to methanol. The focus will be on heterogeneous copper-based catalysts, which are the most commonly used catalysts for the CO_2 hydrogenation reaction. Moreover, special emphasis will

be given to process intensification by coated and structured catalyst and reactors, which can enable local small-scale methanol production for Power-to-Liquid applications.

The aim of the experimental part was to test and compare new formulations of particulate and coated copper catalysts for hydrogenation of CO_2 to methanol in a continuous stirred tank reactor. Moreover, new nanocoating formulations were studied experimentally. A commercial particulate catalyst was also investigated in varying reaction conditions. Finally, the experimental results were compared to simulated results calculated with two commonly used kinetic models for methanol synthesis. The reactor ideality was also experimentally determined applying a step change experiment.

2 Methanol synthesis routes

Methanol is a widely used solvent and an alternative fuel with several industrial applications. The chemical industry uses methanol as a starting material in the production of formaldehyde, aromatics, ethylene, gasoline ethers (MTBE, TAME), acetic acid and other important chemicals. [8] Most of these chemicals are subsequently used to manufacture many of the products in daily life, such as paints and plastics. Worldwide, over 90 methanol plants have a combined capacity of over 75 million tonnes [2]. Figure 1 shows the main methanol consuming industries.

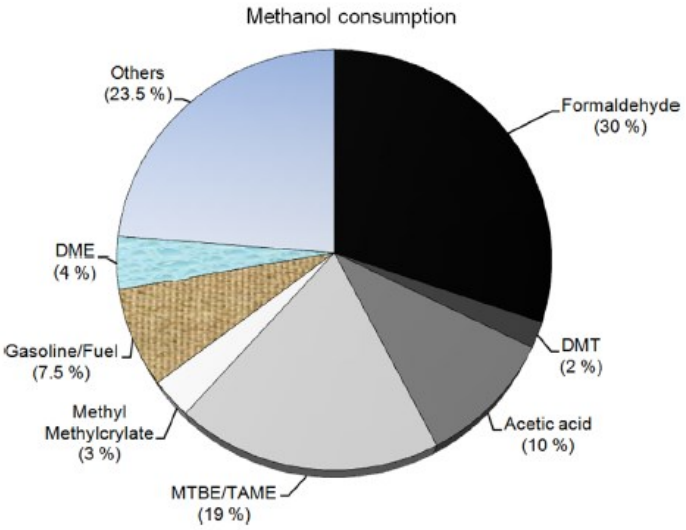

Figure 1. Overview of the methanol consuming industries. [8]

Methanol is highly toxic when ingested in large amounts, causing blindness and death. The toxicity is quoted as a hindrance for its use, but in reality it is not a problem, and it has long been used in consumer products such as washer fluids and antifreezes. [3]

Methanol has been promoted as an energy carrier by several scientists due to its numerous advantages over competing solutions. It has a high octane rating of about 100, and is suitable as an additive for gasoline internal combustion engines (ICE). Though, it only contains about half the energy density of gasoline. A wide commercial use of methanol in ICE vehicles would be readily achievable, since gasoline powered cars can be modified at a modest cost to flexible fuel vehicles (FFV), running on mixtures of methanol and gasoline. [3] Methanol is also used in direct methanol fuel cells (DMFC), where chemical energy is converted to electrical power at ambient conditions. Moreover, methanol can be used for electric power generation in gas turbines, and if needed, methanol can be converted to gasoline by the MTG process developed by Mobil. Therefore, storing electrons in chemical bonds in a liquid is more desirable than in hydrogen gas. [9]

For economic reasons, methanol is currently almost exclusively produced from fossil fuels, but it could be made from any carbon containing feedstock, such as biomass and any CO_2 source in the future. [9] In the next sections both synthesis pathways are presented.

2.1 Methanol from syngas

Currently almost all methanol (MeOH) is produced from synthesis gas (syngas). Syngas is a mixture of hydrogen and carbon monoxide as well as carbon dioxide formed from partial combustion or reforming of coal, natural gas or biomass over a heterogeneous catalyst. [3]

The conversion of syngas to methanol is a well-established technology. Traditionally syngas has been produced by coal gasification. However, currently most syngas is produced by steam methane reforming (SMR) of natural gas on nickel catalyst at 800 – 1000 °C and pressures of 20 – 40 bar, according to reactions (1) and (2) [9]:

$$CH_4 + H_2O \leftrightarrows CO + 3H_2 \qquad \Delta H_{R,298K} = 206 \frac{kJ}{mol} \qquad (1)$$

$$CH_4 + 2H_2O \leftrightarrows CO_2 + 4H_2 \qquad \Delta H_{R,298K} = 165 \frac{kJ}{mol} \qquad (2)$$

Subsequent reactions are carried out to adjust the syngas composition closer to the ideal $\frac{H_2}{CO}$ ratio of 2, which is often called metgas.

The following reactions are the main reactions present in methanol production [6] [10]:

CO hydrogenation:

$$CO + 2H_2 \leftrightarrows CH_3OH \qquad \Delta H_{R,298K} = -90.5 \frac{kJ}{mol} \qquad (3)$$

CO_2 hydrogenation:

$$CO_2 + 3H_2 \leftrightarrows CH_3OH + H_2O \qquad \Delta H_{R,298K} = -49.5 \frac{kJ}{mol} \qquad (4)$$

Reverse water-gas shift (rWGS):

$$CO_2 + H_2 \leftrightarrows CO + H_2O \qquad \Delta H_{R,298K} = 41.0 \frac{kJ}{mol} \qquad (5)$$

The hydrogenation reactions are exothermic and reversible, and according to Le

Châtelier's principle, optimal reaction conditions to shift equilibria to the formation of methanol require higher pressures and lower temperatures. Using modern Cu/ZnO-based catalysts, the process conditions for methanol synthesis from syngas are 200 – 300 °C and 30 – 100 bar. [9] Under these conditions, the single-pass CO conversion is limited to about 15 - 25% due to thermodynamic limitations, and thus the unreacted gases are typically recycled. Therefore, one way to high single-pass conversions is the development of catalysts active at low temperatures. Several companies, such as Lurgi and Mitsubishi, offer commercial methanol synthesis technologies. [6]

Yin and Leung [11] tested methanol synthesis from biomass derived syngas of different compositions. As shown in Figure 2, there is variation in methanol yields with varying CO_2 amounts in the reactant gas.

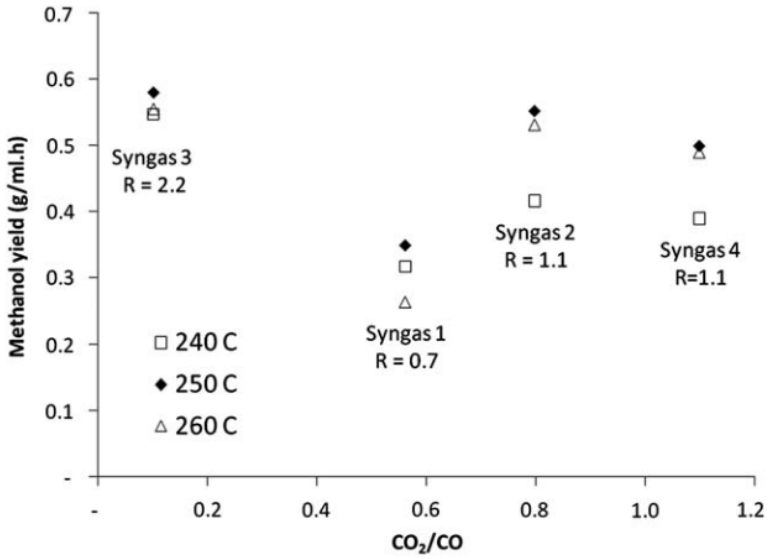

Figure 2. Relationships between methanol yield and the $\frac{CO_2}{CO}$ - and $R = \frac{H_2}{CO+CO_2}$ –feed ratios, when T_R = 240, 250, 260 °C, P_R = 36 bar and GHSV = 7000 h^{-1}. [11]

Operating at pure CO feeds does not result in high yields due to kinetic reasons. However, the commercial processes are equilibrium limited, and hence a high CO_2 concentration pushes the equilibrium towards unfavourable regime. Therefore, a certain amount of CO_2 is needed for reasonable yields. [12]

Several studies show that in industrial conditions methanol formation mainly occurs through CO_2 hydrogenation, despite thermodynamic data showing that direct CO hydrogenation is more favourable. According to these studies, the role of CO in the

CO and CO_2 hydrogenation is to scavenge the absorbed hydrogen to produce surface CO_2. [13] Currently available catalysts do not in fact favour the direct CO hydrogenation reaction. There is still debate about the effect of CO_2 in syngas feeds, and some researchers claim that CO_2 is mainly promotional, and that CO_2 only becomes a major source of carbon when syngas is CO_2-rich. [14] This shows that this industrially established process has for decades been operated only based on empirical knowledge.

2.2 CO_2 hydrogenation to methanol

CO_2 as a feedstock is inexpensive and abundant, it is non-toxic and non-flammable and can be stored in liquid phase under mild pressure and ambient temperature. There are several sources industrial sources for CO_2, like flue gases from gas-fired electric power plants, gaseous streams in industrial processes such as fermentation plants, ammonia and hydrogen manufacturing as well as natural sources, such as natural gas and geothermal energy producing wells. At present, most industries consider CO_2 as a waste with a cost of disposal, however attempts at considering it as a resource is happening. It is estimated that about 5 – 10 % of the total industrial CO_2 emission could be suited for production of fuels and chemical This amount is one order of magnitude higher than the current use of CO_2 in industry. [15] Separation of CO_2 from air with membranes or absorption techniques is also a possibility, and in appropriate conditions also an economically viable solution [6].

Methanol production from CO_2 is the key component in a framework proposed by Nobel laureate George A. Olah [3], called the anthropogenic carbon cycle within the "Methanol Economy". Figure 3 shows this concept.

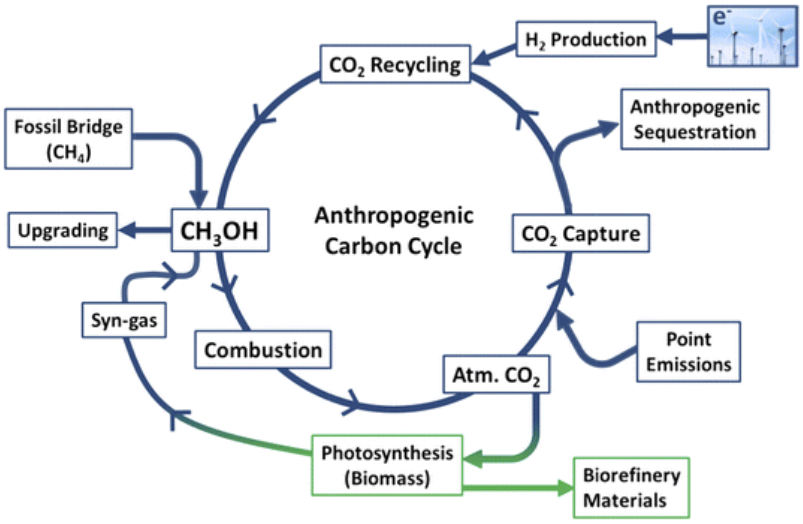

Figure 3. Anthropogenic chemical carbon cycle. [16]

The concept describes an energy/chemical economy based on the capture and recycling of CO_2 via its hydrogenation product methanol. Renewable electricity, e.g. wind and solar power, could be used to produce H_2 by water electrolysis and subsequently used in the methanol synthesis process. The resulting chemicals, like methanol, will become storage of renewable electricity, overcoming many limitations of a hydrogen-based economy. The stored energy can be converted to kinetic energy by either by ICE or fuel cell powered vehicles. Methanol can also be converted by subsequent reactions to nearly all products presently derived from fossil fuels. Centi et al. [17] also agree that the use of CO_2 as the carbon source is an effective approach to introduce renewable energy in the chemical industry value chain, which would limit greenhouse gas emissions.

Therefore, the Methanol Economy is a closed energy provision loop, provided the resulting CO_2 is recycled in a similar manner to nature's own carbon cycle. [16] However, at the center of this concept lies the assumption that CO_2 can be efficiently converted to methanol.

The CO_2 hydrogenation has the same reaction network as the syngas route, but with different feed compositions. Chemists have known how to convert CO_2 and H_2 into methanol since the early 20th century, and some methanol plants in the 1920's and 1930's in the US were actually using CO_2 and H_2, which was obtained from fermentation processes. [9] The methanol yields for the CO_2 hydrogenation are unfortunately lower than for the industrial syngas to methanol route, mainly

because CO_2 hydrogenation has a more severe limitation of the thermodynamic equilibrium [18].

Another approach to produce methanol from CO_2 is called the CAMERE process, where CO_2 is first converted to CO and water with the reverse water-gas shift (rWGS) reaction, after which water is removed, and then the remaining syngas is converted in the conventional way to methanol [19]. Anicic et al. [20] compared this two-step process to the direct hydrogenation of CO_2 from an economical and energy-efficiency viewpoint, and determined the cost of electricity had the greatest on the results. However, the conclusion was that the direct hydrogenation of CO_2 was more energy- and economically efficient. The CAMERE process is out of scope for this work.

The hydrogenation of CO_2 produces water, converting one third of the hydrogen into a non-desirable by-product. This is much more than in the commercial production of methanol from syngas. The CO_2 hydrogenation reaction (4) is also 40 $\frac{kJ}{mol}$ less exothermic than the CO hydrogenation reaction (3).

The most important reaction that occurs in parallel with the CO_2 hydrogenation (4) is the reverse water-gas shift (rWGS) reaction (5). Yang et al. [21] calculated that the competing rWGS reaction has a much lower activation barrier for the rate-limiting step than the CO_2 hydrogenation, and experimental observations have showed that the rWGS is 2 orders of magnitude faster at 300 ◦C on Cu-nanoparticles. The dominant product on a Cu catalyst is consequently CO, rather than methanol.

Other side reactions can also take place to a small extent, like formation of methyl formate, higher alcohols or other hydrocarbons. Subsequent reactions like the dimethyl ether (DME) formation can also happen [22]:

$$2CH_3OH \leftrightarrows CH_3OCH_3 + H_2O \qquad \Delta H_{R,298K} = -23.0\,\frac{kJ}{mol} \qquad (6)$$

Most by-products are actually thermodynamically more favourable than the methanol synthesis, however the reactions are controlled kinetically rather than thermodynamically, because methanol is the main product with typical Cu/ZnO catalysts. This demonstrates the importance of using a suitable catalyst. [23]

There are very few organic syntheses using CO_2, because of its highly oxidized state and thermodynamic stability [6]. CO_2 lies in a potential energy well and often reactions involving CO_2 are endothermic, and need active catalysts to react. [2] Chemical reactions are driven by the difference in Gibbs free energy between the products and reactants. The CO_2 hydrogenation reaction (4) has a Gibbs free energy change of $\Delta G_{R,298K} = 3.4 \frac{kJ}{mol}$, while the CO hydrogenation reaction (3) has $\Delta G_{R,298K} = -25.3 \frac{kJ}{mol}$. The removal of reaction products results according to Le Châtelier's principle in higher methanol yield. [6]

Figure 4 A) shows the temperature effect on the Gibbs free energy of the reactions present in methanol synthesis. Figure 4 B) shows the equilibrium conversions and selectivities at various conditions.

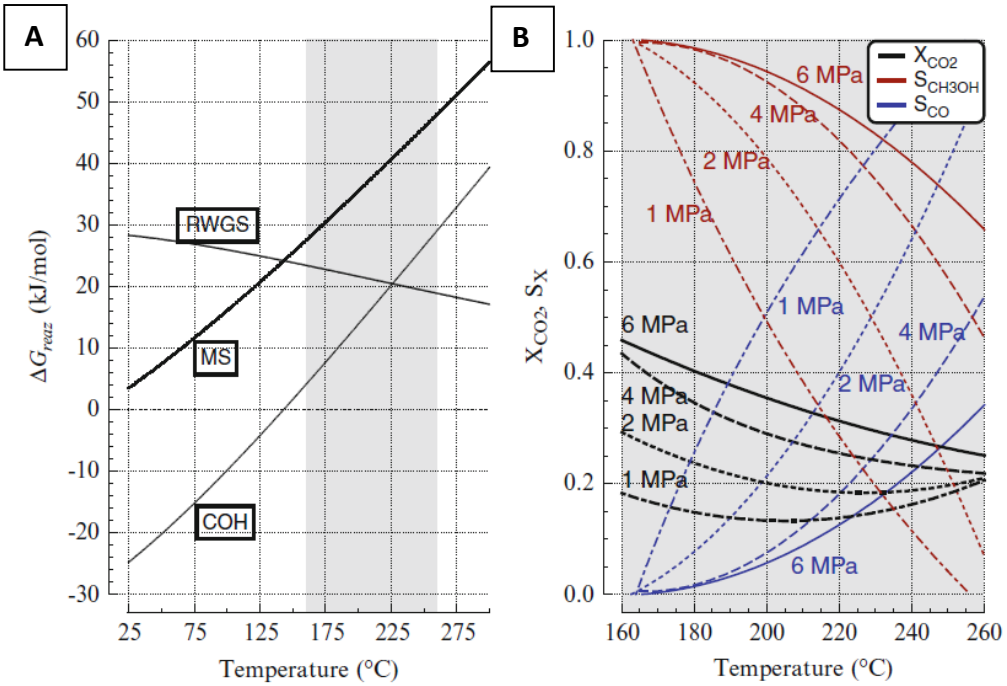

Figure 4. A) Gibbs free energy of the rWGS, CO_2 hydrogenation (MS) and CO hydrogenation (COH) reactions versus temperature. B) Equilibrium conversion/ selectivity values of the CO_2 hydrogenation reaction at various pressures and temperatures. [24]

Both hydrogenation reactions have ΔG_R values that are positive (nonspontaneous), which increase with increasing temperature. Hence, thermodynamically methanol formation favors lower temperatures. The rWGS also has positive ΔG_R values. However, it is decreasing with temperature, meaning that it is more favoured at

higher temperatures. Therefore, at for example constant 40 bar pressure and a temperature change from 180 to 260 °C the theoretical equilibrium methanol yield decreases significantly, from 34 % to 10 %. [24] For maximum methanol yield, a compromise between CO_2 conversion and rWGS reaction rate has to be made. Figure 4 B) shows that increasing the pressure increases the equilibrium CO_2 conversion and selectivity to methanol.

3 Catalysts for CO_2 hydrogenation to methanol

CO_2 conversion to useful chemicals can be driven by homogeneous, heterogeneous and enzymatic catalytic systems. Homogeneous catalysts usually have higher activity, but heterogeneous catalysts have the advantage that they are simpler in terms of reactor design, separation, handling, stability and reusability of the catalyst. [2] Therefore, there has been a preference to convert CO_2 to methanol using heterogeneous catalysts. However, Kothandaraman et al. [25] recently reported of a robust homogeneous ruthenium catalyst system that for the first time achieved one-pot CO_2 capture from air and conversion to methanol. The discovery of such stable homogeneous catalyst that achieved methanol yields up to 79 % will likely increase scientific interest in further homogeneous catalyst development. Still, heterogeneous catalytic hydrogenation of CO_2 has the potential to treat large quantities of CO_2 in a short time. Therefore, this work will exclusively focus on heterogeneous methanol synthesis.

Desirable properties of a good catalyst for the CO_2 hydrogenation include high activity and selectivity toward methanol formation, to minimize by-product formation, as well as long lifetime (up to several years). [8]

Catalyst deactivation can happen through sintering (which is the clustering of active metal sites), carbon deposition or catalyst poisoning. Catalysts that are resistant to poisoning and sintering are highly desirable. [9] Additionally catalysts that are aimed at small scale, decentralized fuel production units would need to be more robust against exposure to air and moisture, compared to industrial-scale catalysts [6].

Several studies on new techniques to develop catalysts with large surface areas, high active site dispersion and small particle size in order to increase activity and selectivity have been made and are presented in this chapter [6]. Special interest is

attributed to catalyst coating techniques on structured surfaces, when for example reactor walls are covered with a thin uniform catalyst layer. This technique offers benefits to for example intensified microchannel reactors. Coated catalysts are tested in the experimental section of this work.

3.1 Cu-based catalysts

Although many different metal catalysts have been tested for the synthesis of methanol, Cu remains as the main active component along with modifiers such as, Zn, Zr, Ce, Al, Ga and Ce. Copper, along with Zn, Cr and Pd are commonly used to minimize by-product hydrocarbon formation and maximize methanol formation. It has been theorized that Cu is so suitable for the methanol synthesis because of its ability to hinder the breaking of the C-O bond, unlike other hydrogenation catalysts, which often instead produce CH_4 [24].

The most general and common catalyst composition for the CO_2 hydrogenation is a $Cu/ZnO/Al_2O_3$ catalyst, which is similar to the ones employed presently in commercial methanol production from syngas. This is to be expected, since both routes according to most researchers share the same mechanisms. Most researchers agree that methanol is formed mainly by hydrogenation of CO_2 of the syngas on the catalyst's surface [22]. In a syngas feed that contains a small fraction of CO_2, the reaction proceeds more rapidly to the equilibrium composition. When steam is present, an initial rapid WGS reaction happens to form the necessary CO_2. [26] Highly efficient catalysts, satisfactory for industrial use, are not available because there is not the necessary mechanistic understanding of CO_2 hydrogenation to be able to control the relevant catalytic properties [27].

Promoters or stabilizers are also added to improve the life of the copper catalyst, since modifying the morphology of the metal particles can be employed to counteract copper sintering. [13] [24] The biggest threat to copper-based catalysts is thermal sintering via a surface migration process, which usually limits reaction temperatures to under 300 ^oC [28]. Catalysts employed for methanol production from syngas tend to deactivate prematurely at high CO_2 levels. Catalysts prepared for long term stability in the presence of CO_2 still have Cu and Zn as their main components, but with added modifiers. [9] The water produced in CO_2 hydrogenation and the rWGS inhibits conventional methanol synthesis catalysts and accelerates sintering. Therefore, catalysts formulated for CO_2 hydrogenation should

have high water tolerance. [24] Additionally, copper is very sensitive to sulphur and chlorine, and trace amounts of them can poison the catalyst. Luckily for the methanol synthesis, these compounds are rarely a problem, since they are removed in pre-treatment. [13]

Catalyst composition and catalyst preparation methods significantly affect the surface structure of the catalyst, which also affects the catalyst performance parameters such as activity and selectivity. [6] Preparation methods, such as co-precipitation, impregnation, and deposition-precipitation affect the results. Co-precipitation is the most common preparation method. The calcination temperature has also been proven to affect the results. Catalyst preparation techniques are often mostly based on empirical knowledge, which slows down the rational design of effective catalysts [9].

Many studies have focused on the synergies between Cu and ZnO in methanol synthesis. Zinc oxide has been proven to improve the dispersion and stabilization of copper. ZnO has lattice oxygen vacancies that have an electron pair in the lattice, which is active for methanol synthesis. High activities have been achieved with Cu/ZnO catalysts due to the formation of flat Cu surfaces, such as Cu(111) and Cu(100). [4] Several modifications of the conventional Cu/ZnO catalyst in terms of preparation method and the addition of modifiers have been considered. In a recent study by Gao et al. [29] the influence of modifiers Mn, La, Ce, Zr and Y on the performance of a typical Cu/Zn/Al catalyst was conducted. The precipitate phase was specially prepared via hydrocalcite-like precursors, which have been studied to increase Cu dispersion. It was found that the Cu surface area and Cu dispersion increased in the modifier order of Al < Mn < La < Ce < Zr < Y, and a similar pattern was found with the number of basic sites. The methanol conversion increased linearly with the increased Cu surface area, and the best results was found with the Cu/Zn/Al/Y catalyst, which achieved 26.9 % CO_2 conversion and a methanol selectivity of 47.1 % with a methanol space time yield (STY) of 0.52 $\frac{g}{g_{cat}h}$ or 16.2 $\frac{mmol}{g_{cat}h}$. The space time yield (STY), or reaction rate for MeOH (r'_{MeOH}), is used to quantify the methanol formation activity, is defined as the methanol quantity (mass, moles or volume) divided by the catalyst mass (or volume) and the time [30]:

$$STY_{MeOH} = \frac{n_{MeOH}}{m_{catalyst}h} \quad (7)$$

Figure 5 illustrates the relationship between Cu surface area and CO_2 conversion.

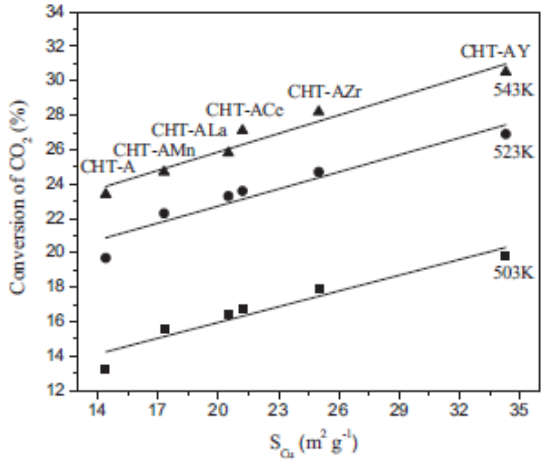

Figure 5. Relationship between conversion of CO_2 and the Cu surface area. CHT-A = Cu/Zn/Al. Reaction conditions: T_R = 230 , 250 and 270 °C, P_R = 50 bar, GHSV = 12 000$\frac{ml}{g_{cat}h}$, $\frac{H_2}{CO_2}$ = 3. [29]

The study verified that the introduction of modifiers to a Cu/Zn/Al catalyst is favourable as conversion and yield for the reaction increased significantly because of the increased Cu surface area [29]. Other researchers have also confirmed that the activity of the catalyst is directly proportional to the metallic copper surface area. However, there is still controversy regarding the contribution of different copper species (Cu^0 and Cu^+) to the activity. Some claim, that the activity is dependent on special copper sites, such as the copper ions, while others argue that the total copper exposed drives the activity. [13]

The support affects the formation and stabilization of the active phase of the catalyst, and tunes the interaction between the copper and the promoter [4]. The common Al_2O_3 support is known to be useful by inhibiting sintering, accelerating the adsorption of CO and improving the stability of the catalyst [8].

The high activity of catalysts containing zirconia is well documented [31] [32] [33] [34]. An et al. [35] found that a fibrous catalyst structure with the addition of 5% of Zr improved the Cu/Zn crystallite dispersion, which lead to a 80 % higher STY than

the most commonly used industrial catalysts for methanol synthesis in China. The fibrous catalyst was further tested by An et al. [34] at different conditions, which verified the high catalytic activity with a maximum MeOH yield of 17.9 % at 250 °C and 40 bar.

Zirconia has been known to be a good promoter or support because of its high stability under reducing or oxidizing atmospheres. Cu/ZnO systems modified with ZrO_2 are well studied, and it has been found that ZrO_2 increases the copper dispersion, as well as lowers the water affinity, compared to Al_2O_3 supported catalysts. [9] It has also been suggested that zirconia containing catalysts have higher water tolerance than aluminium containing catalysts [24]. The crystal types in zirconia have been found to significantly influence the catalyst. Copper supported on monoclinic zirconia, *m*-ZrO_2, is 4.5 times more active compared to tetragonal zirconia, *t*-ZrO2, because of the higher concentration of absorbed active intermediates, such as HCOO and CH_3O. Adding other promoter species has been found to further improve Cu/ZrO_2 catalyst performance, by decreasing the water absorption rate and improving the copper dispersion [4]. Saito et al. [36] found that Cu/ZnO catalysts modified with metal oxides ZrO_2, AI_2O_3, Ga_2O_3, and Cr_2O_3 were more stable over 3400 h experimental runs than commercial catalysts for the CO_2 hydrogenation reaction. Figure 6 shows the results.

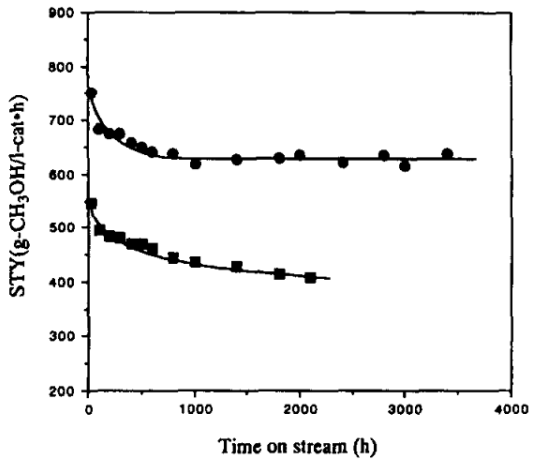

Figure 6. Change in methanol synthesis activities of a multicomponent catalyst $Cu/ZnO/ZrO_2/AI_2O_3/Ga_2O$ (circles) and commercial Cu/ZnO catalyst (squares). T_R = 523 K, P_R = 50 bar, GHSV = 10 000 h^{-1} and maximum T.o.S. = 3400 h. [36]

Both catalysts experienced fast initial deactivation. The multicomponent catalyst activity decreased after 3400 h by 17 %. The commercial catalyst activity decreased to 75 % of its initial activity. [36]

Even though the numerous studies on copper-based catalytic studies are hard to compare, Table 1 with the CO_2 conversions, methanol selectivities and activities summarizes the results of some recent CO_2 hydrogenation studies.

Table 1. Literature experimental results for copper-based catalysts.

Catalyst	**Preparation method**	**P_R (bar)**	**T_R (°C)**	**X_{CO_2} (%)**	**S_{MeOH} (%)**	**STY_{MeOH} ($\frac{mmol}{g_{cat}h}$)**	**Ref.**
Cu/ZrO_2	deposition-precipitation	20	240	6.3	48.8	11.2	[37]
$Cu/Ga_2O_3/ZrO_2$	deposition-precipitation	20	250	13.7	75.5	1.9	[38]
$Cu/B_2O_3/ZrO_2$	deposition-precipitation	20	250	15.8	67.2	1.8	[38]
$Cu/ZnO/Ga_2O_3/SiO_2$	co-impregnation	20	270	5.6	99.5	10.9	[39]
$Cu/Ga_2O_3/ZnO$	co-impregnation	20	270	6	88	11.8	[40]
$Cu/ZnO/ZrO_2$	glycine-nitrate combustion	30	220	12	71.1	-	[41]
$Cu/ZnO/ZrO_2$	urea-nitrate combustion	30	240	17	56.2	-	[32]
$Cu/ZnO/ZrO_2$	solid-state reaction	30	240	15.7	58	-	[42]
$Cu/ZnO/ZrO_2$	co-precipitation	30	250	19.4	29.3	-	[31]
$Cu/ZnO/Ga_2O_3$	incipient wetness	30	270	6.01	28.2	1.4	[43]
$Cu/ZnO/Ga_2O_3$	microwave-assisted precipitation	30	270	15.9	29.7	4.2	[43]
Fibrous $Cu/ZnO/Al/ZrO_2$	co-precipitation	40	240	20.5	61	-	[35]
$Cu/ZnO/ZrO_2$	co-precipitation	40	240	-	-	9.2	[44]
Fibrous $Cu/ZnO/Al/ZrO_2$	co-precipitation	50	250	25.8	69.4	-	[34]
Cu/ZnO/Al/Y	co-precipitation	50	250	26.9	47.1	16.2	[29]
$Cu/ZnO/ZrO_2$	co-precipitation	80	220	21	68	5.6	[33]
$Cu/ZnO/ZrO_2/Ga_2O_3$	citric acid complexing	80	240	17	71	6.6	[45]
$Cu/ZnO/Ga_2O_3/ZrO_2$	co-precipitation	80	250	-	75	10.1	[46]

3.1.1 Reaction conditions

Until the 1960's methanol synthesis from syngas was carried out at 250 – 350 bar pressures and 320 – 450 ^{o}C temperatures. However, since the introduction of more active catalysts by ICI in the 1970's, the conditions have since then been at 50 – 100 bar and 200 – 300 ^{o}C. For the CO_2 hydrogenation reaction similar conditions have been used as for industrial syngas to methanol production. [47]

The activation of CO_2 occurs at a sufficient rate only at temperatures higher than 200 ^{o}C [24]. The reaction rate for CO/CO_2 hydrogenation increases with increasing temperature. However, the equilibrium constants for these reactions decrease with an increase of temperature. As the hydrogenation reactions are exothermic and reversible, the product distribution will be controlled by both thermodynamics and kinetics. [13]

Experimental studies have shown that methanol yield increases up to a certain temperature, usually about 230 ^{o}C, and then starts to decrease at higher temperatures [13]. Guo et al. [32] [41] reported a maximum methanol yield at around 230 – 240 ^{o}C in two different studies using $CuO/ZnO/ZrO_2$ catalysts prepared with two different techniques. The conditions in the experiments studying catalysts prepared with the glycine-nitrate combustion method were 453 - 553 K (180 – 280 ^{o}C) and the pressure of 30 bar and GHSV of 3600 h^{-1} in a fixed bed reactor [41]. Figure 7 shows the results for the temperature impact on CO_2 conversion and methanol selectivity.

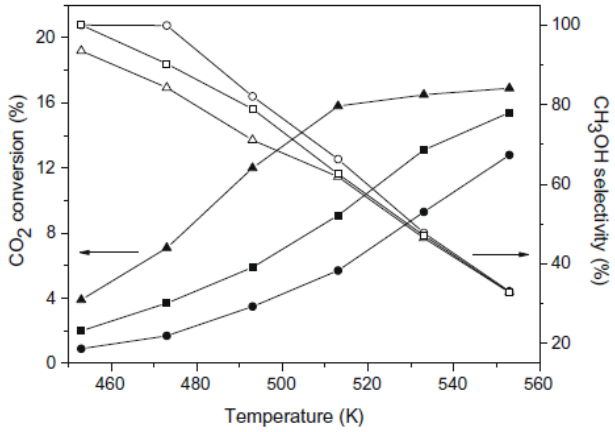

Figure 7. Left: Temperature impact on CO_2 conversion. Right: Temperature impact on methanol selectivity. Triangles represent catalyst prepared with glycine amount that equals 50 % of the stoichiometry, circles 100 % and rectangles 150 % of the stoichiometry. [41]

Compared to methanol synthesis, the rWGS has a higher apparent activation energy. This leads to a faster increase in CO production with increased temperature than that of methanol. [41] Therefore, there is a significant decrease in selectivity to methanol with increasing temperature. Figure 8 presents the temperature impact on methanol yield.

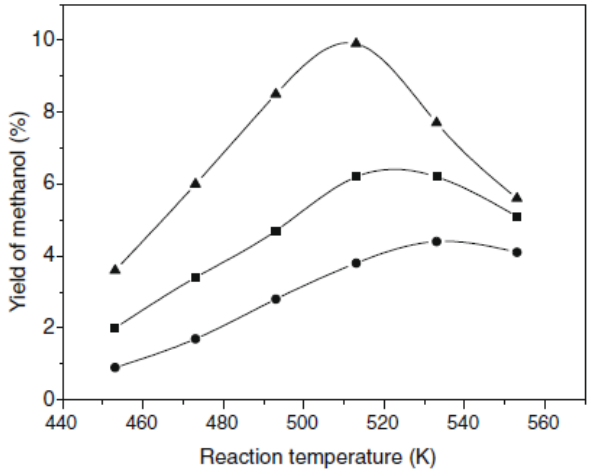

Figure 8. Temperature impact on methanol yield. Triangles represent catalyst prepared with glycine amount that equals 50 % of the stoichiometry, circles 100 % and rectangles 150 % of the stoichiometry. [41]

As shown in Figure 8, the maximum yield is at a plateau, which illustrates the shift of the CO_2 hydrogenation reaction from kinetics- to thermodynamics-limited regime. [13]

The pressure has less of an impact on the results than temperature. Methanol formation is preferred at high pressures. For economic reasons operation at lower pressures than currently typical 50 – 100 bar would be desirable. Cu-catalysts capable of efficient operation at lower pressures have not been reported. There are some studies on Cu/ZnO and Cu/ZrO_2 catalysts operating at less than 20 bar, nevertheless the results do not justify operation at these conditions. [13] Arguments for increasing the reaction pressure to up to 950 bar were made in a study done by Tidona et al. [47] At these conditions the reaction is assumed to take place in supercritical state. Because the syngas to methanol process is thermodynamically more favourable than the CO_2 hydrogenation process, running the CO_2 hydrogenation reaction at higher pressures is an option for higher one-pass methanol synthesis. [47] Figure 9 presents the results from the study with a Cu (18 wt%)/Al_2O_3 catalyst and GHSV varying from 11 900 to 25 000 h^{-1}.

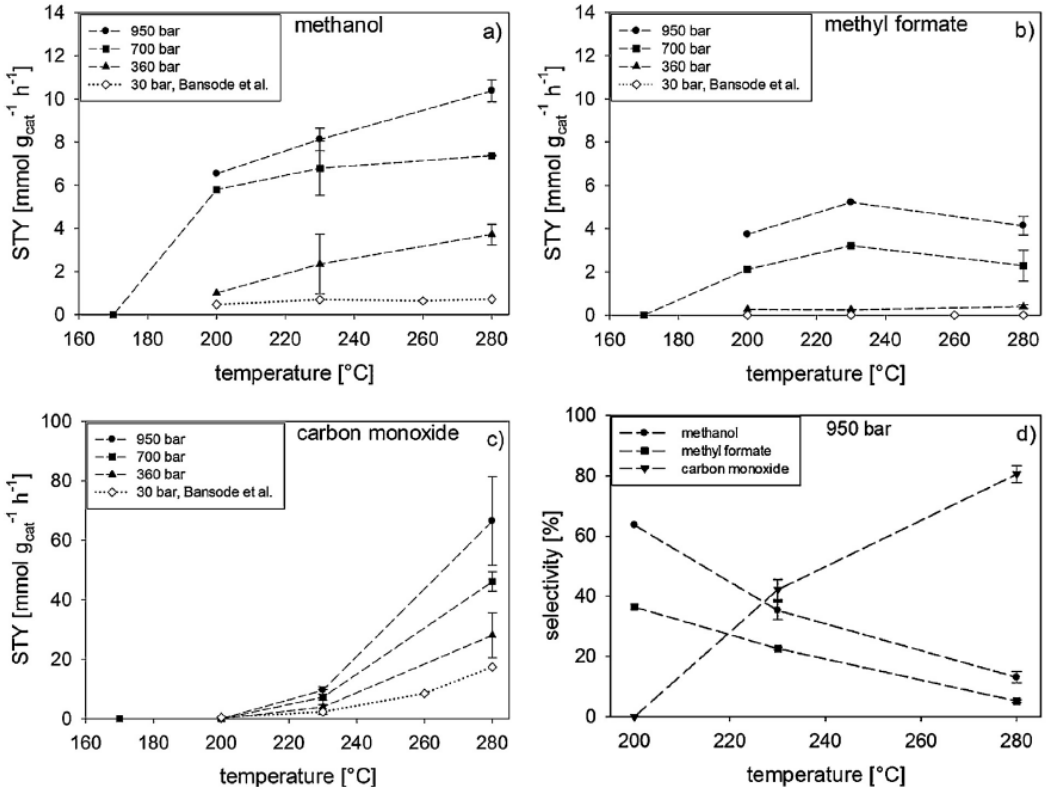

Figure 9. Space time yield versus temperature of: a) Methanol. b) Methyl formate (a side product from the hydrogenation of carbonate). c) Carbon monoxide. Experimentally determined values at 950 bar (circle), 700 bar (square), 360 bar (triangle) and 30 bar (diamond). d) Selectivity at 950 bar versus the reaction temperature. [47]

The STY was an order of magnitude higher in the reaction conditions of 230 °C and 950 bar compared to the conventional 230 °C and 30 bar conditions. The STY was at 950 bar about 10 $\frac{mmol}{g_{cat}h}$, when at 30 bar it was 0.7 $\frac{mmol}{g_{cat}h}$. For comparison, STY using syngas feed at 240 °C and 50 bar with a commercial catalyst was 34 $\frac{mmol}{g_{cat}h}$, which is much higher than in any study with CO_2 as feedstock. The authors argue that the energy efficiency does not significantly suffer from running the reaction at higher pressures. On the other hand, due to the lack of commercial process equipment suitable for these extreme pressures, the team had to develop in-house equipment. [47] This probably limits the usage of such conditions for the hydrogenation of CO_2 in commercial scale.

The space velocity can also affect the reaction rate, mostly due to mass transfer limitations the reactor system. However, increasing the space velocity decreases the MeOH yield. For CO hydrogenation the decrease in MeOH yield has been reported to be more rapid than during CO_2 hydrogenation. [13] The selectivity to methanol in CO_2 hydrogenation has been reported by Sun et al. [48] and Koeppel et al. [49] to increase with the increase of space velocity, which suggest that methanol is the primary product and is formed directly from CO_2 and H_2. As the space velocity increases, the contact time between the reaction gas and the catalyst surface is shorter. If the catalyst is highly active, a longer contact time either triggers a secondary reaction of methanol decomposition (reverse of CO hydrogenation) or increase extent of rWGS reaction. [48] However, Słoczyński et al. [46] did not find any correlation between selectivity to methanol and space velocity in their experimental study. Increasing the space velocity decreased the methanol yield, but increased the MeOH STY.

3.1.2 Reaction mechanisms

The reaction for methanol synthesis has been extensively investigated for over four decades. Still, the reaction pathway over the copper-based catalyst is a topic of debate [6]. Especially questions about how CO_2 is activated over the surface of the catalyst have remained unclear.

Early works on the pathway identified that the production of methanol from syngas is promoted by CO_2, although the synthesis is inhibited at high CO_2 concentrations. Since it was verified by isotope-labelled $^{14}CO_2$ in the late 80's that most of the methanol was produced from CO_2, there was a breakthrough in the understanding of methanol synthesis that also fuelled the interest in pure CO_2 hydrogenation. Later it was theorized that CO_2 does not inhibit methanol synthesis even at large concentrations. Instead the increasing water concentration inhibits the reaction as a result of reaction (4) and the rWGS reaction (5). [6]

The synthesis of methanol is generally regarded as occurring at interfaces of Cu and oxides (of which mainly ZnO and ZrO_2 are used)[6]. These oxides have interesting promoting abilities, and by structural, chemical and electronic effects they can enhance the reactivity of the Cu sites. Oxides also have surface affinity to either CO_2 or H_2 [24]. Bell et al. [50] suggested a dual-site, bifunctional mechanism that has since then been generally accepted. Arena et al. [51] have suggested a similar

mechanism. In this mechanism, there are two active centers involved for a Cu/ZrO_2 catalyst, and the CO_2 adsorbs on the bare oxide as bicarbonate and H_2 can adsorb and dissociate on Cu species. Via spillover, the atomic hydrogen moves from the Cu surface to the oxide site and hydrogenates in a stepwise reaction the adsorbed carbon species into methanol, which then are desorbed from the surface. [51]

The exact ways how the elementary steps happen on the surface are still debated. At least two reaction paths to methanol have been proposed: 1) A reverse water-gas shift, rWGS, thus CO_2 decomposition to CO. 2) A mechanism via an intermediate formate, HCOO [26]. Formate is well-known to be an intermediate in methanol synthesis and WGS. The formation of the formate species is often considered the rate-determining step, and it suggests that CO is formed by methanol decomposition. In the rWGS mechanism CO is formed by reverse water-gas shift, and converted to methanol by the CO hydrogenation reaction. [6] Figure 10 shows illustrated mechanisms for methanol formation for Cu/ZrO_2 and $Cu/ZnO/ZrO_2$ catalysts through a formate intermediate applying spillover hydrogen.

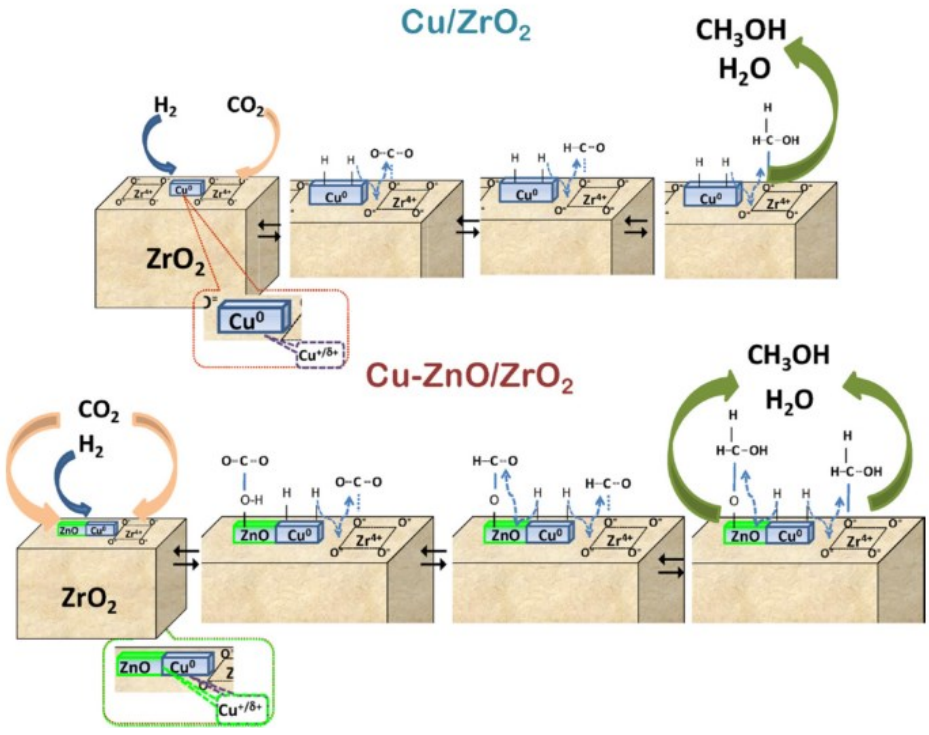

Figure 10. Proposed reaction pathway for the formation of methanol through a formate intermediate on a Cu/ZrO_2 (upper) and $Cu/ZnO/ZrO_2$ (lower) catalyst. [51]

Grabow et al. [52] studied several different reaction paths and surface species and with density functional theory (DFT) calculations identified steps that are likely to be significant for the synthesis of methanol from CO_2 and H_2. It is a formate reaction pathway driven by a partially oxidized Cu facet [24] [53]:

$$H_2\ (g) + 2s \leftrightarrows 2Hs \quad (8)$$
$$CO_2\ (g) + Hs \leftrightarrows HCOOs \quad (9)$$
$$HCOOs + Hs \leftrightarrows HCOOHs + s \quad (10)$$
$$HCOOHs + Hs \leftrightarrows H_2COOHs + s \quad (11)$$
$$H_2COOHs + s \leftrightarrows H_2COs + OHs \quad (12)$$
$$H_2COs + Hs \leftrightarrows H_3COs + s \quad (13)$$
$$H_3COs + Hs \leftrightarrows CH_3OH\ (g) + 2s \quad (14)$$
$$OHs + Hs \leftrightarrows H_2O\ (g) + 2s \quad (15)$$

In this micro-kinetic model the s represents a free surface site and Xs is the adsorbed atom or molecule X. The model was fitted to experimental methanol synthesis rate data which was obtained using a commercial $Cu/ZnO/Al_2O_3$ catalyst. The model showed good fit to the experimental data. [52] Other recent DFT calculation studies, for example by Behrens et al. [54], also favour the formate mechanism. In their study they also used experimental data using a $Cu/ZnO/Al_2O_3$ catalyst system, including imaging methods combined with DFT calculations, and found that the active site consists of Cu steps decorated with Zn atoms which were stabilized by bulk defects and surface species that needed to be present in order for the catalyst to work. This specific structure observed in the very active catalyst sites makes the Zn serve as adsorption site for oxygen-bound intermediates. [54]

However, opposing views of the direct conversion via a formate reaction pathway exist, like for example the study by Yang et al. [55] They argue that methanol synthesis on Cu cannot result from the direct hydrogenation of formate species in simple steps involving adsorbed H species alone. They suggest an indirect methanol formation path from both CO_2 and CO along a WGS-rWGS path, occurring via a more favourable carboxyl (HOCO) route. [55][56] This is also supported by DFT calculations done by Zhao et al. [57], who argue that the formate path does not exist because of the high hydrogenation barrier of HCOO and H_2COO intermediates. The carboxyl pathway to methanol arises from the water-gas shift pool of carboxyl intermediates. They also found that trace amounts of water is a critical reactant in

both the WGS and methanol synthesis reaction. [57] Figure 11 presents the different pathways for CO and CO_2 conversion to methanol over Cu.

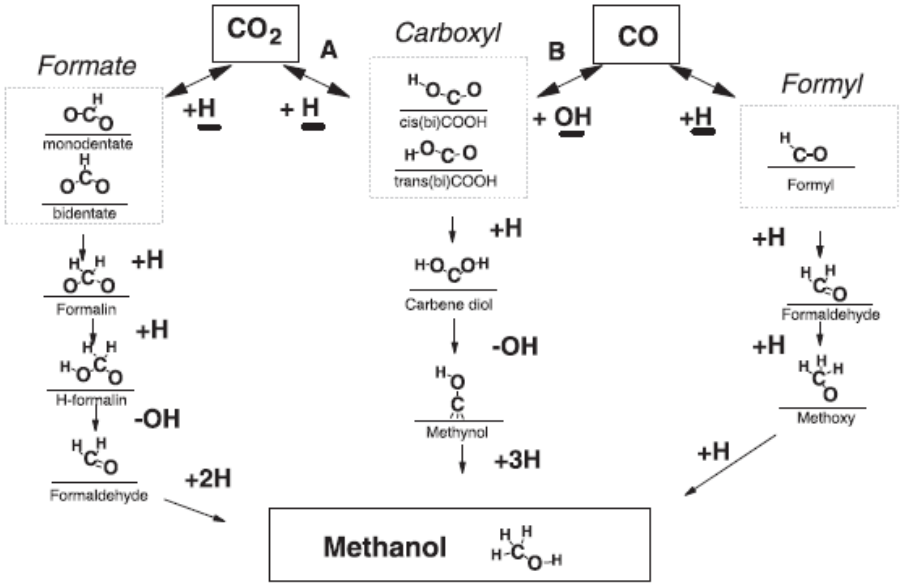

Figure 11. Mechanistic pathways for CO and CO_2 conversion to methanol over Cu. The water-gas shift for CO and CO_2 through the carboxyl intermediate is on the top. The direct conversion of CO_2 through the formate is on the left and direct conversion of CO through a formyl mechanism is on the right. On the middle is the carboxyl mechanism for the methanol synthesis. [56]

The reaction routes for methanol outlined in Figure 11 displays the complexity of the process. It is known that the same molecular species, of similar physico-chemical characteristics, are involved in numerous reactions on Cu-based catalysts. Therefore, it has been suggested that the formation and fate of the several reaction intermediates strictly depends on the state of the catalyst surface under stationary conditions. Consequently, the composition and redox potential of the reacting atmosphere influences the morphology and chemical state of Cu particles. For example the WGS reaction requires oxidative conditions, and the methanol synthesis proceeds under reducing environments. Therefore, each process determines a different state of metal sites, shaping the reactivity of the active Cu phase in the different reactions. [24]

For the development of better catalysts, more complete experimentations and microkinetic modelling is needed to clarify what the actual reaction mechanisms are.

Some things that are already clear based on the current knowledge of the reactions are that a higher surface area of Cu, appropriate adsorption and effective interaction between the active parts of the catalysts are important for the preparation of active catalysts [9].

3.1.3 Kinetic models

Similar to the old mechanism studies, several of the early kinetic modelling studies assumed that the hydrogenation of CO is the only pathway for methanol synthesis. When it was noticed that CO_2 had an effect on the synthesis, Klier et al. [58] published the first kinetic model that included CO_2. The kinetic model developed by Graaf et al. [59] [60] is the most widely employed kinetic model for methanol synthesis simulations. In this model the reactions CO hydrogenation to methanol (3), rWGS (5) and CO_2 hydrogenation to methanol were considered. [61]

The Graaf model assumes that compared to hydrogen and water, carbon monoxide and dioxide adsorb on different active sites. The reactions are assumed to be occurring via a formate mechanism and through statistical model discrimination the authors selected the best kinetic expressions. [62] The rate equations were fitted against a large number of experiments using $CuO/ZnO/Al_2O_3$ catalyst in a gradientless spinning basket reactor in the pressure range of 15 – 50 bar and at temperatures of 207 – 277 °C. [63]

The rate determining steps in the Graaf et al. model for the adsorption reactions are:

$$H_2COs1 + Hs2 \leftrightarrows H_3COs1 + s2 \quad (16)$$

$$HCO_2s1 + Hs2 \leftrightarrows COs1 + H_2Os2 \quad (17)$$

$$H_2CO_2s1 + Hs2 \leftrightarrows H_3CO_2s1 + s2 \quad (18)$$

The reaction rate for the CO hydrogenation reaction in the Graaf model is defined as:

$$r'_{MeOH,3} = \frac{k_3 K_{CO}\left(f_{CO} f_{H_2}^{1.5} - \frac{f_{CH_3OH}}{f_{H_2}^{0.5} K_3^{eq}}\right)}{(1 + K_{CO} f_{CO} + K_{CO2} f_{CO2})\left(f_{H2}^{0.5} + \left(\frac{K_{H_2O}}{K_{H2}^{0.5}}\right) f_{H_2O}\right)} \left[\frac{mol}{kg_{cat} * s}\right] \quad (19)$$

For the rWGS reaction:

$$r'_{rWGS,5} = \frac{k_5 K_{CO_2}\left(f_{CO_2} f_{H_2} - \frac{f_{H_2O} f_{CO}}{K_5^{eq}}\right)}{(1+K_{CO} f_{CO} + K_{CO2} f_{CO2})\left(f_{H2}^{0.5} + \left(\frac{K_{H_2O}}{K_{H2}^{0.5}}\right) f_{H_2O}\right)} \left[\frac{mol}{kg_{cat} * s}\right] \quad (20)$$

For the CO_2 hydrogenation:

$$r'_{MeOH,4} = \frac{k_4 K_{CO_2}\left(f_{CO_2} f_{H_2}^{1.5} - \frac{f_{CH_3OH} f_{H_2O}}{f_{H_2}^{1.5} K_4^{eq}}\right)}{(1+K_{CO} f_{CO} + K_{CO2} f_{CO2})\left(f_{H2}^{0.5} + \left(\frac{K_{H_2O}}{K_{H2}^{0.5}}\right) f_{H_2O}\right)} \left[\frac{mol}{kg_{cat} * s}\right] \quad (21)$$

Where f_i fugacity for species *i*.

k_i rate constant for reaction *i*

K_{i}^{eq} equilibrium constant

K_i adsorption equilibrium constant

However, several studies have neglected the unidealities described by fugacity coefficients, and assumed ideal gas behaviour by using partial pressures in the model with good results. [64] [34]

The values for the chemical equilibria, K_{i}^{eq}, were obtained from an earlier Graaf et al. [65] study. In this study the chemical equilibria of the hydrogenation reactions and the rWGS were determined with a fixed bed reactor at 200 – 270 °C and 10 – 80 bar pressures.

Other noteworthy kinetic models are for example the Skrzypek et al. [66] model and the vanden Bussche and Froment [67] model. In the vanden Bussche and Froment model only the CO_2 hydrogenation and rWGS reactions are considered, and it is assumed that MeOH formation only happens through CO_2 hydrogenation in accordance to the isotope-labelling experiments performed in the 80's. [62] It also considers the inhibitory effect of water. The rate equations are of Langmuir-Hinschelwood-Hougen-Watson (LHHW) type and the adsorption of CO_2 leads to carbonate structures, which are hydrogenated to yield methanol. The water-gas shift reaction occurs via a redox mechanism. [62][67] The experiments used to determine the parameters were performed on an industrial $Cu/ZnO/Al_2O_3$ catalyst in pressures between 15 – 51 bar and at temperatures between 180 – 280 °C.

The rate determining steps are:

$$CO_2(g) + s \leftrightarrows \mathrm{Os} + \mathrm{CO(g)} \quad (22)$$

$$HCO_2 2s + s \leftrightarrows \mathrm{H}_2CO_2 2s + s \quad (23)$$

The reaction rates for the vanden Bussche and Froment model are: [68]

$$r'_{MeOH,4} = \frac{k_1 p_{CO_2} p_{H_2} \left(1 - \left(\frac{1}{K_4^{eq}}\right)\left(\frac{p_{H_2O} p_{CH_3OH}}{p_{H_2}^3 p_{CO_2}}\right)\right)}{\left(1 + k_2\left(\frac{p_{H_2O}}{p_{H_2}}\right) + k_3 p_{H_2}^{0.5} + k_4 p_{H_2O}\right)^3} \left[\frac{mol}{kg_{cat} * s}\right] \quad (24)$$

$$r'_{rWGS,5} = \frac{k_5 p_{CO_2}\left(1 - K_5^{eq}\left(\frac{p_{H_2O} p_{CO}}{p_{CO_2} p_{H_2}}\right)\right)}{1 + k_2\left(\frac{p_{H_2O}}{p_{H_2}}\right) + k_3 p_{H_2}^{0.5} + k_4 p_{H_2O}} \left[\frac{mol}{kg_{cat} * s}\right] \quad (25)$$

The most recent kinetic modelling study was done by Lim et al. [69], where they show that the most accurate model is the one with a formate intermediate, and that CO_2 hydrogenation rate is slower than for CO.

3.1.4 Catalyst deactivation models

Sintering is the main Cu-based catalyst deactivation mechanism, which is often caused by poor heat transfer mechanisms in the reactor. This leads to a thermal misbalance that clusters the copper sites and reduces the effective area. [70] However, sintering of copper occurs relatively slowly at the methanol synthesis conditions, and a catalyst lifetime of several years has been observed. Nevertheless, an initial fast deactivation of up to 60 % is observed with newly reduced catalysts. The Tamman temperature has been used to describe the limit temperature for the crystal growth by atom migration. The Tamman temperature for copper is 397 °C and 887 °C for zinc oxide. Several experimental studies have shown that metallic clusters start to migrate at much lower temperatures, and that the Tamman temperature for copper is as low as 190 – 200 °C. [71] Sintering of Cu is observed in methanol synthesis reaction conditions and becomes severe at 270 – 300 °C, where sintering of zinc has also been observed.

Catalyst deactivation has generally been modelled using simple power law expressions. For conventional methanol synthesis there are number of experimental studies on deactivation modelling. Several studies have confirmed a first order deactivation rate for methanol synthesis after an initial high deactivation rate for the first hours. Simple power law expressions for deactivation are expressed as:

$$\frac{da}{dt} = -K_d(T)a^n \tag{26}$$

Where the deactivation order n can be 1 to 16. Experimentally verified by Sahibzada et al. [72] at 250 °C and 50 bar conditions, an initial deactivation order for the first 10 hours of n = 10 was obtained.

A deactivation model by Lovik [73] for fixed bed reactors can be used to simulate the slow deactivation for longer periods of time. This model has been further improved by Parvasi et al. [64] to consider the effect of different feed compositions (different $\frac{CO}{CO_2}$ −ratios), as conventional Cu-based methanol synthesis catalysts are CO_2 sensitive. The deactivation kinetics for the Parvasi model is:

$$\frac{da}{dt} = -\left(\frac{p_{CO_0}}{p_{CO_{2_0}}}\right)^m K_d \exp\left(-\frac{E_d}{R}\left(\frac{1}{T} - \frac{1}{T_R}\right)\right) a^5 \tag{27}$$

Where the values of K_d and E_d have been reported as 0.00439 1/h and 91270 J/mol. T was the reference temperature, set at 513 K and a is the activity which was initially set to 0.4 by Lovik. [64][73]

The model was validated against process plant data for a time period of 760 days. The parameter m was optimized with reactor plant data, and the value was found to be 0.56.

3.2 Other catalysts

There are a few other heterogeneous catalysts that are selective towards methanol, the most common of them being Pd-based catalysts. Additionally, Au, Pt and Ni/Ga as active metals have been studied for methanol synthesis.

Palladium shows high activity and selectivity towards CO_2 hydrogenation to methanol, and some researchers even consider it to have more potential than Cu-

based catalysts [6]. As with Cu-based catalysts, their performance highly depends on the type of support and the catalyst preparation method. For instance, calcination and reduction temperatures have been reported to have significant impact on Pd/ZnO catalyst performance. [9] Over the past decades Pd catalysts supported on ZnO, Al_2O_3, TiO_2, La_2O_3, CeO_2, Nd_2O_5 and SiO_2 have been tested [74]. In 1995 Fujitani et al. [75] first reported of a Pd-based catalyst that matched a conventional Cu/ZnO catalysts in terms of performance. It was a Pd-Ga_3O_2 catalyst that achieved a yield of 10.1 % in conditions of 523 K and 50 bar. Fujitani et al. postulated that the good activity was due to the optimal amount of the active species of palladium ions Pd^{n+} ($0 < n < 2$) on the surface of palladium that were effectively stabilized by Ga_xO_y. [75]

Recently new types of multi-walled carbon nanotube (MWCNT) supported Pd-catalysts have been developed. MWCNTs have drawn significant interest because of their fascinating features, like the sp^2-C surface and the high mechanical strength. However, most relevant to the CO_2 hydrogenation reaction is the ability for the nanotubes to reversibly adsorb hydrogen. Several studies have been performed on MWCNT-promoted CuO/ZrO_2, yet there are more studies on MWCNT-promoted Pd-catalysts. Liang et al. [76] reported of a MWCNT supported Pd-ZnO which has a low CO_2 conversion of 7.3 %, but almost complete selectivity towards methanol at reaction conditions of 250 ^oC and 30 bar. They concluded that the favourable MWCNT hydrogen adsorption generated a micro-environment of higher concentration of active hydrogen on the surface, therefore improving the rate of hydrogenation reactions. [76] In a more recent study by the same group, Liang et al. [77] modified the nanotubes with palladium, and employed it as a promoter for a Pd/ZnO catalyst. This increased the yield of methanol to 7 % at 50 bar and 270 ^oC. However, selectivity towards side products was considerably high. [77]

The mechanism for Pd-catalysts might not differ from Cu-based catalysts at all. In a study [78] to identify the mechanism for methanol synthesis over Pd/β-Ga_2O_3 using in situ FTIR spectroscopy, it was found that the reaction follows the formate pathway, specifically by the formation of HCOO → H_2COO (dioxomethylene) → CH_3O (methoxy) and finally CH_3OH. The spillover of atomic hydrogen from the Pd surface to the carbon species and the stability of the methoxy species on Ga_2O_3 were theorized to be the reason for the high activity of the Pd/β-Ga_2O_3 catalyst. [78] [4].

Recently, Studt et al. [53] identified, through a computational descriptor-based analysis, a new class of Ni/Ga catalysts. They have unique properties, such as ability to operate at low pressures, and that they hydrogenate CO_2 to methanol without producing large amounts of CO via the rWGS reaction. Tests at ambient pressure and at around 200 °C revealed that especially Ni_5Ga_3 was particularly active and selective, corresponding $Cu/ZnO/Al_2O_3$ in yields, however with much lower CO formation. [53] However, being performed at ambient pressure results in the yields being very low compared to standard CO_2 hydrogenation conditions. Despite this, interesting possibilities would open up from further development of the Ni/Ga catalysts capable of working at low pressure, thus opening possibilities for e.g. decentralized small-scale CO_2 to methanol reactors. Other catalysts, such as gold and platinum, are not as active as palladium catalysts. Some of the results of these alternative catalysts are presented in Table 2.

Table 2. Summarizing table of alternative heterogeneous catalysts for CO_2 hydrogenation to methanol and their performance.

Catalyst	Preparation method	P_R (bar)	T_R (°C)	X_{CO_2} (%)	S_{MeOH} (%)	Y_{MeOH} (%)	Ref.
Au/ZnO	deposition-precipitation (DP)	5	240	0.5	77.8	0.38	[79]
$Au/ZnO/ZrO_2$	co-precipitation	80	220	2	100	2	[79]
Pd/CeO_2	impregnation	20	250	4	27.7	1.2	[80]
Pd/Ga_2O_3	co-precipitation	50	250	19.6	51.5	10.1	[75]
Pd/Ga_2O_3	incipient wetness	50	250	17.3	51.6	8.9	[81]
Pd/Ga_2O_3/MWCNTs	co-precipitation	50	250	16.3	57.5	9.4	[82]
Pd/Zn/MWCNTs	co-precipitation	50	270	19.6	35.6	7	[77]
Pd/Zn/MWCNTs	incipient wetness	30	250	7.3	86.3	6.3	[76]
$PdCa/SiO_2$	incipient wetness	30	250	12.1	65.2	7.9	[74]
Pt/CeO_2	impregnation	30	230	8.1	68.2	5.5	[83]

3.3 Coated catalysts

Structured catalysts, or coated catalysts, are gaining more attention because of the potential benefits they can offer. Coated catalysts are produced by depositing a thin catalyst layer over a support that can either be: 1) An inert parallel longitudinal channel, monolith or foam. 2) Reactor wall. [84] In other words, it is an attempt at utilizing the catalyst more efficiently (improved mass- and heat transfer) in a

process by loading it in a more favourable structure than the typical randomly packed beds. The thin catalyst layer is typically 15 – 100 μm thick, which minimizes the internal diffusional resistances and a high reaction rate can be achieved. Intensified coated microchannel or monolith reactors are also interesting for the CO_2 hydrogenation of methanol.

Monolithic catalyst support structures were first employed in automobile exhaust systems, and since then they have been used in several other environmental applications. [85] Conventional methanol synthesis is almost exclusively conducted in packed bed reactors (PBR). They are filled with catalyst pellets which often suffer from low heat transfer, since only point contacts exist between them. Poor heat transfer leads to design choices where the reactor tubes need to be several meters long in order to be effective, which limits the possibility of developing intensified compact reactors. [86] Coated catalysts are particularly considered for reactions where temperature control is needed, by eliminating the heat transfer resistances that control many reactions. Moreover, the pressure drop is significantly reduced in monolithic reactors or coated microchannel reactors compared to packed bed reactors. [87]

Parallel longitudinal monolith structures are basically a single structure with many thin, vertical, parallel channels, separated by walls. [88] Open-celled foams (OF) are 3D cellular structures, and a trade-off analysis shows that foams in reactors have a pressure drop higher than monoliths, but lower than fixed beds. [84]

There are two basic types of monolithic catalysts when the component distributions and preparation methods are considered: 1) Coated structured catalysts. 2) Incorporated catalysts. For coated catalysts the substrate is most often a ceramic material or metal. Ceramic monoliths are prepared by extrusion while metallic monoliths are manufactured by corrugation. [89]

Producing effective coated catalysts with high specific surface areas and a favourable morphology can be a challenge. The coated catalyst must be thermally and mechanically stable, hence binders are often used. Surface roughness will favour mechanical anchorage, and minimize risk of the coating peeling off. Therefore, an intermediate layer or primer is sometimes used to enhance the adhesion. [84] However, the binder may chemically interact with the catalyst and decrease the activity. Additionally, there are several pre-treatment techniques for the substrate,

often aimed at coating a high surface area (>10 m^2/g) porous oxide on the low-surface-area substrate. [90] Figure 8 illustrates the layers of coating on a substrate.

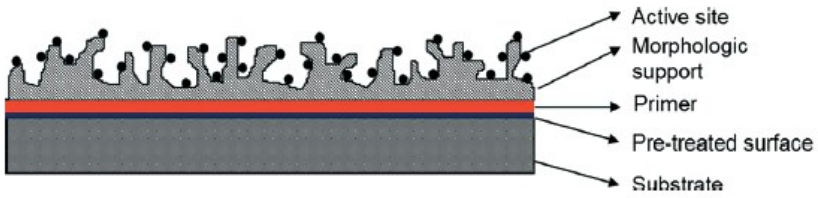

Figure 12. Structured catalyst prepared by coating. [90]

The coating geometry is also critical for the mass and heat transfer phenomena, namely ensuring that a sufficiently thick and homogeneous layer is formed. Therefore, the preparation methods are very important for the monolithic catalyst to function properly. [85]

The most typical ceramic monolith material is cordierite ($2MgO/5SiO_2/2Al_2O_3$), due to its good temperature and mechanical resistance and chemical compatibility with most catalyst coatings. Metal substrates, such as aluminium or FeCrAl alloys, can be laminated with much thinner coatings. They are also more thermally conductive, which is especially beneficial for highly exothermic or endothermic reactions. However, the adherence between the catalytic coating and the metal surface is quite poor, making these coatings more challenging to prepare. The choice of monolith support material depends on the adhesion and chemical compatibility between the substrate and the coating, as well as the properties related to use of the catalyst, such as operating conditions and chemical resistance. [84] [91]

There are various techniques for coating a substrate, the most important being the washcoating or dip coating from a liquid suspension [92]. Figure 13 shows an example of a washcoated microchannel block and a monolith, in the left and the right picture respectively.

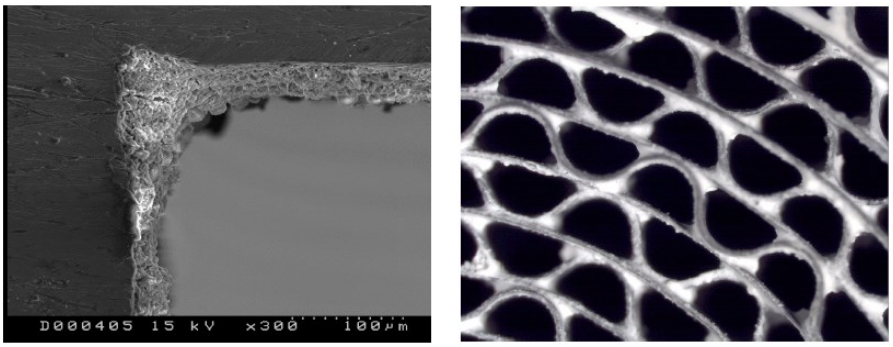

Figure 13. Micrographs of catalyst accumulation by washcoating in a metallic Fecralloy substrate. Left: 700 x 700 µm microchannel block. Right: Monolith structure with 222 $\frac{cells}{cm^2}$. [92]

Furthermore, there are various growth techniques in which the catalyst layer is formed from a liquid solution by growth of the new phase on a substrate. Also less frequent techniques, such as electronic film growth and growth from the vapour phase (PVD, CVD, and ALD) exist. [92]

In washcoating, the structure is coated at a controlled rate with a liquid containing the catalyst, submerging it and then withdrawing it at a controlled rate. The excess liquid is removed, and subsequently calcination is performed to generate a solid layer on the material. The method is very versatile, because it can be applied to any suspension, colloid or sol. However, there are many factors that affect the results, mainly: 1) Properties of the solid, like shape and surface properties. 2) Properties of the liquid, like concentration, viscosity and surface tension 3) Properties of the process, like speed of immersion. [84] Viscosity of the solution is especially important. Low viscosity usually makes coating easy and even, however it requires repeated coatings. Usually viscosity is increased, and a recommended value for good loadings is 10 – 20 cp. [91] Due to surface tension, the washcoated catalyst tends to collect in corners, as can be seen in Figure 13. [93]

Bravo et al. [94] studied the coating of the reactor walls with a commercial BASF $CuO/ZnO/Al_2O_3$ catalysts for the methanol steam reforming reaction. They developed coatings of 25 µm thickness in non-porous capillaries of different diameters, and compared the catalytic activity to a packed catalyst bed. [94] Figure

14 shows the conversion versus space time yield of packed beds and wall coated catalysts.

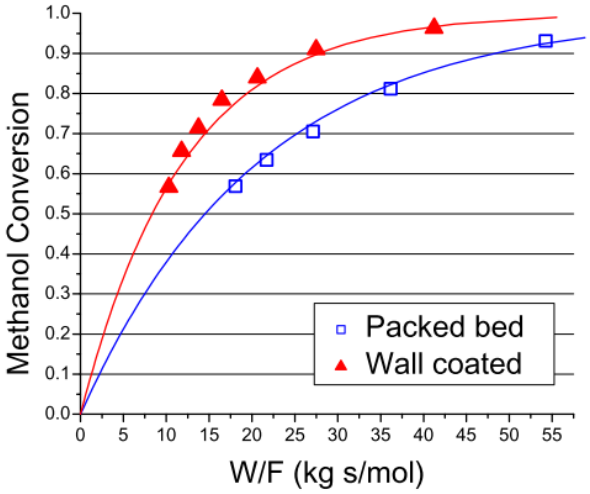

Figure 14. Reactivity for methanol steam reforming with a packed bed reactor and wall coated 4.1 mm diameter quartz tube reactor at $P_R = 0.85$ bar and $T_R = 230$ °C. The contact time, W/F $\left(\frac{m_{catalyst}s}{n_{methanol}}\right)$, is the inverse STY. [94]

The catalytic activity of the wall coated catalyst was higher than for the packed bed catalyst. The coating was adherent and did not peel off during the tests, which lasted for 10 days. Tests were performed in channels as small as 250 µm in diameter. However, at 250 µm channel diameter the deposited thin films became metastable, and capillary forces caused the films to form plugs that blocked flow. [94]

More recently, Montebelli et al. [95] tested the washcoating of highly conductive copper open-cell foams (OF) for methanol synthesis from syngas with a commercial $CuO/ZnO/Al_2O_3$ catalyst. Figure 15 shows the methanol productivity as a function of temperature for a coated catalyst of thickness 75 µm and conventional particulate catalysts.

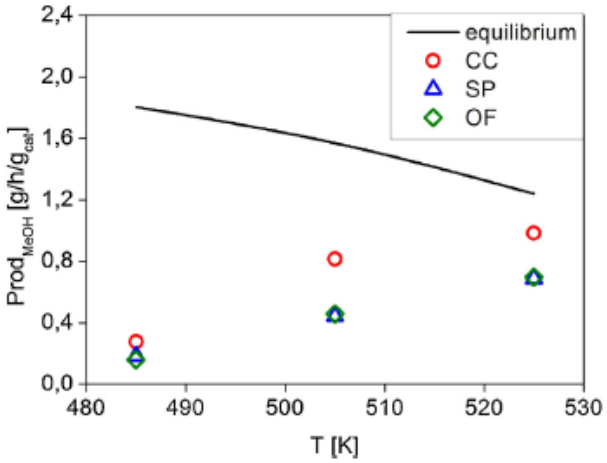

Figure 15. Methanol STY over fresh catalyst samples, where CC (circle) is powdered catalyst, SP (triangle) is slurried powder and OF (diamond) the washcoated foam. Reaction conditions: $T_R = 232$ °C, $P_R = 50$ bar, GHSV $= 15\,000 \frac{dm^3}{kg_{cat}h}$ *at STP*, $\frac{CO}{CO_2} =$ 3.2. [95]

It was found that washcoated copper foams exhibited lower CO_x conversions and methanol productivity than the original catalyst powder. Slurry powders, i.e. dried and calcined powders from slurry, showed the same chemical activity as the washcoated foams. This ruled out any effect of the deposition step on the performance and singling out the slurry preparation or calcination procedure responsible for decreasing the catalyst activity. [95]

Figure 16 shows the evolution of CO_x conversion and methanol productivity over time.

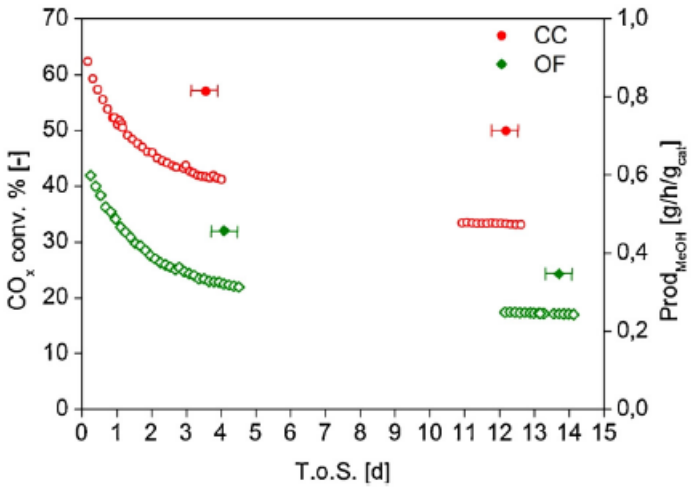

Figure 16. CO_x conversion and methanol productivity as a function of T.o.S. (time on stream). CC (circle) is powdered catalyst and OF (diamond) washcoated foam. Reaction conditions: $T_R = 232$ °C, $P_R = 50$ bar, GHSV $= 15\,000 \frac{\mathrm{dm^3}}{\mathrm{kg_{cat}h}}$ *at STP*, $\frac{CO}{CO_2} = 3.2$. [95]

After two weeks on stream, conversion and productivity decreased about 20 % from their initial steady-state values (taken after four days on stream). The powder and the coated foam showed a similar deactivation trend. [95] The initial deactivation was significant, as reported in other Cu-based catalyst studies.

Catalyst coating is an innovative technique to achieve high void fraction and high volumetric surface areas, hence minimizing pressure drops and mass and heat transfer limitations in reactors. However, their preparation can be challenging and the development of effective structured catalyst systems is still in the development stage, requiring further research [96]. Moreover, coated catalysts are more expensive than conventional catalysts. To compensate for the added costs, they have to show practical benefits for them to become widely used.

4 Reactors for CO_2 hydrogenation to methanol

Chemical reactors form the heart of a chemical production plant, and the choice of reactor is an important engineering decision, especially for catalytic reactions. This chapter presents different interesting reactor technologies for the continuous gas

phase CO_2 hydrogenation to methanol. Even though there have lately been some interesting studies on CO_2 hydrogenation to methanol in special intensified reactors, such as zeolite membrane reactors, emphasis will instead be on interesting new coated catalyst reactors, that mostly have not yet specifically been tested for the CO_2 hydrogenation reaction [6]. Nevertheless, they may offer interesting possibilities for intensified renewable methanol production.

4.1 Packed bed reactors

A tubular reactor is a type of continuous reactor, which involves a cylindrical pipe or pipes usually operated at steady state. The ideal behaviour of tubular reactors is plug flow, in which all non-reacting molecules have equal residence times. There is assumed to be no radial variation in concentration, temperature, reaction rate or axial dispersion of the flow. The reacting fluids are consumed as they flow down the length of the reactor. [30] A tubular reactor with a bed of solid catalyst is often called a packed bed reactor (PBR), or fixed bed reactor (FBR). Packed bed reactors are for heterogeneous catalytic reactions, and are employed for gas-solid, liquid-solid and gas-liquid-solid reactions. [97]

In gas-solid PBRs the reaction gas flows through the solid catalyst particle gaps. There are both simple single fixed bed and multitubular reactor designs available. Multitubular designs increase the tube surface-to-volume ratio, and are used for highly exothermic or endothermic reactions. Single fixed bed reactors are typically operated adiabatically, whereas multitubular reactors are typically heated or cooled by a heating or cooling fluid in the shell of the reactor.

Packed bed reactors are the most common form of reactor for methanol synthesis, in both laboratory- and industrial-scale. One of the most widely used reactors used commercially for methanol production from syngas is the Lurgi multi-tubular packed bed reactor, which has a capacity of about 1200 – 1400 tonnes/day. It has several thousand tubes with 30 – 50 mm diameter and which are filled with catalyst pellets of few millimetres in diameter. [86] The dominant heat transfer mechanism is convection, which implies that high flow rates are needed for acceptable heat transfer coefficients and to properly control the hot-spots in the reactor [95]. Figure 17 shows the industrial Lurgi MegaMethanol process.

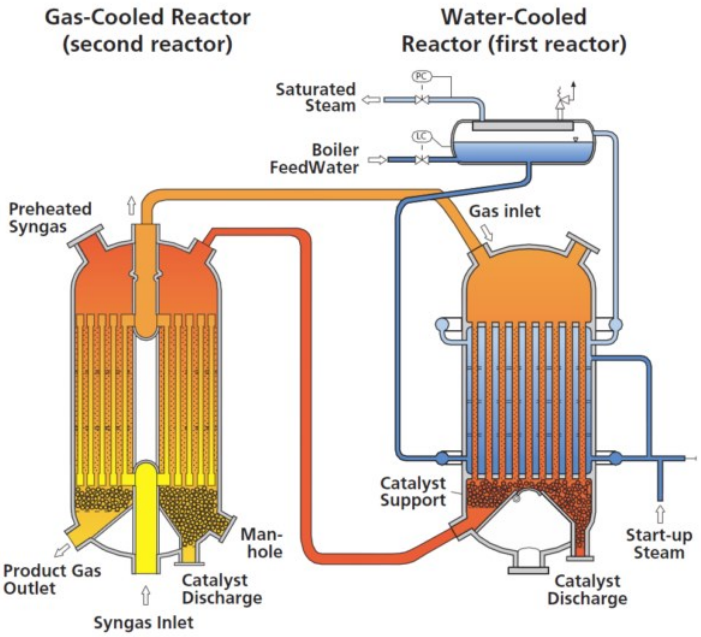

Figure 17. Lurgi MegaMethanol process with two multitubular packed bed reactors. [98]

The syngas enters the first reactor, in which the reaction heat is removed via boiling water, and in the second reactor the cold syngas is counter-currently warmed with the partly converted syngas. Since the methanol synthesis in these conditions is mainly equilibrium limited, the methanol concentration can be increased over the reactor length due to the thermodynamic equilibrium favouring colder temperatures. [98]

Modelling calculations for packed bed reactors can be simplified by making the following assumptions: Generally, radial gradients in concentration, temperature and reaction rates are neglected and assumption is made that the concentration varies continuously in the axial direction, assuming plug flow through the reactor. For heterogeneous catalyst packed bed reactors the reaction rate, the amount of moles of *i* reacting per mass of the catalyst, m_{cat} is: [30]

$$-r'_i = \frac{d\dot{n}_i}{dm_{cat}} \left[\frac{mol\ i}{s * g_{catalyst}}\right] \quad (28)$$

Where $\dot{n}_i$ the flow of reactant *i* ($\frac{mol}{s}$)

m_{cat} the mass of the catalyst (g)

The packed bed reactor design equation used to calculate the catalyst mass needed for a certain conversion is:

$$m_{cat} = \dot{n}_{i,o} \int_0^X \frac{dX_i}{-r'_i} \quad (29)$$

There are numerous detailed modelling studies in literature for packed bed reactors in conventional methanol synthesis. They have generally been modelled as pseudo-homogeneous or heterogeneous systems in one- or two dimensions. [70] In a pseudo-homogeneous model the gas and solid phase are considered a single entity with averaged properties. In the more complex heterogeneous model, the heat and mass transfer is accounted both between the gas and particles and within the particles. Rezaie et al. [99] developed one-dimensional homogeneous and heterogeneous models for methanol synthesis in a Lurgi-type multitubular packed bed reactor with water cooling in the shell-side. The model accounts for accumulation, convection, heat loss of coolant and transport to the solid phase, but neglects the axial dispersion. The molar balance for the solid phase (catalyst) is: [100]

Moles of accumulation on solid surface = moles of diffusion onto solid surface + moles of change due to surface reaction

$$\varepsilon_s c_t \frac{\partial y_{i,s}}{\partial t} = k_{gi}(y_i - y_{is}) + \eta r_i' \rho_B a \quad (30)$$

The solid phase energy balance is:

Heat accumulated on solid surface = heat convection on solid surface + heat generated by reactions

$$\rho_B C p_s \frac{\partial T_s}{\partial t} = a_v h_f (T - T_s) + \rho_B a \sum_{i=1}^{N} \eta r_i' \left(-\Delta H_{f,i}\right) \quad (31)$$

The fluid phase (gas) molar balance is:

Total moles = difference between inlet and outlet moles + moles diffusing from solid phase

$$\varepsilon_B c_t \frac{\partial y_i}{\partial t} = \frac{\dot{n}_t}{A_c} \frac{\partial y_i}{\partial z} + a_v c_t k_{gi}(y_{is} - y_i) \quad (32)$$

The fluid phase energy balance is:

Heat in fluid phase = difference between heat in inlet and outlet + heat convection from solid to liquid + heat transfer from coolant fluid

$$\varepsilon_B c_t Cp_g \frac{\partial T}{\partial t} = \frac{\dot{n}_t}{A_c} Cp_g \frac{\partial T}{\partial z} + a_v h_f (T_s - T) + \frac{\pi D_i}{A_c} U_{shell} (T_{shell} - T) \quad (33)$$

Where

ε_x	void fraction when x = B of catalytic bed, when x = s of catalyst
c_t	total concentration ($\frac{mol}{m^3}$)
y_{is}	mol fraction of component *i* in solid phase
y_i	mol fraction of component *i* in fluid phase
Cp_x	specific heat when x = s of solid, when x = g of gas ($\frac{J}{molK}$)
K_{gi}	mass transfer coefficient for *i* ($\frac{m}{s}$)
η	catalyst effectiveness factor
r_i'	rate of reaction for reactions (3), (4) or (5) ($\frac{mol}{kg_{cat}s}$)
ρ_x	density when x = B of catalytic bed, when x = s of catalyst ($\frac{kg}{m^3}$)
a	activity of catalyst
a_v	specific surface area of catalyst pellet ($\frac{m^2}{m^3}$)
A_c	cross sectional area of each tube (m^2)
$\Delta H_{f,i}$	enthalpy of formation for component i ($\frac{J}{mol}$)
$\dot{n}_t$	total molar flow per tube ($\frac{mol}{s}$)
h_f	gas-solid heat transfer coefficient ($\frac{W}{m^2K}$)
U_{shell}	overall heat transfer coefficient between coolant and process streams ($\frac{W}{m^2K}$)
T	temperature of bulk gas phase (K)
T_x	temperature when x = s of solid, when x = shell of coolant (K)

In the Rezaie et al. study the gas-solid mass transfer coefficients for the components and the overall heat transfer coefficient were estimated from correlations found in literature. Rezaie et al. concluded in the study that the behaviour of the gas phase is very close to the corresponding solid phase behaviour under industrial conditions,

thus a simpler homogeneous model yielded equally satisfactory results, and showed good agreement with historical process data.

Graaf et al. [60] proved that commercial Cu/Zn/Al catalysts exhibit intra-particle mass transfer limitations. For accurate modelling of methanol synthesis, these limitations should be taken into account (like the Rezaie et al. heterogeneous model does). The internal effectiveness factor (ranging from 0 to 1 for isothermal particles) measures how effectively the catalyst is being used. It compares the actual production rate to the absence of internal diffusional resistances. If diffusion is arbitrarily fast, the concentration would be equal to the surface concentration in the whole in the catalyst particle. [30] Graaf et al. [60] developed a dusty gas model for methanol synthesis that describes the intra-particle mass transfer limitations of a Cu/Zn/Al catalyst, and it has been used in several modelling studies, including the Rezaie et al. study. However, Lommerts et al. [61] concluded in a mass transport limitation study, which compared several models for methanol synthesis, that simpler models predict the pore diffusion in catalyst particles equally well. Therefore, the study suggested a simple Thiele modulus approach with linearized pseudo-first-order kinetics for the effectiveness factor calculation. The Thiele modulus is defined for the reaction products MeOH and CO as: [61]

$$\phi_{M,i} = \frac{r_p}{3}\sqrt{\frac{k_i^*\left(K_i^{eq*}+1\right)}{D_{e,i}K_i^{eq*}}} \tag{34}$$

Where k_i^* pseudo-first-order rate constant for *i*= MeOH, CO

K_i^{eq*} pseudo-equilibrium constant for *i*= MeOH, CO

$D_{e,i}$ effective diffusion coefficient of component *i* in the pellet ($\frac{m}{s}$)

r_p catalyst pellet radius (m)

Since the products have the lowest diffusion coefficients, only MeOH and CO are used to calculate the Thiele modulus. [61]

The linearized methanol rates required to achieve the rate constants are as follows: [101]

$$r_i^* = k^*{}_i \left(c_{H_2} - \frac{c_i}{K_i^{eq*}} \right) \tag{35}$$

Where c_i concentration $(\frac{mol}{m^3})$ i = MeOH, CO

The pseudo-equilibrium constants for the products are defined as: [101]

$$K_i^{eq*} = \left(\frac{c_i}{c_{H_2}} \right)_{eq} \tag{36}$$

The equilibrium constants are pseudo-constants because they not only depend on temperature, but also pressure and composition. [61] The pseudo-first-order rates are calculated using the real kinetic rate expressions r'.

The effectiveness factor can be calculated from the Thiele modulus: [61]

$$\eta_i = \frac{1}{\phi_{M,i}} \frac{\left(3\phi_{M,i} \coth\left(3\phi_{M,i}\right) - 1\right)}{3\phi_{M,i}} \tag{37}$$

Modelling programs have to solve heat and mass balances iteratively. The use of the relatively simple Thiele modulus approach for the effectiveness factor helps with modelling the otherwise complex system.

The pressure drop is the mechanical energy loss due to the friction between gas (reaction gas) and solid phases (catalyst). The Ergun equation (38) describes the pressure drop in a packed bed of spherical particles and can be described as a function of the radius of the packing (catalyst particle), void fraction of the packed bed, superficial mass velocity and gas density. The Ergun equation shows that the smaller the catalyst particle size, the larger the pressure drop is. Moreover, the bigger the L/D ratio of the reactor, the larger the pressure drop is. [30]

$$\Delta P = L\frac{G}{\rho d_p}\left(\frac{1-\varepsilon_B}{{\varepsilon_B}^3}\right)\left(\frac{150(1-\varepsilon_B)\mu}{d_p} + 1.75G\right) \quad (38)$$

Where μ fluid viscosity ($\frac{kg}{m*s}$)

G superficial mass velocity ($\frac{m}{s}$)

d_p diameter of catalyst particle (m)

L length of the reactor (m)

The chaotic character of a packed bed leads to non-uniform access of reactants to the catalytic surface and non-optimal local process conditions [102]. Packed bed reactors can suffer from flow maldistributions, which originate from the looser packing of particles near reactor walls. Hence, the reacting fluid bypasses the core of the bed. These maldistributions furthermore lead to limitations in the precision in scale-up and modelling of packed bed reactors [102]. Packed bed reactors are especially unsuitable for highly endothermic or exothermic reactions, where intraparticle temperature gradients become significant, causing hot-spots [103]. Transport resistances and pressure drops can be somewhat alleviated by using packings such as Raschig rings, which increases the void fractions. However the packing nature is still random, and therefore heat and mass transfer resistances are hard to control. [103]

Despite the heat and mass transfer limitations, packed bed reactors are still the most widely used gas-solid catalytic reactor configuration. They are simple to construct and they are practical to operate. For instance, the replacement of catalyst in cases of deactivation is simpler compared to some other reactors (e.g. reactors with coated catalyst structures). [103]

4.2 Stirred tank reactors

Stirred tank reactors (STR) are reactors most often applied for liquid phase homogeneous catalytic reactions, and they can be operated in batch mode or continuously (continuous stirred tank reactor, CSTR) [104]. A batch stirred tank reactor is the simplest of all reactor types and it is the workhorse of the speciality and fine chemical industries [105].

Stirring is used to mix the reagents initially, to maintain homogeneity during the reaction and to enhance the heat transfer at a jacket wall or internal surfaces. Consequently, stirred tank reactors are employed for highly exothermic reactions and processes that require good mass transfer. The prediction of the performance of the reactor mostly depends on the extent how complete the mixing is. [97] An ideal continuous stirred tank reactor (CSTR) is operated at steady state and is assumed to be perfectly mixed, hence there are no spatial variations in the reactor. This means that there is no time dependence or position dependence of the temperature, the concentration or the reaction rate inside the CSTR. Therefore, every variable is the same at every point inside the reactor, and the temperature and concentration in the exit stream are assumed to be the same as those inside the reactor.
The CSTR balance equation can be calculated with the conversion, X_i: [30]

$$V = \frac{\dot{n}_{i,0} X_i}{(-r_i)_{exit}} \tag{39}$$

This is the volume V necessary to achieve a specified conversion X_i.

Ideal mixing is valid if the residence time is 5 – 10 times the mixing time, which is the length of time needed to achieve homogeneity of a mixture of several inputs. There have been several studies on mixing times, but no generalizations have been deduced, because it depends on the geometry and the speed and the power of the agitator. Choi et al. [106] studied how well an agitator mixes a tank by predicting residence time distributions (RTD) by computational fluid dynamics (CFD), and an illustration of the findings can be seen in Figure 18.

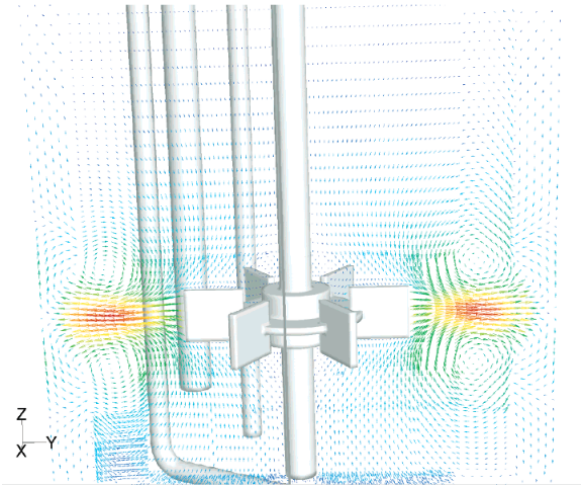

Figure 18. Velocity vector profile for turbulent flow in a 1.4 dm^3 stirred tank, operating at 40 $\frac{cm^3}{min}$ feed flow rate and a mixer speed of 80 rpm. The blue colour represents the slowest velocity (0.01 - 0.1 $\frac{m}{s}$) and the red colour represents the highest velocity (0.7 $\frac{m}{s}$). [106]

The picture shows that the fluid near the impeller is having a much higher velocity, and that some other parts have orders of magnitude slower velocity, which leads to so called “dead volume” and as a result the fluid will pass the reactor more quickly. Choi et al. [106] found that increasing the impeller speed caused the mean and variance of the residence time distribution (RTD) to approach ideal values. The mixing intensity in reality is highly non-uniform, meaning that conditions for effective mixing exist only around the tip of the stirrer [107].

Since continuous stirred tank reactors are rarely employed for gas-solid reactions, only a few heterogeneous methanol synthesis studies are available. However, a number of kinetic studies for methanol synthesis are performed with gradientless recycling reactors, such as a Berty or Carberry reactor. Berty reactors differ from common batch reactors by instead of having a mechanical stirrer a blower recycling the flow to the fixed catalyst basket. [108] Berty reactors are a common gas phase catalyst research tool, and for example Graaf et al. [59] carried out experiments for kinetic modelling in gradientless spinning basket reactors. Moreover, von Wedel et al. [109] performed kinetic studies for methanol synthesis in the slurry phase with a gradientless autoclave. Raudaskoski et al. [31] performed catalyst testing for the CO_2 hydrogenation reaction in a 50 ml stirred tank autoclave with a static catalyst basket.

4.3 Coated catalytic reactors

The process intensification potential of coated reactors has recently gained attention because the local decentralized production of renewable fuels is currently the subject of worldwide research efforts. Especially, catalytic processes involving highly exothermic/endothermic reactions, where large temperature gradients must be avoided to control selectivity or catalyst deactivation, benefit from coated catalysts. Coated catalysts have the potential to be a step forward in enabling efficient small-scale methanol synthesis.

Catalytic reactors can be divided into random and structured reactors based on the procedure how the catalysts are arranged: In an arranged or "random" manner. Coated catalyst reactors are reactors that differ from PB and CSTR reactors by having the catalyst in the form of a porous layer on the walls or the structured passages. Structured reactors like coated reactors could have many advantageous qualities compared to conventional randomly packed reactors: The prevailing heat transfer mechanism may be shifted from convective to conductive, improving the heat transfer coefficients and offering the possibility to adopt more compact reactor designs. Moreover, a higher catalyst specific surface area ensures better mass transfer. In addition, coated reactors typically have smaller pressure drops and less intraporous mass transfer limitations (due to shorter diffusion lengths) than packed beds, which means that they can be operated with limited hot-spots and recycle ratios. [95]

There are essentially two types of coated catalytic reactor types, specifically microchannel and monolithic reactors. [102] These two reactor types are further explained in the following sections.

4.3.1 Monolithic reactors

Monoliths have a compelling use case in the abatement of NOx and CO emissions in cars, and in fact over a billion small monolithic reactors are moving on the roads at present [102]. Recently, other applications in the chemical industry have appeared, such as monoliths used for hydrogenation and oxygenation reactions [88].

Monolithic reactors are filled with monoliths that have catalytic material deposited in the channels of an inert monolithic, ceramic or metallic support. The cross-sections are usually circular, square or triangular in shape. Figure 19 illustrates a shell and tube reactor filled with square channel monoliths.

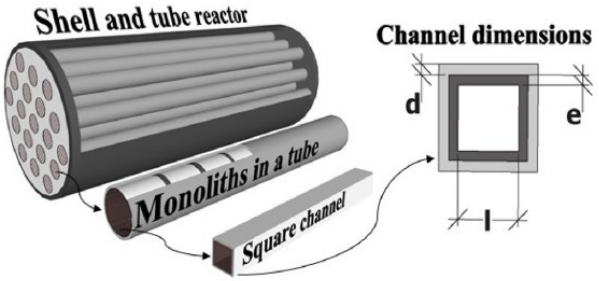

Figure 19. Monolithic reactor. [110]

These catalytic reactors are superior in terms of having high surface areas (improving on mass transfer) without compromise from a high pressure drop, especially at higher GHSV conditions. The pressure drop can be up to 2 to 3 orders of magnitude smaller than with packed beds. [103] The void fraction, the ratio of the sum of the free volume to the overall volume, in monolithic reactors can vary from 0.7 to 0.9, compared to 0.5 for packed beds. The regular structure helps prevent mal-distribution effects and the occurrence of hot spots. This regular structure also makes the scale-up of the reactor more predictable than with conventional reactors because the individual channels are scale invariant. [102]

The most common form of monolith, the square channel cross-sectional monolith, can be geometrically defined by the following parameters: the channel size (d_h) and either wall thickness (d_w) or cell density (which is the number of cells per area). The channel size and shape affects the pressure drop across the channel. Moreover, with coated catalysts the wash coat thickness (d_c) is essential. This affects the catalyst internal effectiveness factor. From these parameters all other parameters used to characterize the monolith structure can be calculated, like the open front area (OFA), geometric surface area (GSA) and hydraulic diameter (d_h). [89] The pressure drop along the channel length in monolithic and microchannel reactors can be described by the following correlation:

$$\Delta P = 2 f_f \frac{\mu L}{d_h^2} u_s \qquad (40)$$

Where f_f Fanning friction factor being 16.00, 15.05, 14.23 and 13.33 for circular, hexagonal, square and triangular monolith channel geometries respectively

L length of the channel (m)

d_h hydraulic diameter (m)

u_s superficial fluid velocity ($\frac{m}{s}$)

Methanol production from syngas in monoliths was first studied by Phan et al. [111]. Metallic monoliths were coated with $CuO/ZnO/Al_2O_3$ by different preparation methods. Metallic monoliths are especially interesting for the exothermic methanol synthesis due to the excellent heat transfer properties. Figure 20 shows the conversion of CO in a slurry coated monolithic reactor as a function of the contact time.

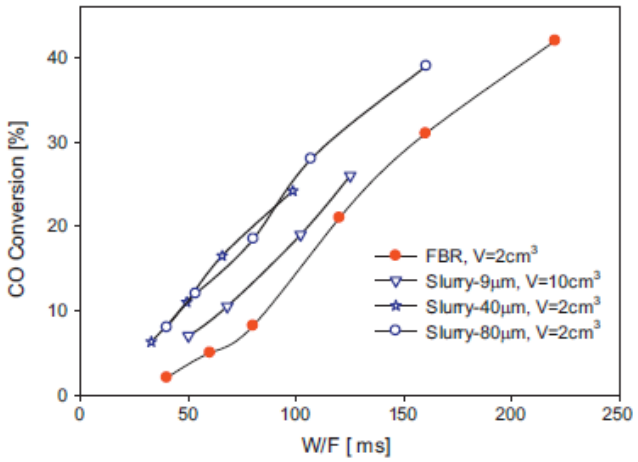

Figure 20. Comparison between monoliths with slurry coatings of 9, 40 and 80 µm thickness, and catalyst powder (FBR) as a function of contact time $\frac{W}{F}$ ($\frac{g_{cat} ms}{cm^3}$). T_{peak} = 255 °C and P = 80 bar. V is the reactor volume. [111]

Slurry coatings offered best performance of all the tested preparation methods. It was found that the thickest tested coating was the most active. All of the slurry coated monoliths had better results in terms catalyst activity than the laboratory-scale fixed bed reactor containing catalyst particles of similar composition and

structure. The better performance was attributed to the better thermal performance of the monoliths. [111]

Arab et al. [110] conducted a theoretical mass and heat transfer study where the impact of catalyst structure was investigated on large-scale production of methanol from CO_2. The study concluded that at smaller GHSVs of about 10 000 h^{-1} the conventional packed bed reactor configuration offers similar performance at lower costs. However, at higher GHSV of 25 000 h^{-1} the packed bed reactor is penalized by such a high pressure drop that the use of monolithic reactors is more suitable for methanol production. [110]

In another modelling study, Montebelli et al. [86] compared highly conductive honeycomb monoliths and open-cell foam reactors with a commercial packed bed reactor by Lurgi for the conventional syngas to methanol reaction. The simulation shows that full-scale packed bed reactors outperform the structured catalyst reactors. However, when the tube lengths were shorter the structured reactors significantly outperformed the packed bed reactor, and showed nearly constant heat transfer coefficients. This was attributed especially to the flow independent conductive heat transfer mechanism. [86] Thus, structured reactors are particularly appropriate for local, small-scale applications, and could enable small power-to-liquids (PtL) or biomass-to-liquids (BtL) cases.

Despite the several benefits monolithic reactors can offer, there are however some drawbacks, which mainly are: 1) Low radial heat transfer rate for ceramic monoliths, complicating temperature control. 2) Poor heat transfer from the monolith to the internal reactor wall. 3) Potential non-uniform fluid distribution, thus lower reactor effectiveness. 4) Catalyst coating difficulty and catalyst replacement difficulty at large scale. [89]

4.3.2 Microchannel reactors

Microchannel and monolithic reactors are similar in many ways and their benefits are largely similar. However, there are notable differences in the designs. First of all, the channels in microchannel reactors are typically in the sub-millimeter range (10^{-6} – 10^{-3} m), whereas monoliths are typically in the millimeter range. Monoliths are mainly straight channelled, whereas microchannels offer a high degree of freedom for non-regular shapes, such as wavy patterns. The materials in microchannels are

not limited to only metals or ceramics, however they are mostly metallic. [103] The ability to use high conductive materials, such as copper, offers the possibility for the microchannel reactors to operate as effective heat exchangers. The main feature of microchannel reactors is their high surface-to-volume ratio, which is in the range of 10 000 – 50 000 $\frac{m^2}{m^3}$, while conventional reactors have typically 100 $\frac{m^2}{m^3}$. [112] When this is combined with the metallic construction, local temperature elevations are immediately dampened by fast heat transport rates at the macro scale. This means that the reactor can operate at true isothermal conditions. This is good for exothermic reactions, such as the methanol synthesis, because thermodynamic limitations are minimized by effective reaction heat removal. The flows in the microchannels are well in the laminar range, directed and highly symmetric. Furthermore, process parameters such as pressure, temperature, and residence time and flow rate are more easily controlled in small volumes. [113] Figure 21 shows an illustration of a lab-scale microchannel reactor chip for methanol steam reforming.

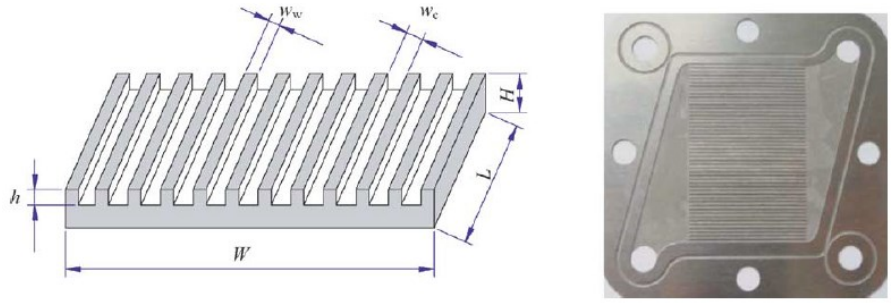

Figure 21. Stainless steel lab-scale microchannel reactor chip. Depth of channel, h, is 0.17 mm, width of channel, w_c, is 0.5 mm and the length, L, is 30 mm. [114]

Microchannel reactors can be randomly packed, however filling the channels with catalyst powder may lead to flow maldistributions and a large pressure drop [115]. Therefore, most research has focused on studying wall-coated microchannels. The geometric surface of the microchannels is often not sufficient for performing reactions efficiently, therefore the surface area is increased in pre-treatment by for example creating a porous layer of alumina by oxidising aluminium alloy [112].

The main technique of introducing microstructures in for example stainless steel platelets is by wet chemical etching [116]. Other techniques include micromilling,

laser micromachining and microelectro discharge machining. Wet chemical etching is fast, economical and is available industrially for most alloys [84]. After the channels are coated with the catalyst, the individual plates are bonded together to form the fluid passages. The assembly of microchannel plates is still complicated and costly, and is one of the main drawbacks of the technology. [116]

Generally, microchannel reactors are a useful tool for catalyst development, since new catalyst formulations can be tested with minimal catalyst amounts. [117]Coated microchannel reactors are for example widely used in testing the endothermic steam reforming of methanol. These reactors are a promising candidate for portable electronics. [113] There are various studies on the production of hydrogen from methanol and the results have been promising. However, for methanol production there are no public studies available.

The challenges of operating a microchannel reactor (and monolithic reactor) are related to ensuring that uniform flow occurs at the inlet of each channel. This directly affects the residence time distribution (RTD), and therefore also temperature evolution and product selectivity. Trouble with microchannel reactors arises from catalyst deactivation. Coke formation on the catalyst can block the channels. Furthermore, the whole unit needs to be replaced if the catalyst is deactivated, which leads to significant down-times and expenses. Consequently, operating conditions that minimizes the catalyst replacement frequency for microchannel and monolithic reactors must be chosen. However, this might not be the optimum reaction conditions. [103]

5 Industrial status and challenges of CO_2 hydrogenation to methanol

The first commercial CO_2 to methanol plant was established in Iceland in late 2011 by Carbon Recycling International (CRI). It produces around 4000 tonnes of renewable methanol per year. It is named the “George Olah Renewable Methanol Plant” and is shown in Figure 22.

Figure 22. Carbon Recycling International (CRI) methanol plant in Svartsengi, Iceland. [118]

It uses locally available cheap geothermal energy (hot water and steam) to produce hydrogen by water electrolysis. This is a method for Iceland to exploit and export its cheap and clean electrical energy. [9] The CO_2 is similarly from geothermal sources, and the approximately 10 % CO_2 is first separated and purified from any sulphur compounds [118]. The renewable methanol has the brand name Vulcanol and is for example blended with gasoline, and exports to other European countries have been planned. Recently CRI signed a long term agreement to deliver Vulcanol to Perstorp [119]. Plans for several bigger plants in Iceland have been prepared as well [118].

Besides the Icelandic plant, there are not many other concrete projects using CO_2 for methanol production. In the 1990's, a CO_2 to methanol pilot plant operated in Japan, producing 50 kg/h at 250 ^oC and 50 bar conditions using a SiO_2 modified Cu/ZnO catalyst [6]. More recently, Mitsui Chemicals built another pilot plant in Japan with a capacity of 100 tonnes per year. The project's aim was to collect design data necessary for a full-scale manufacturing plant. However, no further public information is available of the project since the announcement of the pilot plant in 2008. [120] [6]

The most mature and scalable method of producing renewable methanol from CO_2 is by using water electrolysis for H_2 production and heterogeneous catalytic transformation of CO_2 and H_2. Figure 23 shows one possible process scheme.

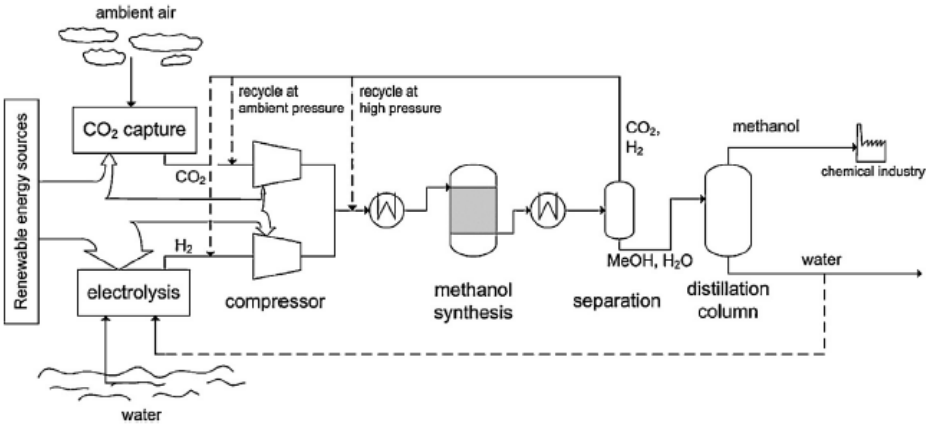

Figure 23. Process scheme for air captured CO_2 and electrically generated H_2 synthesis to renewable methanol. [47]

Areas with the highest energy consumption do not always coincide with areas with the highest resources of renewable energy. In such unbalanced situations decentralized transformation of excess renewable electricity into H_2 and subsequently to methanol may be an efficient and viable renewable energy path. The primary challenge for wider use seems to be the availability and price of CO_2 and renewable H_2. The renewably produced electricity for the production of H_2 is currently too expensive in most locations. [121] Therefore, the first commercial plant was established in Iceland, with nearly free electricity. Also, using the off-peak capacity from nuclear power plants to produce hydrogen and subsequently methanol is techno-economically attractive.

There are still several challenges, besides the cost of renewable energy, to overcome before methanol from CO_2 becomes techno-economically viable. The catalysts need to be improved for a pure CO_2 feed, especially because: 1) The CO_2/H_2 feed is a stronger oxidizing agent than the syngas feed, therefore modifying the active state of the catalyst during reaction 2) Water which forms through rWGS, inhibits the catalyst activity. Moreover, centralized production of renewable methanol is a less efficient option. For that reason, small-scale intensified production near the renewable energy source needs to overcome challenges in developing intensified reactors and suitable catalysts. [122]

6 Aim and content of the experimental part

Heterogeneous catalyst testing for CO_2 hydrogenation to methanol in literature has almost exclusively been conducted in tubular packed bed reactors. In the experimental part of this master's thesis CO_2 hydrogenation to methanol was carried out in a laboratory scale autoclave CSTR. The aim of the experimental part was to test and compare the activity of novel Cu-based in-house particulate catalysts to commercial Cu-based particulate catalysts, as well as test the suitability of new formulations of coated mesh catalysts aimed for small-scale intensified reactors. The behaviour and suitability of novel nanocoatings for the CO_2 hydrogenation reaction was evaluated by comparison of performance of different nanocoatings for both particulate and coated mesh catalysts.

Additionally, the performance of the particulate catalysts was evaluated at different process conditions, by varying operating temperature, operating pressure and space velocity. The particulate catalyst results were compared to the latest studies found in literature. Moreover, the results were compared to results obtained by simulation of two widely used kinetic models. The suitability of the kinetic models was evaluated based on the accuracy of the fit to the experimental results in this work. Finally, the ideality of the reactor was evaluated applying a tracer step change experiment for the determination of the residence time distribution.

7 Materials and research methods

This chapter introduces the experimental setup, how the experiments were executed, as well as analysis and calculation methods of the results.

7.1 Experimental setup

The experiments were carried out at the VTT Technical Research Center of Finland Oy. The experiments were conducted in a laboratory scale 0.2 dm^3 high pressure continuously operated stirred tank reactor. The PI diagram of the experimental setup is presented in Figure 24 and a picture of the reactor can be found in Appendix 1.

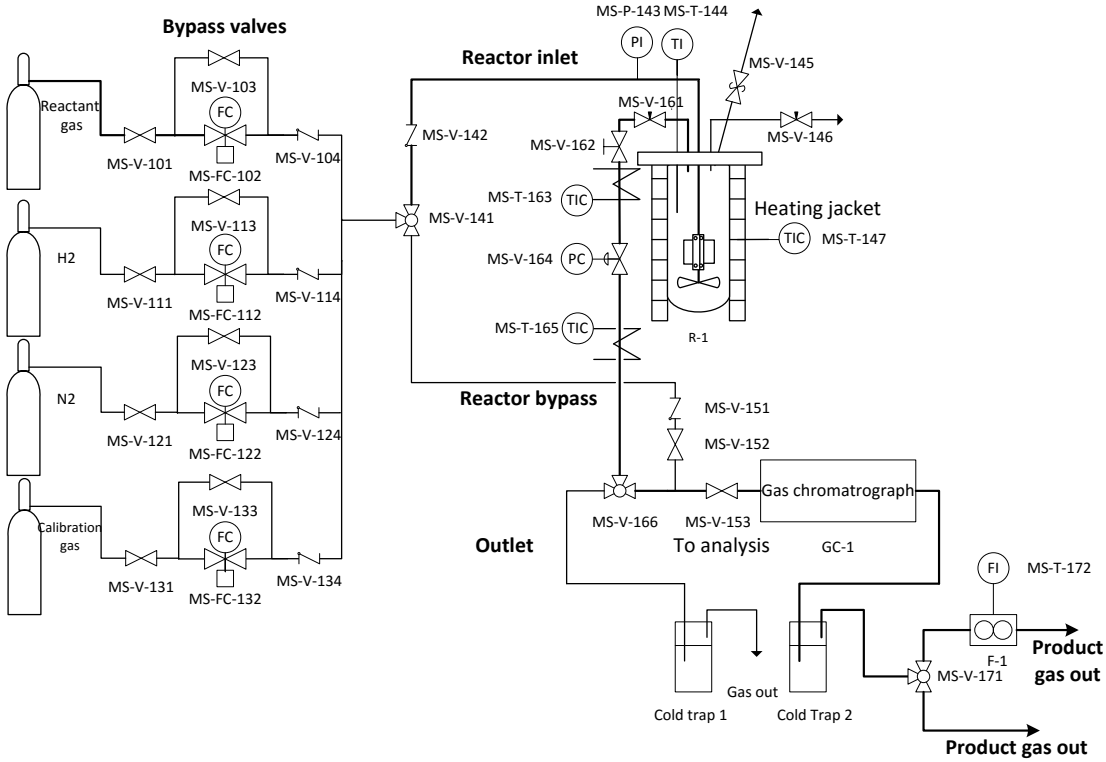

Figure 24. PI-diagram of the CO_2 hydrogenation to methanol experimental setup.

Reactant gases were pre-mixed in a gas bottle in stoichiometric ratio (3:1 for H_2 and CO_2 respectively) along with 5 vol-% of nitrogen that was used as internal standard for GC analyses to calculate the results. The reactant gas bottle and the calibration gas bottle were analyzed and certified by AGA AB. The analysis results of the bottles are provided in Appendix 2 Table 1. The hydrogen was of 99.999 % purity used in catalyst reductions, and the nitrogen bottle was of 99.999 % purity also only used in reductions.

The flow rate to the reactor was controlled with thermal mass flow meters by Bronkhorst (MS-FC-102, MS-FC-112, MS-FC-122 and MS-FC-132) through the gas flow control terminal. The mass flow controllers were calibrated before the experiments with corresponding gases to ensure accurate flow rate. Descriptions of the mass flow meters are available in Appendix 2 Table 3. All the other valves in the system were manual valves. The reactor could be pressurized or flushed with the help of the bypass valves (MS-V-103 MS-V-113 MS-V-123 MS-V-133). The three-way ball valve MS-V-141 controlled the access to either the reactor or bypass. The valve was set to bypass when reacting gases or calibration gases were analyzed. The reactor pressure was controlled with MS-V-164, a manual Tescom 26-1716 backpressure valve, rated at a maximum pressure of 800 PSI (55.16 bar). The

pressure in the system was measured with the pressure gauge MS-P-143, placed in the reactor inlet.

The outlet reactor gases could be directed with three way gate valve MS-V-166 to either the outlet or analysis (GC-1). The analyzed gas flow was furthermore directed with MS-V-171 to either outlet or to the flow meter (F-1). Although not used in the main calculations of the results, the flowrate of the non-condensable outlet gases were measured with F-1, a Kimmon SK25 dry gas meter.

The reactor was heated with a detachable heating jacket, which involved MS-T-147, a K-type thermocouple measuring the temperature at the outer wall of the reactor vessel. Moreover, a K-type thermocouple, MS-T-144, was located in a 4.7 cm deep metallic pocket accessible from the lid of the reactor. It was assumed to be measuring the inside temperature of the reactor. A temperature control terminal collected the temperature data from both thermocouples. The temperature data from MS-T-147 controlled the heating jacket, and thus by adjusting the outside wall temperature a desired temperature inside the reactor could be achieved. Hence, the reactor was manually operated in effectively isothermal mode.
The lines were for the most part ¼ inch (6.35 mm) in inner diameter. The outlet line of the reactor measured 2.45 m from reactor outlet to gas chromatograph inlet. This line was heated with heating elements in its entirety to prevent condensation of reaction products such as water or methanol before analysis. The pressure side of the line was heated with MS-T-163, a heating element set to a temperature of 220 ^{o}C. The atmospheric side of the line was heated with MS-T-165, set to 220 ^{o}C. Furthermore, the heated lines were thoroughly insulated in order to minimize heat losses.

7.1.1 Autoclave

The reactor was manufactured by Autoclave Engineers, and Figure 25 is a sketch of it.

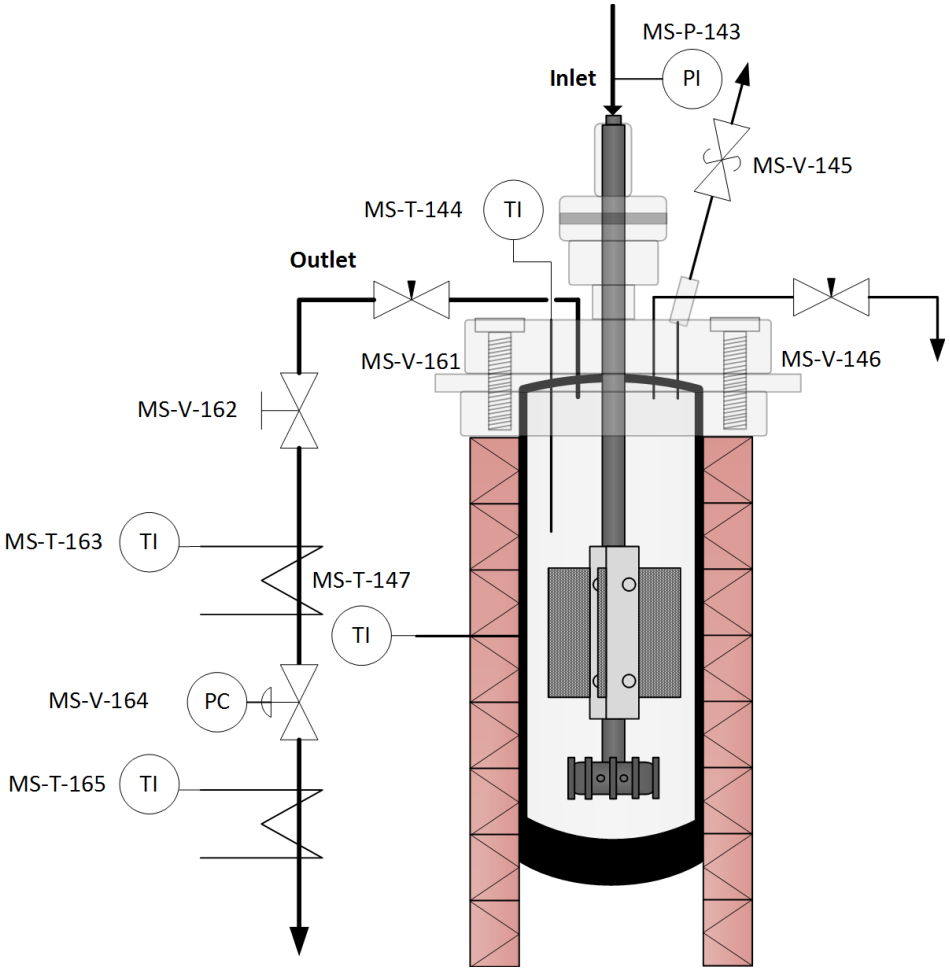

Figure 25. Autoclave CSTR sketch.

A larger version of the sketch, including the dimensions, can be found in Appendix 3. The reactor lid was of bolted closure type and had a Gasche-type metal gasket for an effective metal-to-metal pressure seal. The reactor was rated at pressures up to 372 bar at a maximum of 343 °C, making it suitable for the high pressure methanol synthesis conditions. [108] The reactor vessel had been modified from the standard 0.3 dm^3 configuration to a 0.2 dm^3 configuration.

The reacting gases entered the reactor from the top through a hollow stirrer shaft. The gas entered the reactor through the rotating impeller, which was a Dispersimax turbine shown in Figure 26.

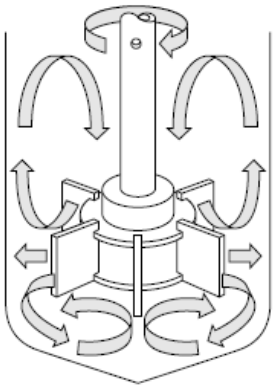

Figure 26. The Dispersimax turbine impeller with a hollow shaft. [108]

This type of impeller is suitable for gas/liquid applications and it provided radial flow and good dispersion as the gas passed through the turbine rotating at high speeds.

The stirrer was operated by a rubber belt drive system connected to an electrical motor that could be manually adjusted for different agitation speeds. The default stirring speed was set to around 400 (max. was around 1000), and the speed was read from the temperature control terminal. Figure 27 shows the catalyst basket or mesh attached to the rotating shaft.

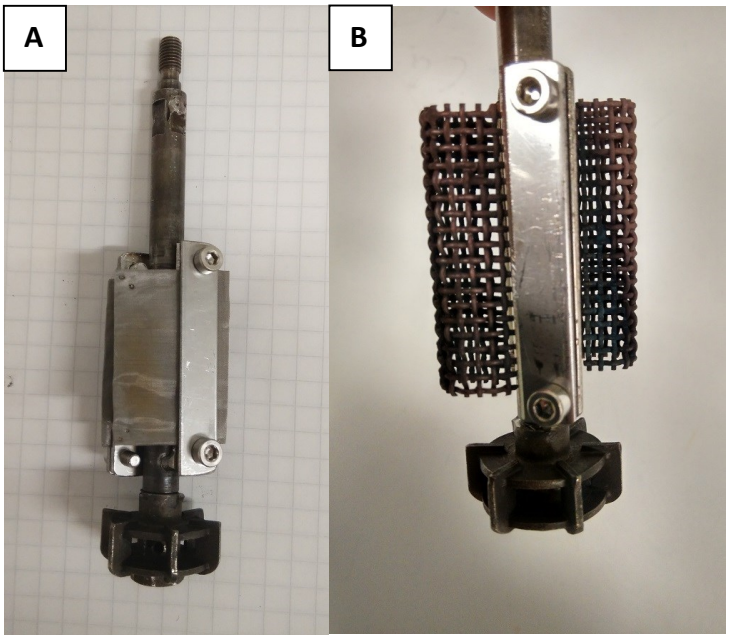

Figure 27. A) Particulate catalyst in a basket attached to the stirrer shaft and B) coated catalyst mesh attached to the stirrer shaft.

The stirrer shaft was modified to include two pairs of metal plates on both sides. In-between the plates a catalyst basket or a metallic web could be attached (in a similar fashion to how a Carberry spinning basket catalyst reactor works [123]). The idea behind attaching the catalyst to the rotating shaft was to maximize the gas-solid(catalyst) mass transfer in the catalyst, and thus facilitate high catalyst activity. The gas entered the reactor under the catalyst from within the turbine, and then rose to the rotating catalyst level, where the CO_2 hydrogenation and rWGS reactions occurred. The gas exited the reactor from the lid, through the needle valve MS-V-161. The reactor lid also had a sampling valve MS-V-146, and a safety valve MS-V-145.

The basket for the particulate catalyst, shown in Figure 27 A), was custom made from 100 µm metallic net. The dimensions of the net were 3.1 x 4.35 cm, and when attached to the metallic plates. The effective dimensions of the volume where the catalyst was located was about 2 x 4.35 cm.

7.2 Product analysis

The product gas was analyzed with an on-line Agilent 6890N gas chromatograph (GC). On-line gas chromatographs offer easy operation and excellent accuracy within the scope of this work. The gas chromatograph was equipped with two detector modules: A thermal conductivity detector (TCD) was used to analyze the non-condensable gases present in the system H_2, N_2, CO and CO_2, and a flame ionization detector (FID) was used to analyze MeOH. The GC working principle is illustrated in Figure 28.

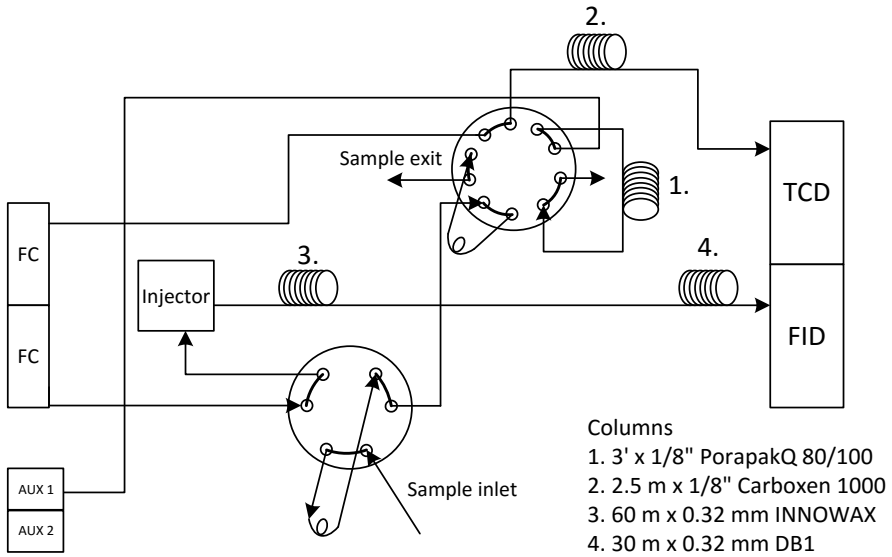

Figure 28. Gas chromatograph internals sketch.

The TCD was connected to a PorapakQ-pre-column and a Carboxen 1000 column. The FID detector had the polar INNOWAX and nonpolar DB1 columns. For the TCD the carrier gas was argon (20 cm^3/min) and for the FID helium (2 cm^3/min). The gas chromatograph oven temperature program was set to 1) 40 ^oC, hold for 3 minutes. 2) rise to 150 ^oC, 10 ^oC/min. 3) 150 ^oC, hold for 0 min. The program lasted in total about 20 minutes.

The gas chromatograph was calibrated for the non-condensable gases (TCD) before each experimental run with the calibration gas bottle provided by AGA. Methanol (FID) was calibrated once by preparing a solution of heptane and methane with known mass fractions and injected into the GC.

7.3 Catalysts

In the experiments tests were carried out with two types of Cu- based catalysts. One was the conventional particulate catalysts inside a metallic basket, and the other was a coated catalyst, where a metallic mesh was covered with the catalyst formulation.

7.3.1 Particulate catalysts

There were two types of particulate catalysts tested: Commercial catalysts which were available on the market, and experimental catalysts or “in-house” catalysts,

that were manufactured specifically for these experiments. Commercial particulate catalysts included Cu-based BASF RP-60 (hereafter named BASF), Süd Chemie G-66MR (hereafter named S-C or Süd Chemie) and different in-house nanocoated formulations of these. The commercial catalysts were chosen based on their suitability for the methanol synthesis as well as availability at the VTT lab. Appendix 2 Table 4 presents the properties of the two commercial catalysts.

The in-house catalysts formulations developed at VTT, hereafter named "49", "61" and "75", and nanocoated versions of these were Cu-based particulate catalysts. The compositions and the preparation of the in-house catalysts is beyond the scope of this work. Furthermore, particulate catalysts developed at the University of Porto engineering faculty (FEUP) in Portugal in a joint research effort to study CO_2 hydrogenation catalysts were also tested. Five different formulations were tested, hereafter named FEUP, FEUP Cu1, FEUP Cu2, FEUP Cu3 and FEUP 44c. They were also Cu-based catalysts. A table with all tested catalysts is available in Appendix 4.

All particulate catalysts were sieved to a particle diameter of 200 – 300 μm, to ensure equal particle sizes. Most catalysts were initially in fine powder form, and as a result had to be pelletized first before crushing and sieving. The pelletization was performed with a manual hydraulic press, which compressed the powder catalyst into brittle pellets that could be ground. The manual pelletization process was time consuming and caused a part of the catalyst being wasted. Therefore, in certain cases too little of the desired particle size catalyst was obtained. Information on which catalysts were first pelletized and catalyst loadings in each run can be found in Appendix 4.

Each VTT in-house catalyst and commercial catalysts was also in-house nanocoated. For the commercial BASF catalyst a total of 7 different nanocoatings formulations was applied for initial screening. The best performing nanocoating was applied to the rest of the catalysts. FEUP catalysts were the only tested catalysts that were not nanocoated.

The amount of catalyst placed in the metallic baskets was weighed and the total amount of catalyst placed in the reactor was fixed in the particulate catalyst activity tests to about 2.09 g, unless there was less catalyst available.

7.3.2 Coated mesh catalysts

The coated mesh catalysts were prepared with different coating materials as support, specifically Al_2O_3 and ZrO_2 and combinations of these. The catalytically active Cu was always nanocoated on the support material along with other species in either nanocoating formulation A, B or C. Table 3 shows the different formulations of the coated mesh catalysts.

Table 3. Coated mesh catalyst formulations.

	Mesh 1	**Mesh 2**	**Mesh 3**
Mesh material	Inconel	Inconel	Inconel
Support	Al_2O_3	ZrO_2	Al_2O_3-ZrO_2
Prepared nanocoating formulations	Blank	Blank	NC-A
	NC-A	NC-A	
	NC-B	NC-B	NC-A (not pre-calcined)
	NC-B	NC-C	
Tested nanocoating formulations	Blank	Blank	NC-A (not pre-calcined)
		NC-A	
		NC-B	

The coated mesh catalysts were pre-calcined before nanocoating at 700 °C for 24 h, and after nanocoating the catalysts were calcined at 350 °C for 1 h in 0.2 dm^3/min air. An exception to this was Mesh 3 NC-A which was neither pre-calcined nor calcined after nanocoating.

Since especially the Al_2O_3 containing coatings were very uneven in mass and colouring, only a part of the coated mesh catalysts were tested. Some uneven coatings included clogged mesh channels, and some had the coating crumbling off, such as the one pictured in Figure 29 B). Results of such coated catalysts would have been meaningless and impossible to compare, and therefore it was decided that the uneven coated mesh catalysts would not be tested and the preparation technique would instead be further developed.

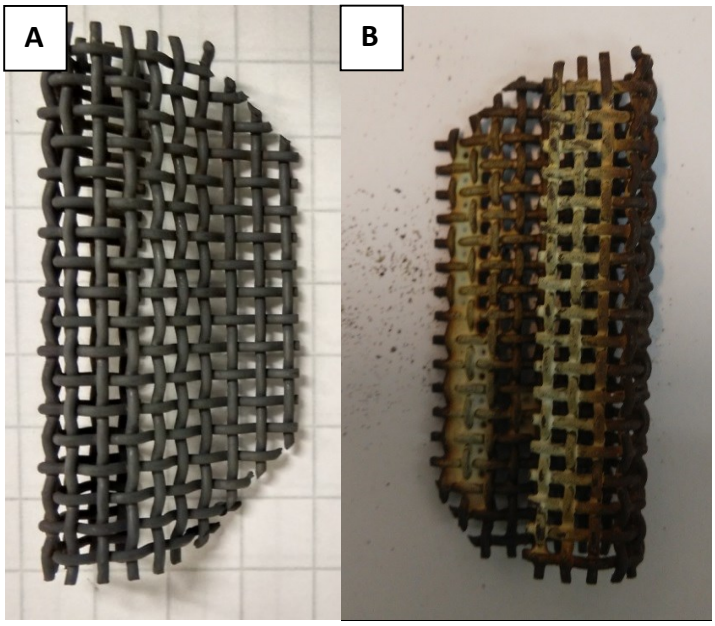

Figure 29. Comparison between A) An even coating, Mesh 2. B) Uneven and crumbling coating, Mesh 1.

Of the coated mesh catalysts that contained catalytically active Cu, 4 of 7 prepared catalysts were tested, Mesh 2 NC-A, NC-B and Mesh 3 NC-A.

7.4 Execution of experiments

There were three different experiments performed. The main experiment compared different particulate and coated mesh Cu-based catalysts at fixed operating conditions. The second experiment included tests performed with the BASF catalyst at different conditions by changing temperature, pressure and flow rate. In the final experiment the reactor ideality/non-ideality was tested in a tracer step change experiment. The conditions for the experiments are presented in Table 4.

Table 4. Conditions for the tests perfromed in this work.

	Catalyst activity comparison (particulate and mesh)		Condition test				Step change experiment
Catalyst	All		BASF RP-60				-
Catalyst particle size (µm)	200 - 300		200 - 300				-
Set T_R (°C)	240		200	220	240	250	240
Set P_R (bar(g))	50		30		50		50
Set WHSV (1/h)	Particulate catalysts: 3.17	Mesh catalyst: Not set	1.58		3.17	6.34	- (0.134 $\frac{dm^3}{min}$ at STP
Set stirrer speed	400 - 430		400				430

As seen in Table 4 the activity test conditions were 240 °C and 50 bar gauge pressure (bar(g)), WHSV of 3.17 1/h and a stirrer speed of 400 – 430. These conditions were used to compare differences in catalytic activities and product distributions. In the condition tests the temperature, pressure and WHSV were varied, and only one type of catalyst was used.

In total the experimental work lasted for 20 weeks of which about 9 weeks was spent on building and testing the system. The reactor system was old and had been used for totally different purposes. The unavailability of mass flow controllers suitable for the high pressure conditions of the experiment caused problems that were discovered during the initial runs of the system. The build-up phase of the reactor included: 1) Cleaning the reactor lid and vessel, changing all the reactor outflow lines and valves with isopropanol and methylene chloride. 2) Assembling the lines, checking for leaks with a hydrogen detector, changing leaking connections, changing gaskets in the reactor and backpressure valve and wrapping the lines in insulation material. 3) Calibrating mass flow controllers, testing operation at 50 bar pressure, changing faulty mass flow controllers. 4) Finding the right line heating temperature. 5) Finding the optimal settings for the stirrer motor for reliable operation.

7.4.1 Reaction experiments

The reaction experiments were performed applying the following steps: 1) The GC was calibrated by taking three samples from the calibration bottle to calibrate H_2,

CO, CO_2 and N_2 gases. The reactant gases were analyzed by taking three samples from the reactant gas bottle. The first sample was ignored and the two similar consecutive samples were used in calculations of the results. 2) When the reactor had been loaded with catalyst by attaching the basket or bed to the stirrer shaft, the reactor was closed with six bolts that were tightened according to manufacturer suggestions in the following manner: 8 Nm, 15 Nm, 20 Nm, 30 Nm and finally 40 Nm. (40 Nm was the maximum allowed torque for the reactor lid). A pressure test was performed with N_2 at 50 bar(g) pressure and held for 1 – 2 minutes. 3) The heating jacket was attached to the reactor and switched on. The stirring was set to a value of 400 – 430 in the terminal, and the stirrer water cooling was switched on. 4) The catalyst was reduced "in situ" with a stream of 50 cm^3/min H_2 and 50 cm^3/min N_2 for 1 h at 250 ^oC and atmospheric pressure. 5) The reactor temperature was set to desired reaction conditions. 6) The reaction experiment was initiated by pressurizing the reactor with reactant gas. The reaction temperature was manually operated to stay roughly at the desired temperature. Samples for GC analysis were taken every 20 – 30 minutes and the reaction was run for 3 – 4 h to ensure that a rough stationary state at the operating conditions was reached. Depending on the sampling interval, either the last 3 or 5 samples were used in calculations of the results. In general, samples used in calculations were taken during the stationary operation within the last 1.5 h of the run. 7) After the reaction experiment, the reactor was flushed with nitrogen and the reactor was cooled to ambient temperature.

A table of all experiments with the measured temperatures, pressures, stirrer speeds as well as catalyst masses and flow rates for each catalyst run can be found in Appendix 4.

7.4.1 Tracer step change experiment

The goal of the experiment was to determine the ideality of the reaction system (CSTR) by injecting an inert "tracer" into the reactor pressurized with N_2 at time 0, and comparing the experimental results of the composition changes over time in the outlet with calculated ideal values. This determines the residence time distribution (RTD). The RTD describes the probabilistic distribution of how long the species spend in the reactor. The RTD of a CSTR tells if the operation is perfect or if there is non-ideal behaviour, such as bypassing or dead volume, where materials either

leave too quickly or stay for too long compared to the ideal residence time, τ. Thus, the tracer experiment is method to diagnose problems in real reactors. [30]
For this experiment the reactor did not have any catalyst loading, and the reactant gases H_2 and CO_2 acted as the inert tracer gases. The reactor was first pressurized to 50 bar(g) with N_2, and the experiment was started with the initiation of reactant gas flow. The flow rate was measured with the flow meter, and the average value of three 15 minute long measurements was used for the calculation of the results.

7.5 Calculation methods

To be able to compare differences in catalyst activities, representative parameters are essential. CO_2 conversion (X_{CO_2}), methanol selectivity (S_{MeOH}) and methanol yield (Y_{MeOH}) and carbon monoxide yield (Y_{CO}) were chosen as parameters to assess the performance of the different catalysts. Furthermore, reaction rates (STY) with respect to catalyst mass were also calculated to compare the catalyst activities.

7.5.1 Thermodynamic calculations

The thermodynamic equilibrium compositions for the methanol synthesis process were calculated with the Aspen Plus V8.6 process simulator using the Gibbs reactor block. The Gibbs reactor minimized the Gibbs free energy of the compounds present in the process (i.e. a ratio of 3:1 for H_2 and CO_2 respectively) to obtain the equilibrium concentrations of the products. The property method was the RKS-MHV2 (Redlich-Kwong-Soave equation of state with modified Huron –Vidal-2 mixing rule), which was a predictive (thus no binary interaction parameters were needed) cubic equation of state model that was suitable for high pressures. This property method could also handle the components that were present in the system, such as H_2. [124] [125]

7.5.2 Analysis calculations

In this study the nitrogen present in the reactant gas acted as an internal standard and was the basis for the results obtained. Since the volumetric composition of the reactant gas was known (coming from an analyzed bottle), reactant *i* molar flow was calculated in the following way:

$$\dot{n}_{i_0} = \frac{\frac{V\%_{i_0} * \dot{v}_o}{100}}{V_m} \quad (41)$$

Where $V\%_i$ volume percentage of component i in reactant

$\dot{v}_o$ reactant total volume flow rate ($\frac{dm^3}{min}$) at STP

V_m molar volume, 0.022414 $\frac{dm^3}{mmol}$ at STP

STP was defined as 273.15 K and 1.01325 bar. The volume flow rate was known from the calibration of the mass flow controllers.

Because the nitrogen was not consumed in the reaction it was assumed that:

$$\dot{n}_{N_{2_0}} = \dot{n}_{N_2} \quad (42)$$

Thus, the amount of nitrogen in the reactor outlet was always known, and by knowing the peak area relationships of the components present in the system to the internal standard N_2, all the outlet component amounts could be calculated.

The response factor for component *i* in the gas chromatograph TCD detector was defined as:

$$RF_i = \frac{\frac{A_i}{V\%_i}}{\frac{A_{N_{2_0}}}{V\%_{N_{2_0}}}} \quad (43)$$

Where A_i average TCD peak area for component *i*, where *i* = H_2, CO_2 or CO.

$A_{N_{2_0}}$ average TCD peak area for N_2

The response factor accounted for differences in TCD detector response between the analyte and standard. [126] The TCD response factor was calculated before each new reaction experiment from the average of the reactant gas sample peak areas for the components H_2 and CO_2. The RF for CO was calculated from the calibration gas samples. Average RF values from all of the experiments were calculated and the results are available in Appendix 2 Table 2.

The molar flows at the outlet were calculated with the following equation:

$$\dot{n}_i = \frac{\left(\frac{A_i}{RF_{H_2}}\right)}{A_{N_2}} * \dot{n}_{N_2} \quad (44)$$

Where A_i average H_2, CO_2 or CO TCD peak area in outlet gas

RF_i average H_2, CO_2 or CO response factor

A_{N_2} average nitrogen TCD peak area in outlet gas

Thus, the TCD detected component molar outflows were calculated, but for obtaining results for methanol, which peak area only showed in the FID detector, the relationship between the detectors was calculated with the help of the calibration gas methane, which showed in both detectors:

$$\frac{FID}{TCD} = \frac{A_{CH_4,FID}}{A_{CH_4,TCD}} \quad (45)$$

Where $A_{CH_4,FID}$ average methane FID peak area

$A_{CH_4,TCD}$ average methane TCD peak area

This gave a link between the peak areas from the two detectors. However, the methanol response factor in relation to methane, $RF_{\frac{MeOH}{CH_4}}$, was also needed. The TCD response factor of MeOH in relation to the TCD response factor of methane was found in literature to be 1.52. [127] The amounts of methane calculated with both the TCD and FID peak areas would need to be equal, and thus a correction factor was experimentally determined by injecting heptane and methanol solution with known concentrations. The correction factor was 1.222, and thus $RF_{\frac{MeOH}{CH_4}}$ was 1.857.

Thus, the methanol molar flow in the outlet was obtained:

$$\dot{n}_{MeOH} = \frac{A_{MeOH}}{\left(\frac{FID}{TCD}\right) * RF_{\frac{MeOH}{CH_4}} * A_{N_2}} * \dot{n}_{N_2} \quad (46)$$

Where A_{MeOH} methanol FID peak area in outlet

A_{N_2} nitrogen peak area in outlet

Neither the TCD nor the FID detected water, a product in both the CO_2 hydrogenation reaction and the rWGS reaction. Therefore, to obtain the molar balance, the molar flow of water was calculated using the stoichiometry of reactions (4) and (5) to obtain:

$$\dot{n}_{H_2O} = \dot{n}_{MeOH} + \dot{n}_{CO} \quad (47)$$

An assumption that the only reaction products formed in the system were MeOH, CO and H_2O was made. The other products that the GC detected were short hydrocarbons, mostly C_2, C_3 and C_4 compounds. However, the combined amounts of these were so small, under 0.1 vol-%, that they were ignored for simplicity of calculations. Moreover, gas bag samples of non-condensable product gases from the run with VTT in-house catalyst 75 were further analyzed in a Micro-GC. The results are presented in Appendix 7. The conclusion of the micro-GC results was that there was neither DME formation nor anything else that the on-line GC could not detect.

There were two methods for calculating the conversion for H_2 and CO_2. The first method was:

$$X_i = \frac{\dot{n}_{i_0} - \dot{n}_i}{\dot{n}_{i_0}} * 100\ [\%] \quad (48)$$

Where $\dot{n}_i$ H_2 or CO_2 outlet gas molar flow rate

The remaining reactants in the outflow were used to calculate the conversion. However, the CO_2 and H_2 GC peak areas between samples proved to be fluctuating more than expected, and therefore the conversion results often did not match with

the amounts of products formed. Especially with catalysts with low conversions or with blank runs the problem became apparent. Blank runs indicated conversions up to 2 %, even though there was neither MeOH nor CO forming. To mitigate this, the conversions were calculated from the yields of the two main products, MeOH and CO:

$$X_i = Y_{MeOH}^i + Y_{CO}^i \ [\%] \tag{49}$$

Where Y_{MeOH}^i yield of methanol calculated from reactant *i*

Y_{CO}^i yield of CO calculated from reactant *i*

In literature often only CO_2 conversions are presented, and in this work the CO_2 conversion was used as the basis for results.

The MeOH yield calculated on the basis of hydrogen could be calculated based on reaction stoichiometry in the following way:

$$Y_{MeOH}^{H_2} = \frac{3\dot{n}_{MeOH}}{\dot{n}_{H_{2_0}}} * 100 \ [\%] \tag{50}$$

The MeOH yield on the basis of CO_2 was calculated:

$$Y_{MeOH}^{CO_2} = \frac{\dot{n}_{MeOH}}{\dot{n}_{CO_{2_0}}} * 100 \ [\%] \tag{51}$$

The CO yield from H_2 was:

$$Y_{CO}^{H_2} = \frac{\dot{n}_{CO}}{\dot{n}_{H_{2_0}}} * 100 \ [\%] \tag{52}$$

And from CO_2:

$$Y_{CO}^{CO_2} = \frac{\dot{n}_{CO}}{\dot{n}_{CO_{2_0}}} * 100 \ [\%] \tag{53}$$

The rWGS reaction consumed H_2 and CO_2 in equal amounts, as opposed to the CO_2 hydrogenation reaction where H_2 consumption was 3 times higher. Consequently, the CO yield from hydrogen was about 3 times lower than the CO yield from CO_2.

The selectivity in generalized form was:

$$S_j^i = \frac{Y_j^i}{X_i} * 100\ [\%] \tag{54}$$

Where Y_j^i yield of product *j* (MeOH or CO) calculated from reactant *i* (H_2 or CO_2).

Space time yield, or the product formation rate $r'_{prod.}$, takes into account the catalyst amount in the catalyst activity evaluation. It was calculated in the following way:

$$STY_i = r'_{prod.} = \frac{\dot{n}_i * 60\frac{min}{h}}{\frac{m_{cat}}{1000}} \quad [\frac{mmol}{g_{cat} * h}] \tag{55}$$

Where $\dot{n}_i$ molar flow in the out gas of product *i* (MeOH or CO)

Since the catalyst bed volume was not measured, the GHSV was not calculated. However, to obtain a parameter that evaluates the reactant flowrate in direct relation to the amount of catalyst in the reactor, the weight hourly space velocity WHSV was defined as:

$$WHSV = \frac{\dot{m}_o * 60\frac{min}{h}}{m_{cat}} \left[\frac{1}{h}\right] \tag{56}$$

Where $\dot{m}_o$ total mass flow of reactants ($\frac{g}{min}$)

m_{cat} catalyst mass (g)

The reactant total mass flow was obtained by:

$$\dot{m}_0 = \sum_{i=1}^{n} \dot{n}_{i_0} * M_i \left[\frac{g}{min}\right] \quad (57)$$

Where M_i molar mass of reactant component i ($\frac{g}{mol}$), for H_2 = 2.02$\frac{g}{mol}$, CO_2 = 44.01 $\frac{g}{mol}$ N_2 = 28.01 $\frac{g}{mol}$

The amount of heat released by the exothermic CO_2 hydrogenation reaction (4) was:

$$\dot{Q}_4 = \Delta H_4(T_r) * \frac{\dot{n}_{MeOH}}{60\frac{s}{min}} \ [W] \quad (58)$$

Where $\Delta H_4(T_r)$ reaction enthalpy of CO_2 hydrogenation at reacting temperature $T_{r,}$ in $\frac{kJ}{mol}$

And the heat absorbed by the endothermic rWGS (5) reaction was:

$$\dot{Q}_5 = \Delta H_5(T_r) * \frac{\dot{n}_{CO}}{60\frac{s}{min}} \ [W] \quad (59)$$

The heats of formation for the reacting species at specific reaction temperatures were estimated in Aspen using the RKS property method. The heats of formations and heats of reaction calculation methods and results at different temperatures and pressures are presented in Appendix 5 in Table 1 and Table 2.

Therefore, the total heat generated/absorbed in the reactor was:

$$\dot{Q}_{tot} = \dot{Q}_4 + \dot{Q}_5 \ [W] \quad (60)$$

7.5.3 Step change calculations

For the step change experiment the ideal tracer concentrations over time was calculated from the reactor balance for comparison with the experimental results.

For an ideal CSTR the average residence time, or space time, was calculated in the following way: [30]

$$\tau = \frac{V_{reactor}}{\dot{v}_o} \ [min] \tag{61}$$

Where $V_{reactor}$ reactor volume (dm^3)

$\dot{v}_o$ volumetric flow rate of inlet ($\frac{dm^3}{min}$)

The CSTR balance for an inert species was: In – Out = Accumulation, since no generation was happening. Therefore, the volume percentage balance was:

$$V_{reactor} \frac{dV\%_i}{dt} = v_i(V\%_{i_o} - V\%_i) \tag{62}$$

Where $v_i = v_{i_o}$ flow rate of inert *i* in both the inlet at and the outlet of the reactor

$V\%_{i_o}$ the volume percentage of inert component *i* in the inlet

$V\%_i$ the volume percentage of inert component *i* in the outlet

The balance was defined with the residence time in the following way:

$$\frac{dV\%_i}{dt} = \frac{1}{\tau}(V\%_{i_o} - V\%_i) \tag{63}$$

Thus, the response to a step tracer was:

$$V\%_i(t) = V\%_{i_o}\left(1 - \exp\left(\frac{-t}{\tau}\right)\right) \ [\text{vol-\%}] \tag{64}$$

The flow rate at STP was obtained from the mass flow controller calibration. The flow rate was corrected to reaction conditions by rearranging the ideal gas formula (with compressibility factor Z):

$$\dot{v}_2 = \frac{P_1 \dot{v}_1 Z_2 T_2}{P_2 Z_1 T_1} \left[\frac{dm^3}{min}\right] \quad (65)$$

Where Z_i gas compressibility factor in conditions i, Z_2 was the compressibility factor for gases at the experimental conditions, obtained from Aspen Plus with the RKS property method by dividing the calculated non-ideal volume of inlet gases divided by the ideal volume of gases. Z_1 was 1, because it was the compressibility factor at STP.

The experimental volumetric concentrations were known by the GC peak areas and the known inlet volumetric concentrations:

$$V\%_i = A_i \frac{V\%_{i_o}}{A_{i_o}} \quad (66)$$

Where i reactant components H_2, CO_2 or N_2

The H_2 and CO_2 known initial peak areas A_{i_o} were obtained from the analysis of the reactant gas. In this case, the A_{i_o} of N_2 was taken from the analysis of the calibration gas bottle for accuracy reasons, since it had a larger concentration of N_2 than the reactant gas.

7.5.4 Kinetic model simulation

The two main kinetic models presented in chapter 3.1.3, the model presented by Graaf et al. (hereafter the Graaf model) and the vanden Bussche and Froment model (hereafter the vanden Bussche model), were implemented in Aspen Plus for calculating the model-based reaction rates. In Aspen, the CSTR block was used for the simulations with the RKS-MHV2 property method.

The kinetic models could not directly be implemented into Aspen, since Aspen only accepts certain types of equations. One of the models is the LHHW model, which consists of a kinetic factor, a driving force expression and an adsorption term: [128]

$$r_i' = \frac{[Kinetic\ factor][Driving\ force]}{[Adsorption\ expression]^m} = k_i * \exp\left(\frac{-E_i}{RT}\right) \frac{\left(K_1\left(\prod c_i^{v_i}\right) - K_2\left(\prod c_j^{v_j}\right)\right)}{\left(\sum K_i\left(\prod c_k^{v_k}\right)\right)^m} \quad (67)$$

Where the K term is expressed in Aspen in the following logarithmic form:

$$\ln(K) = A + \frac{B}{T} \quad (68)$$

Thus, the Graaf model had to be rearranged to fit the built-in Aspen model. Temperatures were expressed in Aspen in Kelvins and pressures in Pascals. Rearranging the equations and units of the original models to Aspen form is a daunting task, luckily already completed and verified by Kiss et al. [128] for the Graaf model:

For CO hydrogenation:

$$r'_{MeOH,3} = a_{MeOH,3} * k_{MeOH,3} * exp\left(\frac{-E_{a,3}}{RT}\right) \frac{K_{CO} f_{CO} f_{H_2} - \frac{K_{CO}}{K_3^{eq}} f_{MeOH} f_{H_2}^{-0.5}}{(adsorption\ expression)} \quad (69)$$

For rWGS:

$$r'_{rWGS,5} = a_5 * k_5 * exp\left(\frac{-E_{a,5}}{RT}\right) \frac{K_{CO_2} f_{CO_2} f_{H_2} - \frac{K_{CO_2}}{K_5^{eq}} f_{H_2O} f_{CO}}{(adsorption\ expression)} \quad (70)$$

For CO_2 hydrogenation:

$$r'_{MeOH,4} = a_4 * k_4 * exp\left(\frac{-E_{a,5}}{RT}\right) \frac{K_{CO_2} f_{CO_2} f_{H_2}^{1.5} - \frac{K_{CO_2}}{K_4^{eq}} f_{H_2O} f_{MeOH} f_{H_2}^{-1.5}}{(adsorption\ expression)} \quad (71)$$

The adsorption term was the same for all three reactions and was expressed in Aspen compatible form as:

$$(adsorption\ expression) = f_{H_2}^{0.5} + \frac{K_{H_2O}}{K_H^{0.5}} f_{H_2O} + K_{CO} f_{CO} f_{H_2}^{0.5} + \frac{K_{CO} K_{H_2O}}{K_H^{0.5}} f_{CO} f_{H_2O} + K_{CO_2} f_{CO_2} f_{H_2}^{0.5} + \frac{K_{CO_2} K_{H_2O}}{K_H^{0.5}} f_{CO_2} f_{H_2O} \quad (72)$$

Where a_i activity of the catalyst in respect to reaction *i*

The reactions were set in Aspen to occur in vapor phase and the reaction rate was based on catalyst weight. Partial pressures were used instead of fugacities for the driving force. The reaction equilibrium constants used were the Graaf et al. [65] correlations. The experimental data used by Kiss et al. [128] for the Aspen unit conversion was the data from An et al. [34] for the highly active fibrous Cu/Zn/Al/Zr catalyst. The values for the expressions are presented in Appendix 6 Table 3 for the kinetic factor, Table 4 for the driving force and Table 5 for the adsorption.
Since the vanden Bussche model already was a LHHW type equation it didn't need to be rearranged. However, since the original model used bar for partial pressures the kinetic constants and the units of equation were changed by Van-Dal et al. [68] to fit the Aspen logarithmic form:

For CO_2 hydrogenation:

$$r'_{MeOH,4} = a_4 \frac{K_1 p_{CO_2} P_{H_2} - K_6 p_{H_2O} p_{MeOH} p_{H_2}^{-2}}{\left(1 + K_2 p_{H_2O} p_{H_2}^{-1} + K_3 p_{H_2}^{0.5} + K_4 p_{H_2O}\right)^3} \quad (73)$$

For rWGS:

$$r'_{rWGS,5} = a_5 \frac{K_5 p_{CO_2} - K_7 p_{H_2O} p_{CO} p_{H_2}^{-1}}{1 + K_2 p_{H_2O} p_{H_2}^{-1} + K_3 p_{H_2}^{0.5} + K_4 p_{H_2O}} \quad (74)$$

The kinetic factor was set to 1 and the parameters were instead included in the driving force. The experimental data for the parameters were from the original vanden Bussche and Froment. However, Van-Dal et al. used the readjusted activation energies by Mignard and Pritchard [129], which represented other

experimental results better, and extended the applicability of the vanden Bussche model up to 75 bar. [130] The parameter values for the vanden Bussche Aspen model are available in Appendix 6 Table 6. Further information on the kinetic models and experimental data used for the parameters is available in Appendix 6 Table 1 and Table 2.

8 Results and discussion

This chapter presents the results from the thermodynamic equilibrium calculations, catalyst comparison tests, condition test as well as the CSTR step change experiment and the kinetic model simulations.

8.1 Thermodynamic equilibrium

Figure 30 A) shows the results for the equilibrium composition as molar-% at different temperatures varied with 5 ^{o}C increments and constant 50 bar pressure. Figure 30 B) shows the equilibrium CO and MeOH yields and the CO_2 conversion.

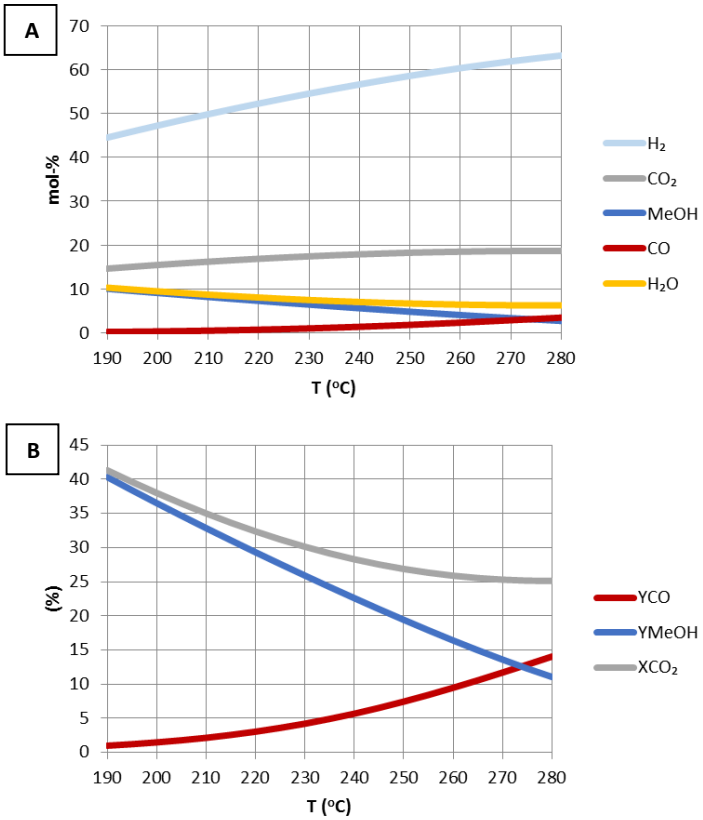

Figure 30. Equilibrium calculations at 50 bar pressure in varying temperatures. A) equilibrium compositions of all components in mol-%. B) Equilibrium MeOH (blue) and CO (red) yields and CO_2 (grey) conversions.

Figure 30 B) shows that the rWGS reaction is favoured at higher temperatures due to its endothermic character. The CO_2 hydrogenation is favoured at lower temperatures. MeOH yield becomes equilibrium limited at higher temperatures, and from an equilibrium perspective the reaction should be carried out at as low temperature as possible.

Figure 31 A) shows the equilibrium composition as molar-% at different pressures varied with 5 bar increments and constant 240 °C temperature. Figure 31 B) presents the equilibrium CO and MeOH yields as well as the CO_2 conversion.

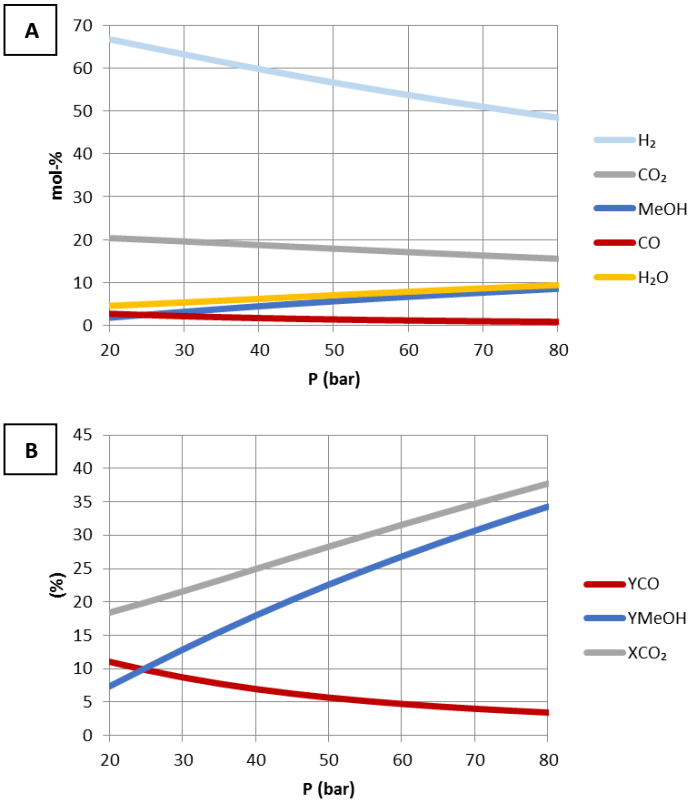

Figure 31. Equilibrium calculations at 240 °C temperature in varying pressures. A) Equilibrium compositions of all components in mol-%. B) Equilibrium MeOH and CO yields and CO_2 conversions.

The yield curves of the products MeOH and CO show that MeOH yield is maximized at high pressures, since the CO_2 hydrogenation reaction favours higher pressures and the rWGS favours lower pressures.

8.2 Catalyst activity

The standard conditions for the catalyst comparison tests were 240 °C and 50 bar(g) pressure and WHSV of 3.17 1/h. The 240 °C temperature was based on literature, where maximum methanol yield for most experiments was achieved at 230 – 240 °C temperatures. [41] [45] Higher pressure according to thermodynamic equilibrium calculations and experimental results from literature indicated a positive effect on methanol yield and selectivity, and therefore the standard pressure in the experiments of this work was set to 50 bar(g), which was close to the maximum allowed pressure of the system.

To verify that the reaction system worked as expected, a blank run was performed in identical conditions to the catalyst activity tests.

The results for the two commercial catalysts and the blank run are presented in Figure 32, in which figure A) displays the conversions (as numbers above the bars) and yields in terms of MeOH and CO. B) shows the STY of MeOH and CO.

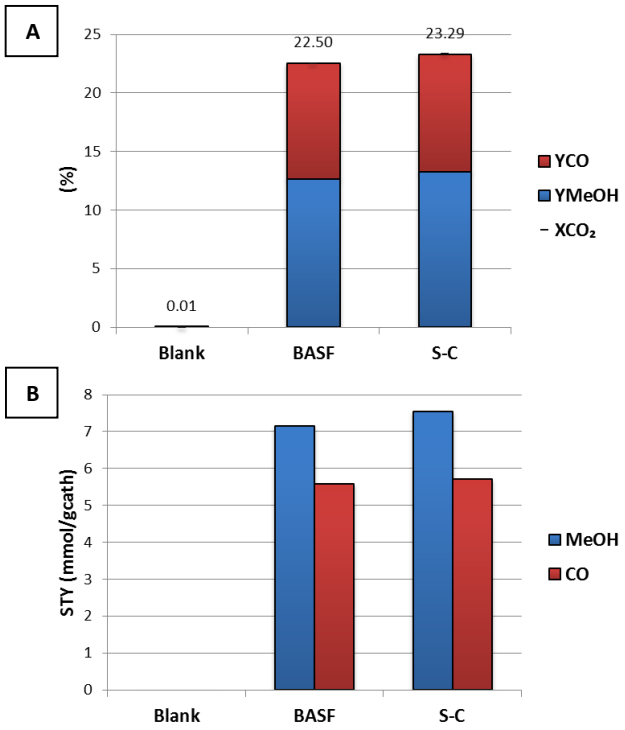

Figure 32. Blank, BASF and Süd Chemie particulate catalyst results at fixed conditions. A) MeOH (blue) and CO (red) yields and CO_2 conversion in %. B) MeOH (blue) and CO (red) space time yield in $(\frac{mmol}{g_{cat}h})$.

There was virtually no MeOH or CO formation in the blank run. This confirms that the system was working properly, and that there were no significant amounts of impurities or catalyst traces in the lines that would have contributed and skewed the results. The difference between the two commercial catalysts was hardly noticeable in terms of conversion of CO_2 and product distribution. Both runs had high CO_2 conversion and high CO yields. The CO formation was in fact higher than the equilibrium CO composition at the reaction conditions. In these conditions, including the 5 vol-% N_2 in the feed, the equilibrium CO yield is about 6 %, which is significantly less than the experimental results of around 10 %. This indicates that equilibrium in the system was not fully reached. The fact that the rWGS is very fast

contributes to this, since there are no significant kinetic limitations hindering the reaction, like with the CO_2 hydrogenation. [128] Solely looking at the rWGS equilibrium, shows the following CO yields at 50 bar pressure:

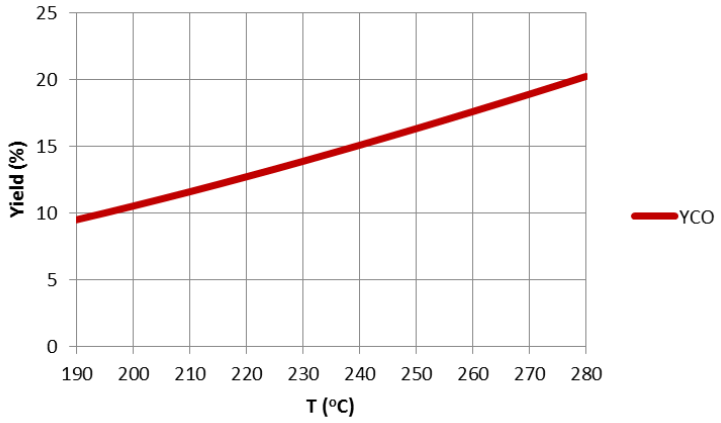

Figure 33. rWGS equilibrium CO yield at varying temperatures and 50 bar for a reactant gas composition of $\frac{H_2}{CO_2} = 3$.

Figure 33 displays that the equilibrium yields for CO is significantly higher when only rWGS is considered for equilibrium calculations. This shows why systems, which are not in equilibrium, can have experimental CO yields higher than the equilibrium calculations with all involved reactions would indicate.

The molar balance for the BASF experiment is shown in Appendix 8 Table 1, and the elemental balance is shown in Appendix 8 Table 2. The elemental balance shows excellent agreement, with only a few percentage point deviations between the inlet and outlet molar amounts. The outlet compositions as well as the elemental balances for all experimental runs are available in Appendix 8 Table 3.

The complete results for the blank, BASF and S-C runs are presented in Table 5. The reaction heat was about -0.15 W for BASF and for S-C -0.16 W, meaning that only a small amount of heat was released. Thus, there were mostly likely no significant temperature gradients inside the reactor caused by the reactions. This finding also supports the assumption of isothermal operation inside the reactor, since the CO_2 hydrogenation and rWGS reaction heats effectively canceled each other out.

Table 5. Results for the blank, BASF and Süd Chemie particulate catalysts at fixed conditions of 240 °C, 50 bar(g) and WHSV 3.17 1/h.

Catalyst	WHSV (h^{-1})	T.o.S. (min)	X_{CO_2} (%)	S_{MeOH} (%)	$Y_i^{CO_2}$ (%)		STY_i ($\frac{mmol}{g_{cat}h}$)		$\dot{Q}$ (W)
					MeOH	CO	MeOH	CO	
Blank	-	223	0.0	100.0	0.0	0.0	-	-	0
BASF	3.17	224	22.5	56.1	12.6	9.9	7.1	5.6	-0.15
S-C	3.19	237	23.3	56.9	13.3	10.0	7.5	5.7	-0.16

Figure 34 illustrates how the reactant conversion and product formation evolved over the course of the run for both commercial catalysts. The reaction was calculated to start when the reactor was pressurized to reaction pressure with reactant gas.

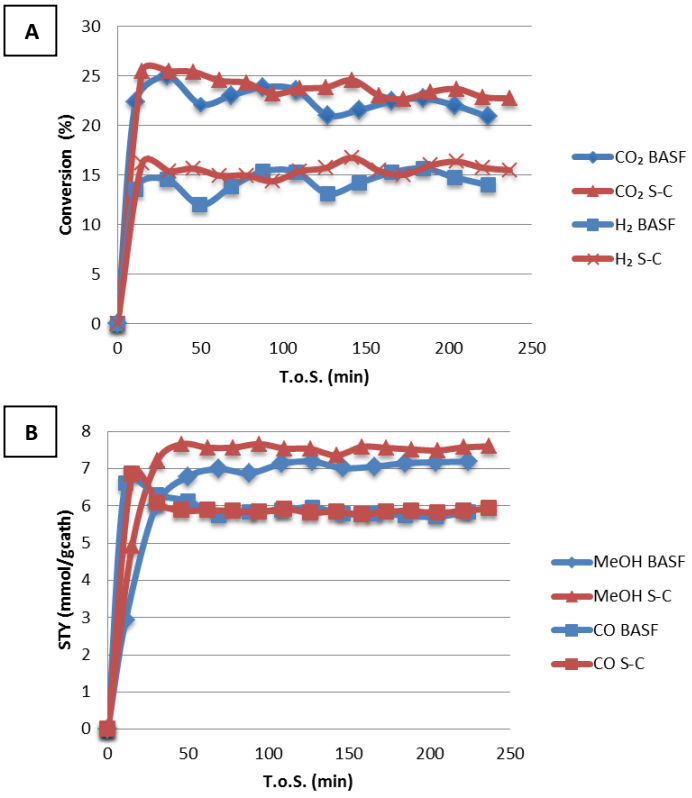

Figure 34. BASF (blue) and Süd Chemie (red) particulate catalyst results over time on stream (T.o.S.) at fixed conditions. A) Conversion of CO_2 and H_2. B) Methanol and CO STY.

The system achieved stable conditions quickly, and conversions and yields were more or less constant after 1.5 h on stream. Therefore, it is safe to say that the total run time of typically 3-4 h and sampling within the last 1.5 h of the run was sufficient time for the reactor outlet compositions to have stabilized. However, as already explained, these stabilized compositions do not necessarily represent equilibrium compositions.

In Figure 34 B) the CO yield was maximized right in the beginning of the experiment. The MeOH formation is not as high initially, and there is no peak formation at the beginning. This indicates that the rWGS reaction was faster than the CO_2 hydrogenation reaction, which is in agreement with findings in literature. [21]

8.2.1 In-house particulate catalysts

The in-house particulate catalyst activities were compared to the two commercial catalysts, BASF and S-C. The tests were performed in the standard conditions of 240 ^{o}C, 50 bar(g) pressure and WHSV of 3.17 1/h. The results of the runs for the VTT in-house catalysts are illustrated in Figure 35. The detailed results are available in Table 6.

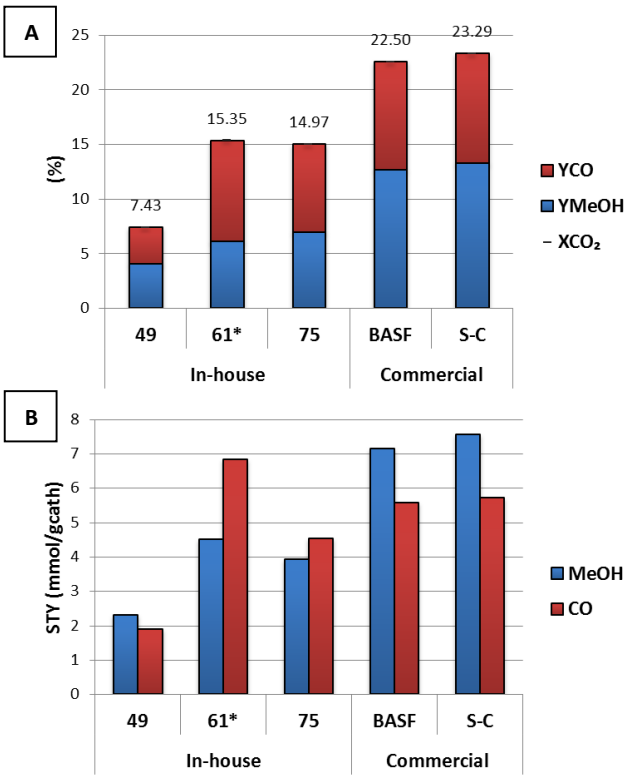

Figure 35. VTT in-house 49, 61 and 75 particulate catalysts compared with commercial catalysts at fixed conditions. A) MeOH and CO yields and CO_2 B) MeOH and CO STY. * denotes that impurities that affected the results existed in the reactor system.

The experiment with in-house catalyst 61 had several problems which are now addressed: Residues of another catalyst was detected in the reactor lines during the run of this catalyst, hence the results are not entirely comparable since the foreign catalyst contributed to the formation of hydrocarbons other than MeOH and also initiated higher CO formation rate. A control run with the BASF RP-60 catalyst with the same foreign catalyst contamination showed a 25 - 30 % lower MeOH yield than typical for the catalyst Moreover, the loading of catalyst 61 was significantly lower than the set WHSV would have required. Therefore, the catalyst 61 results are not entirely comparable to the other results. Nevertheless, the results from Figure 35 B) show that the MeOH STY for catalyst 61 was the highest of the VTT in-house catalysts. Catalyst 49 exhibited the best selectivity to methanol of the VTT in-house catalysts, but suffered in turn from very low MeOH STY. Compared to the commercial catalysts, the results for the VTT in-house catalysts were worse by all metrics. The MeOH yields were significantly lower for all the in-house catalysts, and

especially the selectivity to MeOH was significantly lower for the in-house catalysts. In fact, catalysts 61 and 75 showed higher CO formation rates than MeOH rates. Low MeOH yields combined with high CO yields are attributes that are not desirable for a methanol synthesis catalyst, and indicates that the in-house formulations need to be further developed.

Five different formulations of the FEUP catalyst, developed at the University of Porto, were tested and compared to the commercial catalysts. The results of the runs for catalysts FEUP, FEUP Cu1, FEUP Cu2, FEUP Cu3 and FEUP 44c are illustrated in Figure 36.

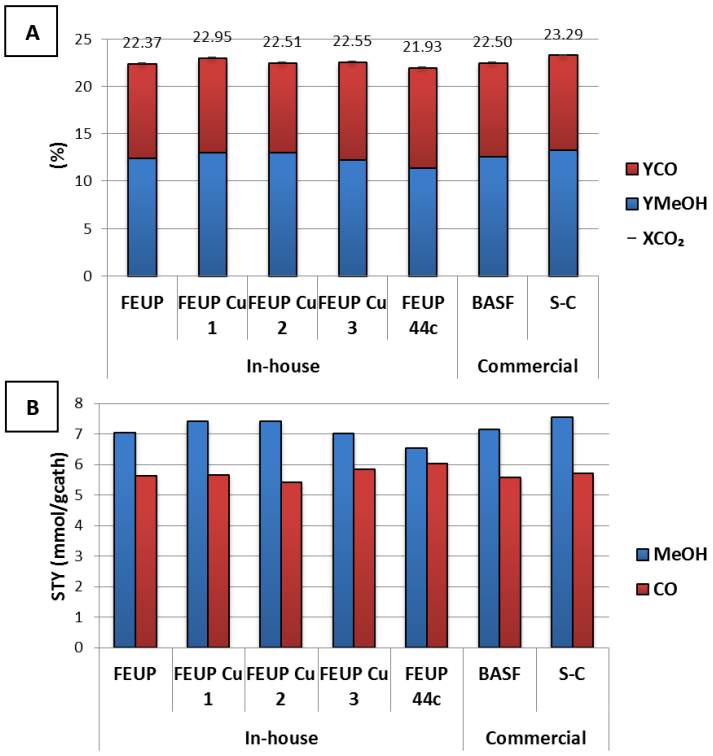

Figure 36. University of Porto particulate catalysts FEUP, FEUP Cu1, FEUP Cu2, FEUP Cu3 and FEUP 44c compared with commercial catalysts at fixed conditions A) MeOH and CO yields and CO_2 conversion. B) MeOH and CO STY.

The FEUP catalysts matched the commercial catalysts in terms of performance. Especially FEUP Cu1 and Cu2 performed well, with similar MeOH formation rate to BASF and S-C. FEUP Cu2 had slightly higher selectivity to MeOH than the commercial catalysts. The performance differences between the FEUP formulations were fairly small, and the MeOH STY difference between the best formulation, Cu1, and the

weakest, 44c, was about 12 %. The performance differences are within the margin of error. The detailed results of the in-house catalysts can be found in Table 6.

Table 6. Results for the VTT and FEUP in-house particulate catalysts at 240 °C and 50 bar(g).

Catalyst	WHSV (h^{-1})	T.o.S. (min)	X_{CO_2} (%)	S_{MeOH} (%)	$Y_i^{CO_2}$ (%)		STY_i ($\frac{mmol}{g_{cat}h}$)		$\dot{Q}$ (W)
					MeOH	CO	MeOH	CO	
49	3.17	231	7.4	54.8	4.1	3.4	2.3	1.9	-0.05
61	4.14	210	15.3	39.8	6.1	9.2	4.5	6.8	-0.02
75	3.16	215	15.0	46.5	7.0	8.0	3.9	4.5	-0.05
FEUP	3.17	231	22.4	55.6	12.4	9.9	7.0	5.6	-0.14
FEUP Cu1	3.19	245	23.0	56.8	13.0	9.9	7.4	5.6	-0.16
FEUP Cu2	3.19	247	22.5	57.8	13.0	9.5	7.4	5.4	-0.16
FEUP Cu3	3.19	215	22.5	54.5	12.3	10.3	7.0	5.8	-0.14
FEUP 44c	3.20	231	21.9	52.0	11.4	10.5	6.5	6.0	-0.11

8.2.2 Nanocoated particulate catalysts

The BASF catalyst was coated with seven different nanocoating formulations for an initial nanocoating activity screening. Figure 37 shows the performance of the nanocoated BASF and Süd Chemie particulate catalysts.

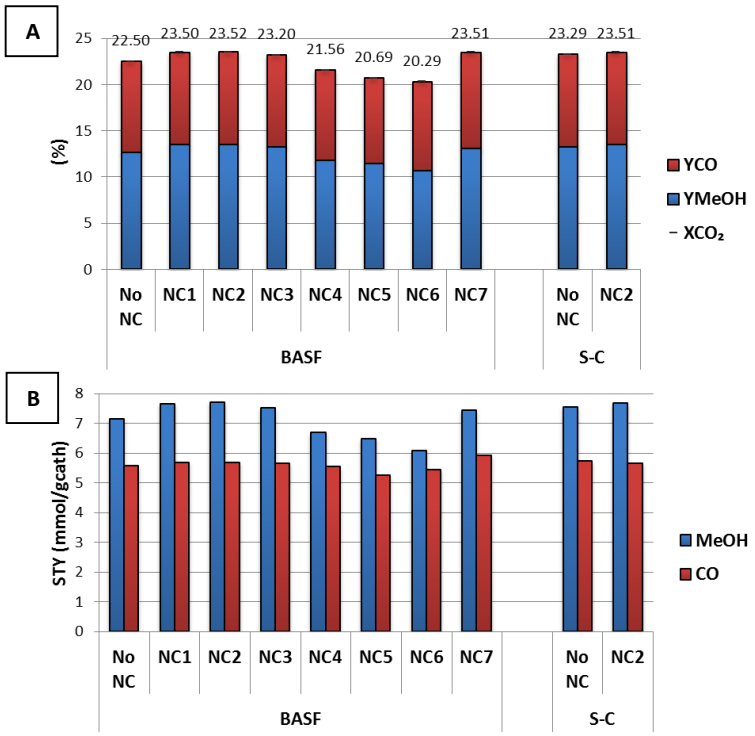

Figure 37. In-house nanocoated commercial particulate catalyst formulation comparison at fixed conditions. A) MeOH and CO yields and CO_2 conversion B) MeOH and CO STY.

The results show that different nanocoating formulations affected the performance. However, the performance difference from non-nanocoated catalyst was typically very small and most likely falls within the margin of error. Formulations NC1, NC2, NC3 and NC7 exhibited higher MeOH STY than standard BASF catalyst, whereas NC4, NC5 and NC6 had lower MeOH STY. The best performing formulation, NC2, showed a MeOH formation rate improvement of about 7 % over the standard BASF catalyst. The best performing BASF nanocoating formulation, NC2, was applied to the other catalysts. The Süd Chemie NC2 catalyst proved to be better than the non-nanocoated Süd Chemie catalyst, although only by a small margin.

The catalyst loadings for the nanocoated in-house catalyst experiments were not constant as aimed. The nanocoated catalyst runs had partly because of this significantly higher weight based space velocities than the non-nanocoated catalysts, as seen in the detailed results in Table 7. Figure 38 shows the results of the nanocoated VTT in-house catalysts.

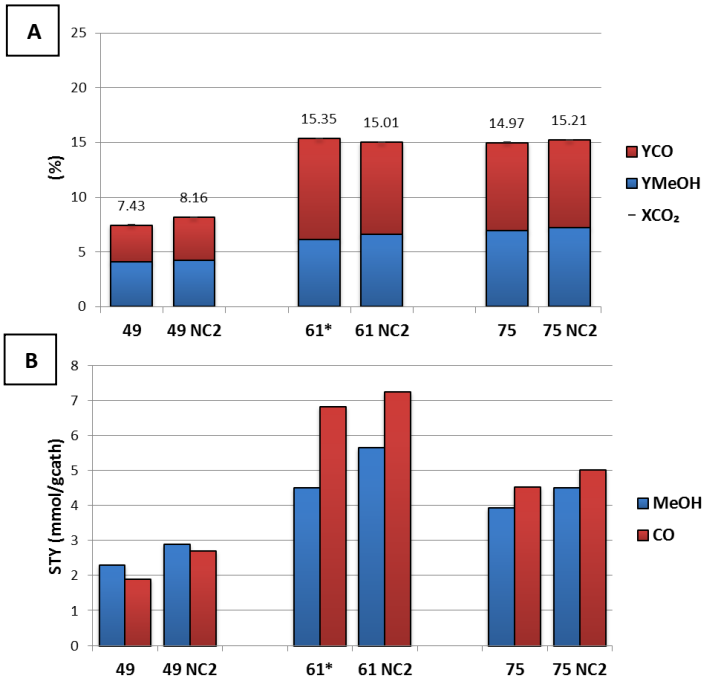

Figure 38. Nanocoated VTT in-house catalysts compared with non-nanocoated formulations at fixed conditions. A) MeOH and CO yields and CO_2 conversion B) MeOH and CO STY. * denotes that impurities that affected the results existed in the reactor system.

Despite the lower catalyst loadings, all of the nanocoated catalysts performed slightly better in terms of MeOH yield. The MeOH STY showed larger differences in favor of the nanocoated catalysts. Since all of the nanocoated catalysts achieved similar or higher methanol yields with smaller catalyst loadings, it can be concluded that nanocoating can be favorable in terms of performance.

Even with nanocoatings, the VTT in-house catalysts MeOH formation rates were still significantly lower than for the commercial catalysts. Nanocoating did not significantly improve on the selectivity to MeOH either, and thus catalysts 61 and 75 runs still had higher rWGS reaction rates than CO_2 hydrogenation rates. Table 7 shows the detailed results of the nanocoated catalyst experiments

Table 7. Results for the in-house nanocoated particulate catalysts at 240 °C and 50 bar(g).

Catalyst	WHSV (h^{-1})	T.o.S. (min)	X_{CO_2} (%)	S_{MeOH} (%)	$Y_i^{CO_2}$ (%)		STY_i ($\frac{mmol}{g_{cat}h}$)		$\dot{Q}$ (W)
					MeOH	CO	MeOH	CO	
Commercial									
BASF NC1	3.17	223	23.5	57.4	13.5	10.0	7.6	5.7	-0.17
BASF NC2	3.18	214	23.5	57.6	13.5	10.0	7.7	5.7	-0.17
BASF NC3	3.18	175	23.2	57.1	13.2	10.0	7.5	5.6	-0.16
BASF NC4	3.17	221	21.6	54.7	11.8	9.8	6.7	5.5	-0.13
BASF NC5	3.17	241	20.7	55.2	11.4	9.3	6.5	5.3	-0.13
BASF NC6	3.17	224	20.3	52.7	10.7	9.6	6.1	5.4	-0.11
BASF NC7	3.18	270	23.5	55.7	13.1	10.4	7.4	5.9	-0.15
S-C NC2	3.17	217	23.5	57.5	13.5	10.0	7.7	5.7	-0.17
In-house									
49 NC2	3.85	262	8.2	51.7	4.2	3.9	2.9	2.7	-0.04
61 NC2	4.82	222	15.0	43.8	6.6	8.4	5.7	7.3	-0.04
75 NC2	3.51	221	15.2	47.3	7.2	8.0	4.5	5.0	-0.06

Nanocoatings may not only improve catalyst activity, but for example improve catalyst stability in oxidative atmospheres. Thus, the success of a particular nanocoating formulation cannot solely be evaluated on catalyst performance, even though this work only performed activity testing. Appendix 9 Table 1 presents the performance of all the particulate catalysts in terms of relative performance to BASF.

8.2.3 Coated mesh catalysts

Due to problems with the quality of the coating, only Mesh 2 NC-A, NC-B, NC-C and Mesh 3 NC-A(not pre-calcined) were tested. The results are illustrated in Figure 39 and detailed results are presented in Table 8.

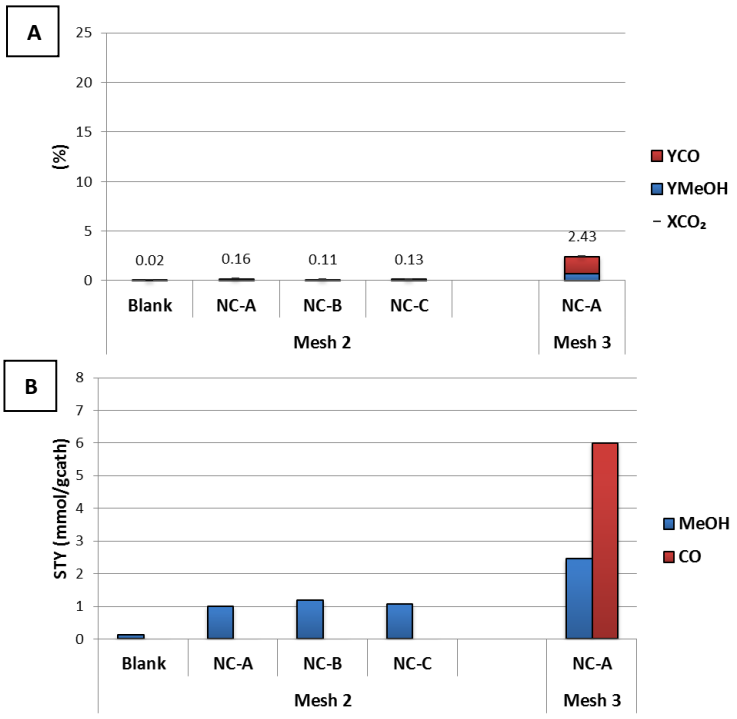

Figure 39. In-house coated mesh catalysts at fixed conditions. A) MeOH and CO yields and CO_2 conversion B) MeOH and CO STY.

The catalytic activities were generally low, especially for Mesh 2, which had very low MeOH formation rates and surprisingly, no CO formation. One reason for why the results showed no CO formation was that the CO amounts could be below GC TCD detection limits, though this is not proven. The non-nanocoated Mesh 2 catalyst was also tested for control, and as expected, it produced virtually no MeOH or CO. Mesh 3 showed best performance, but unfortunately suffered with Mesh 1 from quality issues, and therefore further formulations were not tested.

An interesting phenomenon with Mesh 3 NC-A and Mesh 2 NC-B was the significantly (>5x) higher formation rate of other hydrocarbon products, specifically C_2 and C_4 hydrocarbons, than for any other tested catalyst. The mol-% of other products than MeOH or CO was still very low though, accounting for under 0.1 mol-% in the outlet gas, and thus wasn't included in the products. Still, the higher formation rates of higher hydrocarbons shows that the catalyst formulations were not methanol synthesis specific, and other reaction paths were simultaneously catalyzed.

Table 8. Results for the mesh catalysts at 240 °C and 50 bar(g).

Catalyst	WHSV (h^{-1})	T.o.S. (min)	X_{CO_2} (%)	S_{MeOH} (%)	$Y_i^{CO_2}$ (%)		STY$_i$ ($\frac{mmol}{g_{cat}h}$)		$\dot{Q}$ (W)
					MeOH	CO	MeOH	CO	
Mesh 2 Blank	35.35	202	0.0	100.0	0.0	0.0	0.1	0.0	0.00
Mesh 2 NC-A	34.73	230	0.2	100.0	0.2	0.0	1.0	0.0	0.00
Mesh 2 NC-B	60.30	211	0.1	100.0	0.1	0.0	1.2	0.0	0.00
Mesh 2 NC-C	45.91	218	0.1	100.0	0.1	0.0	1.1	0.0	0.00
Mesh 3 NC-A	19.44	240	2.4	29.1	0.7	1.7	2.5	6.0	0.01

Considering that the catalyst amounts when using a coated catalyst are generally smaller than for a typical packed bed reactor, it is essential for the coated catalyst to be more active for comparable results. The coated catalysts in this study did not achieve high activities for MeOH synthesis, and thus need to be further developed.

8.3 Condition testing

The commercial BASF catalyst was used to test the system at different conditions by changing one parameter at the time. Even though only BASF was used in the testing, the other catalysts can be expected to roughly follow similar trends, since they all were Cu-based catalysts. The parameters that were varied in this work were space velocity, reaction pressure and temperature, as explained in Table 4.

8.3.1 Effect of space velocity

The WHSV was varied by doubling and halving the flow rate from the original set point of 0.186 dm^3/min at STP. Therefore, the new flow rates were 0.093 and 0.370 dm^3/min at STP. The results are illustrated in Figure 40. The equilibrium CO_2 conversion was added to the graph as a reference, and was calculated with Aspen RKS-MHV2 property set for a feed containing 5 mol-% N_2 (similar to the experimental reactant gas).

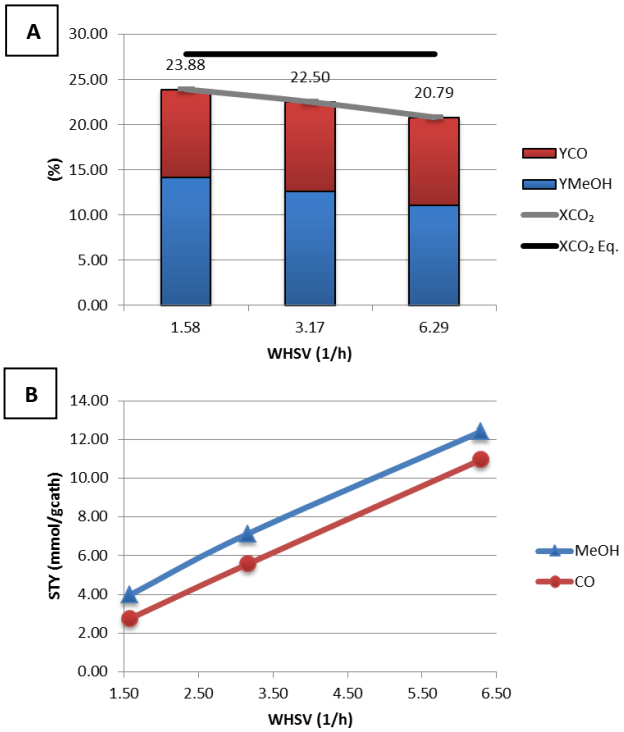

Figure 40. Effect of space velocity on BASF particulate catalyst performance at T_R = 240 °C and P_R = 50 bar(g). A) MeOH and CO yields, equilibrium CO_2 conversion and experimental conversion B) MeOH and CO STY.

The lower space velocity result shows slightly higher CO_2 conversion, MeOH and CO yields, but significantly lower formation rates per mass of catalyst. Therefore, increasing the space velocity increased also the STY of the products, which indicates that mass transfer limitations existed within the tested range. The change in WHSV can be thought of as a change in catalyst loading, and the results might also indicate that the CO_2 hydrogenation reaction was kinetically limited, since an increase in catalyst loading (lower WHSV) lead to an increase in methanol yield. [128] Interestingly, the CO yield was more or less constant with varying WHSV within the tested range, indicating that the rWGS was, contrary to CO_2 hydrogenation, equilibrium limited. Słoczyński et al. [46] reported with a $Cu/ZnO/ZrO_2$ catalyst with various metal oxide additives a similar relationship between and STY and space velocity. Table 9 shows the detailed results in the different flow rates.

Table 9. Measured reaction conditions and results of the BASF runs at varying space velocities.

Catalyst	T_{meas} (°C)	P_{meas} (bar(g))	WHSV (h^{-1})	X_{CO_2} (%)	S_{MeOH} (%)	$Y_i^{CO_2}$ (%)		STY_i ($\frac{mmol}{g_{cat}h}$)	
						MeOH	CO	MeOH	CO
BASF Run 1	240	49.8	**1.58**	23.9	59.1	14.1	9.8	4.0	2.8
BASF Run 2	239	49.3	**3.17**	22.5	56.1	12.6	9.9	7.1	5.6
BASF Run 3	240	50	**6.29**	20.8	53.1	11.0	9.7	12.4	11.0

The selectivity to methanol decreased with increasing WHSV, and hence the behaviour of increasing selectivity to methanol with increasing WHSV reported by Sun et al. [48] was not observed within the tested range of this work.

8.3.2 Effect of pressure

The effect of pressure was tested at 30 and 50 bar(g) pressures. Figure 41 shows the experimental results.

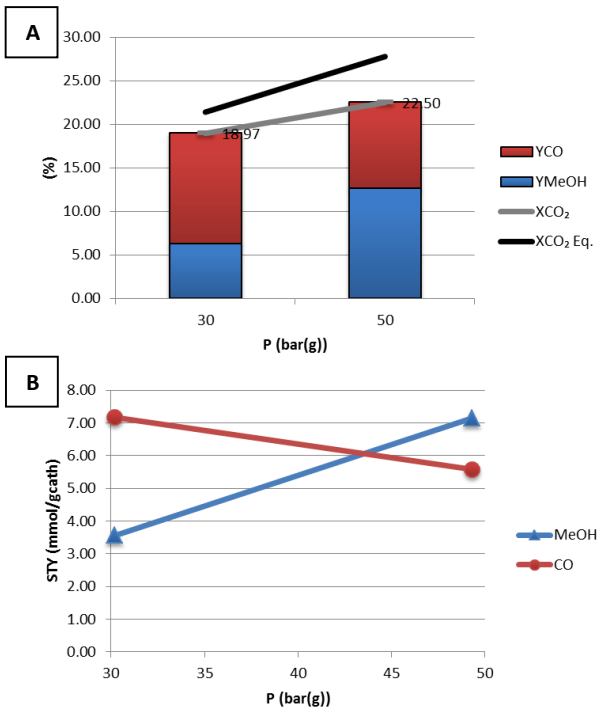

Figure 41. Effect of pressure on BASF particulate catalyst performance at $T_R = 240$ °C and WHSV = 3.17 1/h. A) MeOH and CO yields, equilibrium CO_2 conversion and experimental conversion B) MeOH and CO STY.

The results showed a similar behaviour as to what the equilibrium calculations predicted, meaning that the methanol formation rate decreased and the CO formation rate increased with decreasing pressure. At 30 bar(g) the CO formation was higher than MeOH formation. In fact, Figure 41 B) displays that the crossing point of MeOH and CO space time yields occurred somewhere between 30 and 50 bar reaction pressure.

The equilibrium conversion of CO_2 for the CO_2 hydrogenation increased with higher pressure, and thus the MeOH yield was higher. The rWGS equilibrium conversion decreased with increasing pressure. However, the pressure also affects the kinetics of the reactions. A higher reaction pressure leads to higher reactant gas partial pressures, which increases the reaction rate. Table 10 shows the detailed results of the runs in the different pressures.

Table 10. Measured reaction conditions and results of the BASF runs at varying pressures.

Catalyst	T_{meas} (°C)	P_{meas} (bar(g))	WHSV (h^{-1})	X_{CO_2} (%)	S_{MeOH} (%)	$Y_i^{CO_2}$ (%)		STY_i ($\frac{mmol}{g_{cat}h}$)	
						MeOH	CO	MeOH	CO
BASF Run 7	240	**30.2**	3.16	19.0	33.2	6.3	12.7	3.6	7.2
BASF Run 2	239	**49.3**	3.17	22.5	56.1	12.6	9.9	7.1	5.6

8.3.3 Effect of temperature

The effect of reaction temperature was tested at 4 set points, which were specified as 200, 220, 240 and 250 °C. The results are presented in Figure 42.

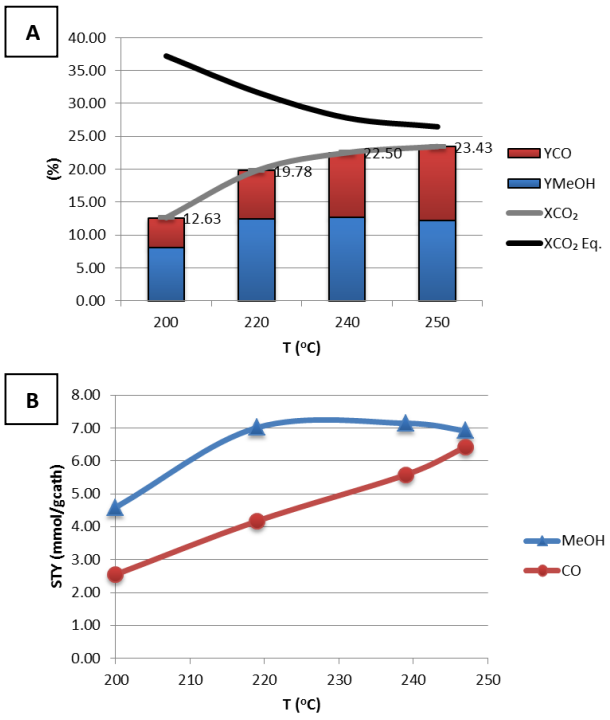

Figure 42. Effect of temperature on BASF particulate catalyst performance at P_R = 50 bar(g) and WHSV = 3.17 1/h. A) MeOH and CO yields, equilibrium CO_2 conversion and experimental conversion B) MeOH and CO STY.

Increasing the reaction temperature increased the MeOH yield and STY up to a certain point, until it fell again in the highest tested temperature of 250 °C. This

suggests that with the increasing temperature the CO_2 hydrogenation gradually developed into a more equilibrium limited reaction instead of a kinetically limited one. The yield of MeOH for the BASF catalysts was highest at 240 °C. However, the yield was not much lower at 220 °C. The CO yields and STY increased constantly with an increasing reaction temperature, and as a consequence the CO_2 conversion also increased with an increase of temperature, although the increase slowed down at higher temperatures. A similar study was performed with the FEUP catalyst in a narrower temperature range of 200 – 240 °C. The results were similar, with the exception of lower MeOH yield at 220 °C. The results for the BASF and FEUP tests in varying conditions is available in Table 11.

Several studies in literature examined the relationship between catalyst activity and reaction temperature and the results obtained in this experimental work resemble those findings. In literature, Guo et al. [41] reported of a maximum methanol yield at 230 – 240 °C for different catalyst formulations at 30 bar and GHSV 3600 1/h, and Madej-Lachowska et al. [45] 220-240 °C for different formulations at 80 bar. An et al. [34] found that their highly active fibrous catalyst had the highest methanol yield at a higher temperature of 250 °C at 50 bar conditions.

Table 11. Measured reaction conditions and results of the BASF runs at varying temperatures.

Catalyst	T_{meas} (°C)	P_{meas} (bar(g))	WHSV (h^{-1})	X_{CO_2} (%)	S_{MeOH} (%)	$Y_i^{CO_2}$ (%)		STY_i ($\frac{mmol}{g_{cat}h}$)	
						MeOH	CO	MeOH	CO
BASF Run 4	**200**	49.8	3.16	12.6	64.3	8.1	4.5	4.6	2.6
BASF Run 5	**219**	49.8	3.16	19.8	62.7	12.4	7.4	7.0	4.2
BASF Run 2	**239**	49.3	3.17	22.5	56.1	12.6	9.9	7.1	5.6
BASF Run 6	**248**	49.1	3.18	23.4	51.9	12.2	11.3	6.9	6.4
FEUP Run 1	**200**	50.0	3.17	11.5	61.4	7.0	4.4	4.0	2.5
FEUP Run 2	**220**	50.0	3.17	18.2	59.0	10.7	7.5	6.1	4.2
FEUP Run 3	**239**	49.4	3.17	22.4	55.6	12.4	9.9	7.0	5.6

8.4 Comparison with literature

Comparing the in-house and commercial catalyst results to those found in literature in Table 1 shows many similarities. The CO_2 conversion in literature for the pressure range 30 – 80 bar and temperature range 220 - 270 °C has generally been 15 – 25 %. The best performing particulate catalysts in this work was the BASF NC2, which achieved at the standard catalyst comparison conditions a CO_2 conversion of 23.5 % and a MeOH selectivity of 57.6 %. The selectivities to methanol in literature were found to be varying more widely, generally between 30 – 70 %. Since each experimental setup is unique, and the reaction conditions most likely differ from the ones in this work, no direct comparison between the results from this study and the results found in literature can be made. Nevertheless, general observations of the differences in results can still be useful. Selected results from literature presented in similar units as the results in this work with detailed condition information are presented in Table 12.

Table 12. Detailed results from literature.

Study and catalyst	**T_R (°C)**	**P_R (bar)**	**WHSV (1/h)**	**$Y_i^{CO_2}$ (%)**		**STY_{MeOH} ($\frac{mmol}{g_{cat}h}$)**
				MeOH	**CO**	
Gao et al. [29]						
Cu/Zn/Al	250	50	7.1	7.8	11.8	10.9
Cu/Zn/Al/Zr	250	50	7.1	11.9	12.7	15.7
Cu/Zn/Al/Y	250	50	7.1	12.7	14.1	16.7
Frei et al.[44]						
$Cu/ZnO/ZrO_2$	240	40	3.4	-	-	9.2
Industrial cat.	240	40	3.4	-	-	8.3
Guo et al. [32]						
$50\text{-}CuO/ZnO/ZrO_2$	240	30	1.2	9.6	7.4	-
$100\text{-}CuO/ZnO/ZrO_2$	240	30	1.2	7.0	5.3	-
$150\text{-}CuO/ZnO/ZrO_2$	240	30	1.2	4.7	3.1	-
Raudaskoski et al. [31]						
$Cu/ZnO/ZrO_2$-12h	230	30	1.8	5.1	11.6	-
$Cu/ZnO/ZrO_2$-24h	230	30	1.8	5.3	9.9	-
An et al. [35]						
Fibr. Cu/Zn/Al/Zr	240	40	6.4	12.5	8.0	-
Industrial cat.	240	40	6.4	6.9	9.3	-

At the Gao et al. experimental conditions the yields for the various catalyst formulations were between 7.8 – 12.7 % and 11.8 – 14.1 % for MeOH and CO

respectively. The study was performed at a high space velocity, and the results showed a low selectivity to MeOH compared to results for catalysts in this work. The study by Frei et al. was performed in largely similar conditions to this study, with the exception of a lower pressure of 40 bar. The STY of MeOH was between 9.2 and 8.3 $\frac{mmol}{g_{cat}h}$, which was a bit higher than the best results in this work. The Raudaskoski et al. study was the only study performed in a similar, but smaller, autoclave reactor to the one used in this work. The results showed low MeOH yields of around 5 % for the catalysts. However, the space velocity and pressure was significantly lower than in this work, 1.8 1/h and 30 bar respectively, making comparison challenging.

Based on these findings, it suggests that the commercial catalysts and the best performing in-house catalysts (FEUP and its formulations) were active at catalysing the CO_2 hydrogenation to MeOH, and that the results were comparable to the latest studies in literature for catalysts specifically formulated for the MeOH production from CO_2.

8.5 Tracer step change experiment

In the step change experiment conditions, the compressibility factor Z_2 was calculated in Aspen Plus to be 1.0134. At STP, the flow rate was 0.134 dm^3/min. The flow rate at experimental conditions of 49.2 bar(g) and 240 ^oC was calculated to be:

$$\dot{v} = \frac{0.134\frac{dm^3}{min}1.013\ bar*1.0134*513\ K}{50.213\ bar*1*273.15\ K} = 0.00513\ \frac{dm^3}{min}$$

Therefore, the mean residence time was:

$$\tau = \frac{0.2\ dm^3}{0.00513\frac{dm^3}{min}} = 38.97\ min$$

An estimation for when the H_2 and CO_2 first reached the GC was made, based on the experimental results. CO_2 and H_2 were first detected in the outlet in the second GC sample at 20 min. Thus, a value of slightly under 20 min, about 17 min, was obtained as an estimation. It was used as the t=0 point of the theoretical calculations. The

results for the experimental concentrations over time and the calculated ideal results are presented in Figure 43.

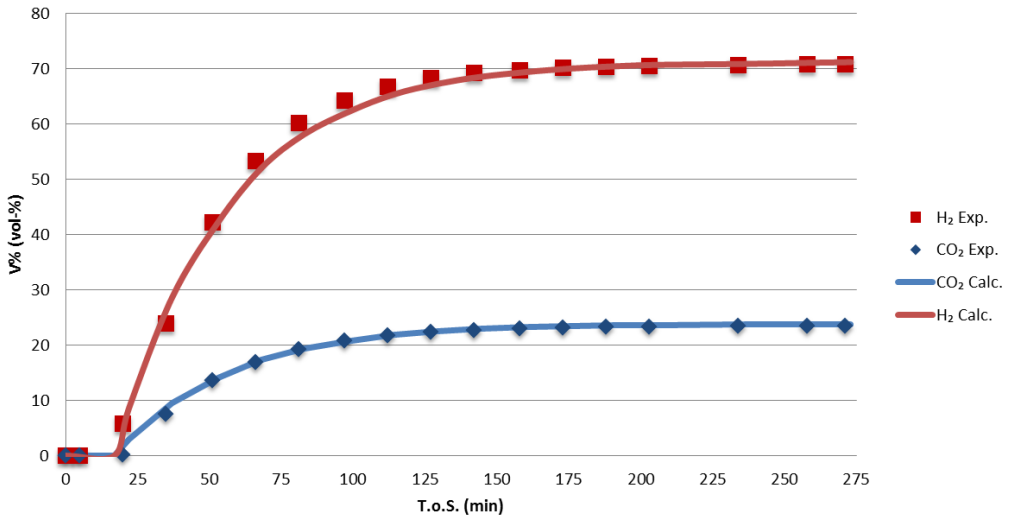

Figure 43. Calculated H_2 and CO_2 outlet concentrations, with start at T.o.S. 17 min, and experimental H_2 and CO_2 concentrations.

The results show that the experimentally obtained concentrations were very close to the calculated perfectly operating CSTR concentrations. The H_2 results show a bit poorer fit to the calculated curve than the CO_2 results. With the results obtained in this experiment it is still safe to assume ideal operation of the reactor with gaseous species.

As T.o.S approaches infinity, the $V\%_i$ asymptotically approaches $V\%_{i_0}$, and therefore steady state condition (i.e. no accumulation). The time for an ideal CSTR to reach 95 % steady-state condition is roughly 3x residence time, which is proven by the following calculation:

$$\frac{V\%}{V\%_0} = 0.95 = 1 - \exp\left(-\frac{t_{95\%}}{\tau}\right)$$

$$-\frac{t_{95\%}}{\tau} = \ln(1 - 0.95) = \ln(0.05)$$

$$t_{95\%} \approx 3\tau$$

The time to reach 95 % steady-state condition in the step change experiment was about 117 min. With the standard flow rate, used in the catalyst activity testing, of 0.186 dm^3/min at STP (τ = 28 min), the $t_{95\%}$ was about 84 min.

8.6 Kinetic model simulation

Two common kinetic models for methanol synthesis process simulations were implemented in Aspen Plus for comparison with the experimental results obtained with the particulate BASF catalyst. The motivation was to establish a rough overview of how well the kinetic models fit with the results obtained with the CSTR within the range of applied tested conditions. However, the low amount of data points and the narrow range of reaction conditions tested prevented any conclusive statements of the fit with a kinetic model.

The kinetic model rate constants were adjusted with the activity factor *a*, to fit calculated and experimental catalyst activities. The models were simulated with similar conditions as the experimental runs in the Aspen CSTR block.

8.6.1 The Graaf model

Figure 44 A) shows simulations with the Graaf model implemented with the parameter calculations by An et al. [34] with varying temperatures at standard 50 bar(g) pressure and *a* values of 1, 0.1 and 0.01. Figure 44 B) shows the simulated results with varying pressures and activities at constant 240 ^oC temperature. The condition testing results with particulate BASF catalysts at all tested temperatures and pressures are also presented in the figures. In terms of results, changing activities for single reactions did not differ significantly from changing all the activities at the same time. The reason for this was that the Graaf model assumes that almost all MeOH formation happens through the CO hydrogenation, so the rWGS reaction has to first convert CO_2 to CO (in cases with only CO_2 in the feed). Therefore, the activity values were simultaneously changed for all 3 reactions.

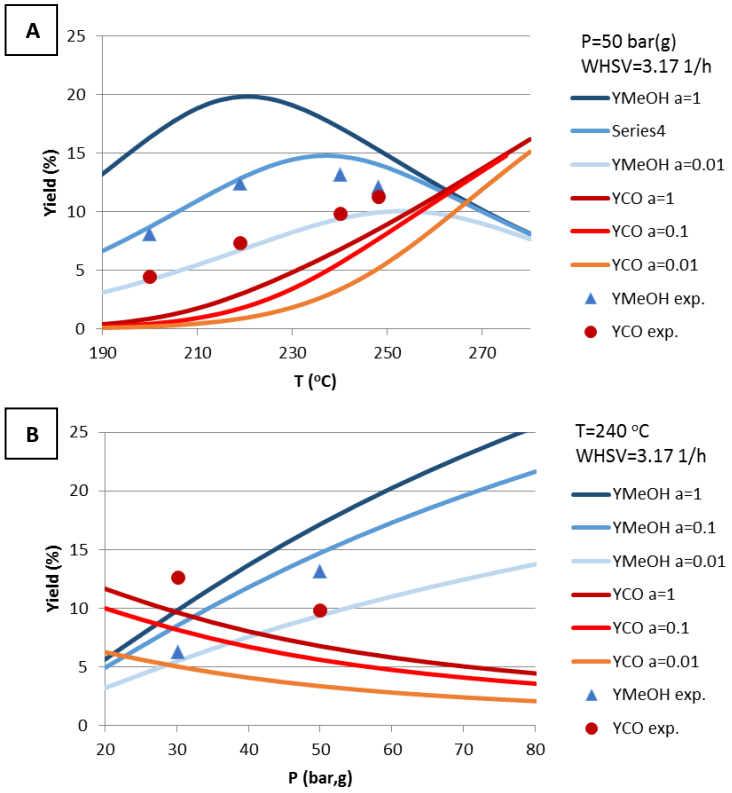

Figure 44. The Graaf model simulation results with varying activities, *a*, compared with experimental results obtained using particulate BASF (circles and triangles). A) MeOH and CO yields at varying temperatures B) MeOH and CO yields at varying pressures.

Compared to the results in this work, the Graaf model (with a = 1) displayed significantly higher catalyst activity for methanol synthesis and significantly lower activity for CO synthesis in all conditions. In Figure 44 A) the maximum methanol yield at 50 bar(g) was 20 %. The CO formation was very low, and at 240 °C and 50 bar(g) the yield was only 6.3 %. The limited amount of experimental data points made comparison challenging.

The activity was adjusted for the MeOH yield to fit with the experimental results as closely as possible. The Graaf model CO yield could not be adjusted with mere activity adjustments. The best fit was found with an activity of about 0.06, which simulated the MeOH yields in the following way:

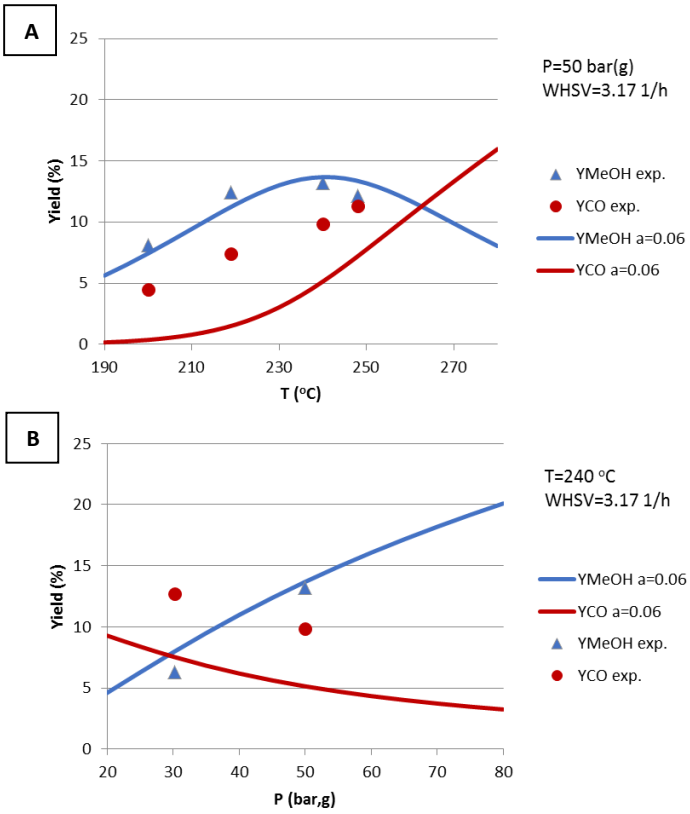

Figure 45. The Graaf model simulation results with $a = 0.06$ compared with experimental results. A) MeOH and CO yields at varying temperatures B) MeOH and CO yields at varying pressures.

The Graaf model, with a = 0.06, exhibited maximum methanol yield at a temperature of about 230 - 240 °C. This is similar to the experimental results, and the pressure effect on MeOH yield matched the experimental results moderately well. Nevertheless, the Graaf model failed to fit with the experimental CO results, and thus is not suitable as a model for the whole process.

Finally, the activity adjusted Graaf model was simulated with different space velocities and compared to the experimental BASF results with different flow rates. The results, shown with WHSV on a logarithmic scale, are presented in Figure 46.

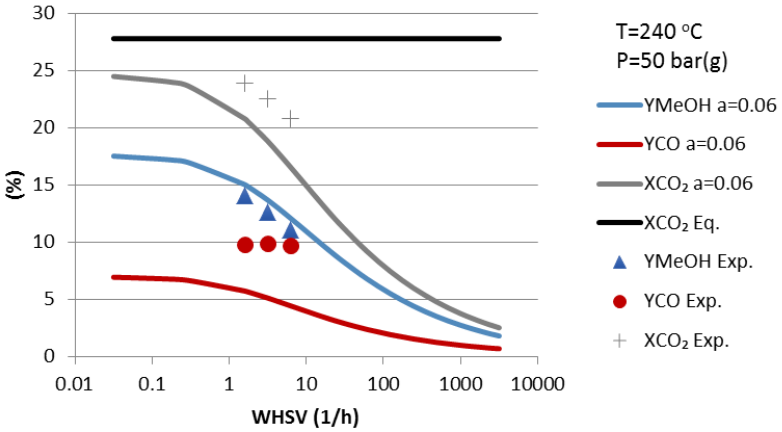

Figure 46. The Graaf model with $a = 0.06$ simulated at varying space velocities and compared with experimental results. Results are presented using MeOH and CO yields and CO_2 conversion.

The simulated results for MeOH yield agreed with the varying WHSV experimental results in the test range of 1.6 – 6.3 1/h, exhibiting a similar descending slope. For the CO formation, the simulated results plateaued at WHSV of less than 1 1/h. The experimental results indicated that the plateau occurs at a higher WHSV, since the CO yields of the experimental results were essentially identical despite the varying space velocities.

8.6.2 The vanden Bussche model

The simulation of the vanden Bussche model was conducted in a similar way as with the Graaf model, with varying activities (a = 1 – 3) for both reactions at different temperatures and pressures. Figure 47 shows the results.

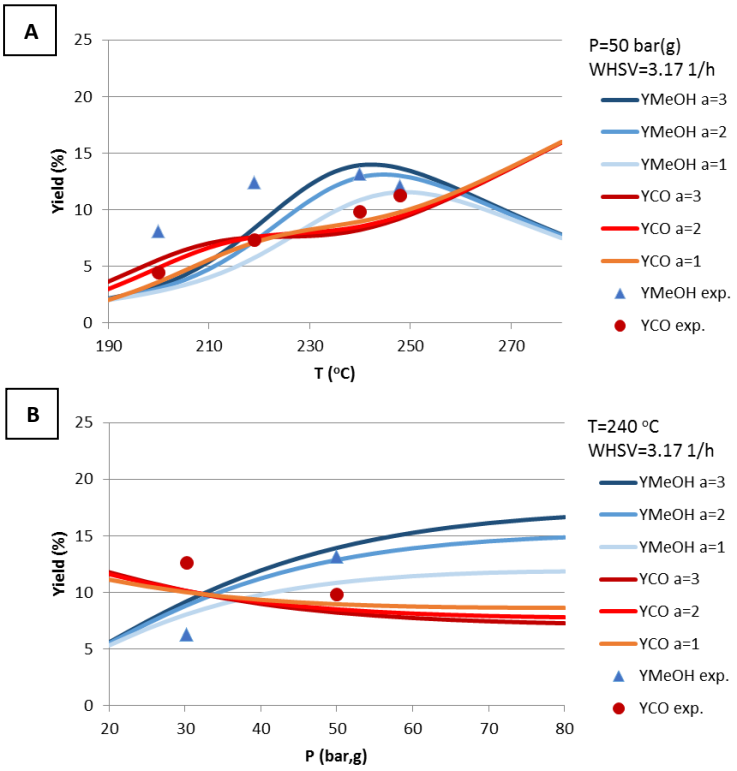

Figure 47. The vanden Bussche model simulation results with different activities, *a*, compared with experimental results obtained using particulate BASF. A) MeOH and CO yields at varying temperatures B) MeOH and CO yields at varying pressures.

Figure 47 A) shows that the simulated yields for MeOH with catalyst activity a = 1 was lower than the experimental yields. The simulated CO yields were much closer to those observed in experimental results than with the Graaf model. However, a significant difference from experimental results was especially seen with MeOH at low temperatures, where the simulated yields were lower. The high temperature CO yields also differed, and were lower than the experimental ones. In Figure 47 B) it can be seen, similarly to the Graaf model, that the model differs from the experimental results at the 30 bar(g) point with higher MeOH yields. The simulated CO yield at 30 bar(g) was also higher than the experimental observation.

Higher activity improved the fit of the model to the experimental MeOH results, and slightly worsened it for the CO. An activity of 3 was chosen as the best fit. However, as illustrated in Figure 48, it was noticed that the vanden Bussche MeOH yield curve did not fully match the experimental results.

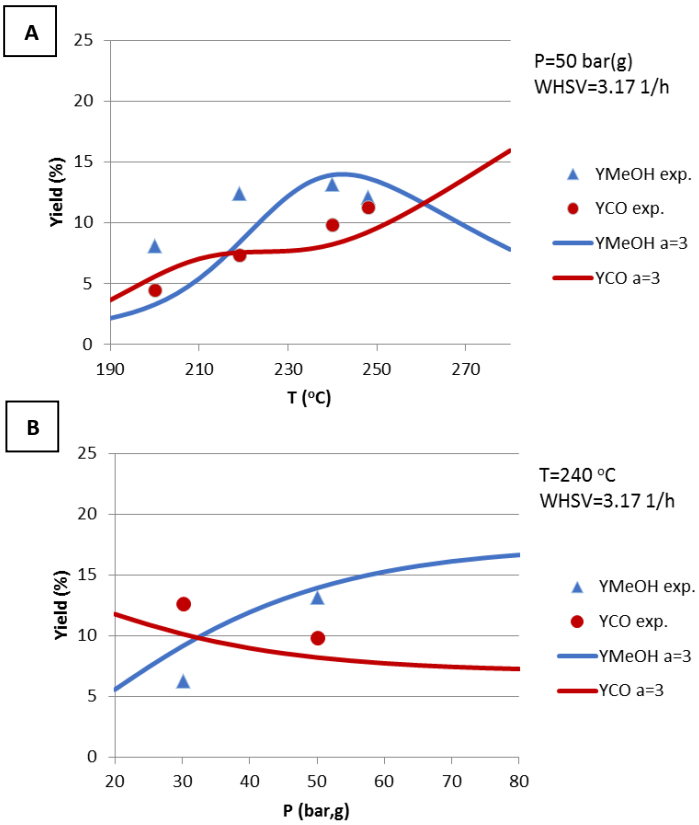

Figure 48. The vanden Bussche model simulation results with a = 3 compared with experimental results. A) MeOH and CO yields at varying temperatures B) MeOH and CO yields at varying pressures.

The simulated MeOH yield lags the experimental results at especially lower temperatures. With a shift of the simulated yields to a 10 °C lower temperature in Figure 48 A), the MeOH and CO yields would match the experimental results significantly better. However, the results in varying pressures at a 10 °C lower temperature would not have been better than the unadjusted results, and for that reason any temperature adjustment was discarded.

All in all, the vanden Bussche model (with and without a temperature adjustment) described the experimental data better than the Graaf model, due to the more accurate CO fit. However, regarding the MeOH formation at different conditions, the Graaf model reproduced better the experimental results.

Figure 49 illustrates the effect space velocity for the activity adjusted vanden Bussche model.

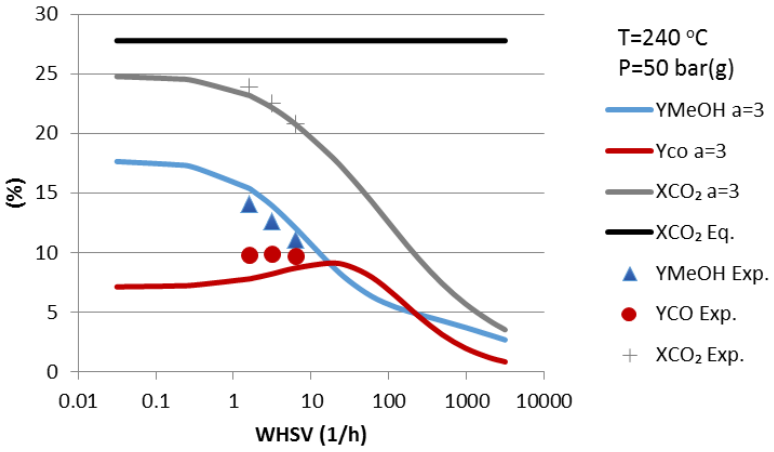

Figure 49. The vanden Bussche model with $a = 3$ simulated at varying space velocities and compared with experimental results. Results are presented as MeOH and CO yields and CO_2 conversion.

Contrary to the Graaf model, the vanden Bussche model results had a CO yield curve more in line with experimental results. The vanden Bussche model also simulated the MeOH yield in line with the experimental results.

9 Error estimation

This chapter discusses the most significant error sources of the experimental work and the results.

9.1 Reaction system

The experimental setup had several error sources that could have affected the results, of which one was the reactor heating system. The detachable electric heating jacket was wrapped around the reactor vessel, but was not insulated. Thus, a part of the vessel was always left exposed, and as a consequence the reactor was unevenly heated. Furthermore, the temperature measurement inside the reactor was probably not representative of the catalyst temperature, the temperature in which the reactions actually occur. The thermocouple was placed in a metallic pocket a few cm above the catalyst baskets or meshes 1 cm from the reactor wall. Thus, the measured reactor inside temperature cannot be assumed to be representing the

catalyst temperature without some error. On the other hand, the stirring was most likely effective, which minimized the temperature gradients in the reactor. The heat released by the reactions was also so small, that the temperature gradients from the heat of the reactions were probably minimal.

Another possible error source was the relatively small reactor system leakage, which was never completely eliminated. The pressure tests performed before each run indicated a pressure drop of about 0.05 – 0.1 bar/min throughout the experiments.

The catalyst comparison experiments were designed to be performed at fixed conditions. However, many factors complicated this in practice. Deviations in conditions affected the catalyst activities. Pressure was the factor that was the most difficult to control due to problems with the backpressure valve. Despite this, the pressure was generally managed to be kept within 1 bar of the set point. The stirrer speed had to be changed halfway through the experimental runs, due to unforeseen problems with the stirrer motor. The set value for the stirrer speed was 400, and at the end of the runs the set value was 430. The deviations from the set point conditions for reaction temperature, pressure and stirrer speed for all runs can be found in Appendix 4. All in all, the reaction conditions were assumed to be same for the runs in activity tests, but in reality this was not the case.

Two repeatability tests with the BASF catalyst were performed. The first repeatability test was performed multiple times with the same catalyst loading over a 1 week time span. The testing conditions were the same as in the catalyst comparisons, i.e. 240 ^{o}C, 50 bar(g) and WHSV of about 3.17 1/h. Figure 50 illustrates the results for the repeatability tests with samples taken at different T.o.S.

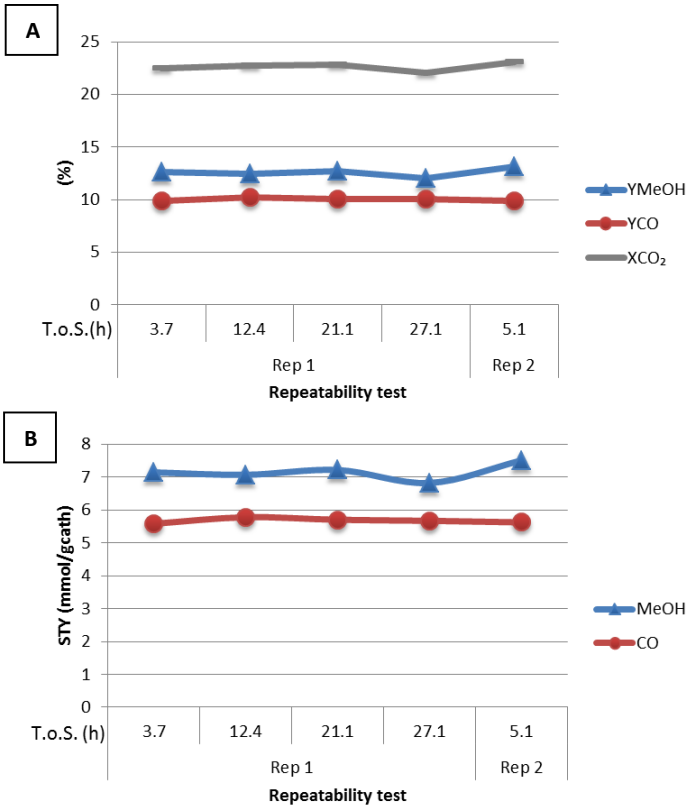

Figure 50. Repeatability test, with BASF particulate catalyst. Rep 1 is performed at multiple T.o.S. A) MeOH and CO yields and CO_2 conversion B) MeOH and CO STY.

The results from repeatability test 1 were performed during the condition testing, which results were presented in chapter 8.3. Every third run was a repeatability test to verify that the system worked as planned. Rep 1 was performed with the same catalyst loading, with a total on stream time of 27 h. Rep 2 was a separate test, and it was the final experiment for this work. Table 13 shows the complete results for the repeatability tests.

Table 13. Results of repeatability tests 1 and 2.

	T.o.S. (min)	T_{meas} (°C)	P_{meas} (bar(g))	WHSV (h^{-1})	X_{CO_2} (%)	S_{MeOH} (%)	$Y_i^{CO_2}$ (%)		STY_i ($\frac{mmol}{g_{cat}h}$)	
							MeOH	CO	MeOH	CO
Rep 1	224	239	49.3	3.2	22.5	56.1	12.6	9.9	7.1	5.6
	742	240	49.8	3.2	22.7	55.0	12.5	10.2	7.1	5.8
	1263	240	49.9	3.2	22.8	55.9	12.8	10.1	7.2	5.7
	1627	239	50	3.2	22.1	54.6	12.1	10.0	6.8	5.7
Rep 2	306	240	49.2	3.2	23.1	57.2	13.2	9.9	7.5	5.6

The MeOH STY varies from 6.8 $\frac{mmol}{g_{cat}h}$ (after 1627 min T.o.S. for Rep 1) to 7.5 $\frac{mmol}{g_{cat}h}$ (after 306 min T.o.S. for Rep 2). There is significantly smaller variation in CO STY.

9.2 GC analysis and calculation methods

The outlet gas compositions were based gas chromatograph results. However, the gas mixture in the GC had to be assumed to be representative of the outlet gas compositions for this to be true. Thus, no product condensation was assumed to be taking place in the line leading to the GC. The lines were heated properly and the backpressure valve was constantly inspected for signs of condensation. Nevertheless, condensation of products as an error source needs to be considered when evaluating the results.

The GC was calibrated before each run with the calibration gas bottle for the components detected by the TCD. However, methanol was calibrated only once for the FID.

As a precaution, the results were calculated with another method that evaluated the conversions based on the measured flow rates of the outlet. With known measured flow rates the molar flow rates of the non-condensable gases were known. The yields of CO and MeOH were deduced from the conversion and the known stoichiometries of the reactions. The method proved to be less reliable than the method presented in chapter 7.5. Nevertheless, the two methods showed very similar results, which gives further assurance that the results were calculated correctly.

10 Conclusions and proposals for future studies

Methanol is almost exclusively produced from syngas. However, there is an alternative route of CO_2 hydrogenation for methanol production. This reaction is typically heterogeneously catalysed, a gas-solid reaction, with typical conditions of 30 – 100 bar and 200 – 300 ^{o}C. A competing reaction that is much faster, the reverse water-gas shift, simultaneously converts CO_2 to CO. The main active component in catalysts has typically been copper. The Cu-based catalysts are structure sensitive, and the catalyst activity linearly depends on the copper surface area and dispersion.

Thermodynamically, the exothermic CO_2 hydrogenation to methanol is not as favourable as the syngas route. Consequently, the development of highly active catalysts with good stability for the CO_2 hydrogenation reaction is the priority in catalyst research.

In the experimental part of the work new formulations of Cu-based particulate catalysts and coated catalysts for CO_2 hydrogenation were tested in a laboratory-scale continuous stirred tank reactor at fixed conditions. Particulate catalysts included commercial catalysts, VTT in-house formulations and experimental catalysts developed at the University of Porto. New in-house nanocoating formulations for particulate catalysts were also screened. Moreover, a condition test was performed with a commercial particulate catalyst. Lastly, the CSTR was investigated in a tracer step change experiment, which indicated that the reactor operated almost as an ideal CSTR.

The activity testing at 240 ^{o}C and 50 bar(g) revealed that the commercial particulate catalysts were highly active in catalyzing the CO_2 hydrogenation to methanol reaction, along with high CO formation by rWGS. The results graphed over time on stream suggested that the rWGS reaction was faster than the CO_2 hydrogenation. The VTT in-house particulate catalysts were significantly less active for MeOH formation than the commercial catalysts. They suffered from high CO yields, which often exceeded MeOH yields, suggesting that the catalysts were not formulated correctly to specifically MeOH synthesis. The FEUP catalysts on the other hand showed comparable results to the highly active commercial catalysts, with high CO_2 conversions and reasonable selectivities to MeOH. The performance of the best performing particulate catalysts was in a remarkably narrow range, with MeOH yields at around 12 – 13 %, and MeOH selectivities at around 55 %.

The nanocoating screening test was performed on the BASF catalyst and the results showed that nanocoatings have marginal effect on catalyst performance. The best nanocoating formulations improved MeOH STY by 2 - 7% compared to the non-nanocoated catalyst. The best performing nanocoating, NC2, was applied to the VTT in-house catalysts, and results showed improved activities and especially higher MeOH formation rates. Although, still not comparable to the commercial catalysts or the FEUP catalysts.

The coated mesh catalysts performed poorly, with MeOH yields an order of magnitude lower than for particulate catalysts with nonexistent CO formation. Furthermore, there were quality problems with the coatings.

The commercial BASF catalyst was tested at different temperatures, pressures and WHSV. The behaviour of the catalyst generally agreed with results found in literature. Tests for different space velocities revealed noticeable mass transfer limitations within the tested range. The results for the particulate catalysts were similar to the latest studies in literature, both in terms of MeOH and CO formation. However, in terms of CO_2 conversion and selectivity to MeOH, the best performing catalysts in this work did not match with the best performing catalyst found in literature.

Finally, the implementation of the two kinetic models, the Graaf model and the vanden Bussche model, revealed that the Graaf model (when activity adjusted) failed to simulate similar CO yields to the experimental results, but the predicted MeOH yields were better than the vanden Bussche model. All in all, the simpler vanden Bussche predicted the experimental results as a whole slightly better.

Coated catalysts have promising process intensifying applications, and therefore further testing of the coated mesh catalysts is recommended, despite the problems with coated catalysts in this work. There is also room to improve the VTT in-house catalysts, to reach better catalytic activity and selectivity to MeOH. Nanocoating is still a novel technology, but the results in this work indicated a beneficial effect of this technique for catalyst performance. Therefore, further nanocoating improvements and testing is recommended as well.

Bibliography

[1] C. Song, “Global challenges and strategies for control, conversion and utilization of CO2 for sustainable development involving energy, catalysis, adsorption and chemical processing,” *Catal. Today*, vol. 115, no. 1–4, pp. 2–32, 2006.

[2] A. Dibenedetto, A. Angelini, and P. Stufano, “Use of carbon dioxide as feedstock for chemicals and fuels: Homogeneous and heterogeneous catalysis,” *J. Chem. Technol. Biotechnol.*, vol. 89, no. 3, pp. 334–353, 2014.

[3] G. a. Olah, G. K. S. Prakash, and A. Goeppert, “Anthropogenic chemical carbon cycle for a sustainable future,” *J. Am. Chem. Soc.*, vol. 133, no. 33, pp. 12881–12898, 2011.

[4] W. Wang, S. Wang, X. Ma, and J. Gong, “Recent advances in catalytic hydrogenation of carbon dioxide.,” *Chem. Soc. Rev.*, vol. 40, no. 7, pp. 3703–3727, 2011.

[5] “Neo Carbon Energy,” 2015. [Online]. Available: http://www.neocarbonenergy.fi/. [Accessed: 26-Aug-2015].

[6] S. G. Jadhav, P. D. Vaidya, B. M. Bhanage, and J. B. Joshi, “Catalytic carbon dioxide hydrogenation to methanol: A review of recent studies,” *Chem. Eng. Res. Des.*, vol. 92, no. 11, pp. 2557–2567, 2014.

[7] E. V Kondratenko, G. Mul, J. Baltrusaitis, G. O. Larrazabal, and J. Perez-Ramirez, “Status and perspectives of CO2 conversion into fuels and chemicals by catalytic, photocatalytic and electrocatalytic processes,” *Energy Environ. Sci.*, vol. 6, no. 11, p. 3112, 2013.

[8] K. A. Ali, A. Zuhairi, and A. R. Mohamed, “Recent development in catalytic technologies for methanol synthesis from renewable sources : A critical review,” *Renew. Sustain. Energy Rev.*, vol. 44, pp. 508–518, 2015.

[9] A. Goeppert, M. Czaun, J.-P. Jones, G. K. Surya Prakash, and G. a Olah, “Recycling of carbon dioxide to methanol and derived products - closing the loop.,” *Chem. Soc. Rev.*, vol. 43, no. 23, pp. 7995–8048, 2014.

[10] J. Lange, “Methanol synthesis: a short review of technology improvements,” *Catal. Today*, vol. 64, no. 1–2, pp. 3–8, 2001.

[11] X. Yin, D. Y. C. Leung, J. Chang, J. Wang, Y. Fu, and C. Wu, “Characteristics of the synthesis of methanol using biomass-derived syngas,” *Energy and Fuels*, vol. 19, no. 1, pp. 305–310, 2005.

[12] O. Martin and J. Pérez-Ramírez, “New and revisited insights into the promotion of methanol synthesis catalysts by CO2,” *Catal. Sci. Technol.*, vol. 3, no. 12, p. 3343, 2013.

[13] X. Liu, G. Lu, Z. Yan, and J. Beltramini, “Recent advances in catalysts for methanol synthesis via hydrogenation of CO and CO2,” *Ind. Eng. Chem. Res.*, vol. 42, pp. 6518–6530, 2003.

[14] A. Egbebi and J. Spivey, “Bioderived Syngas to Alcohols,” *Thermochem. Convers. Biomass to Liq. Fuels Chem.*, no. 1, pp. 125–145, 2010.

[15] G. Centi and S. Perathoner, “Opportunities and prospects in the chemical recycling of carbon dioxide to fuels,” *Catal. Today*, vol. 148, no. 3–4, pp. 191–205, 2009.

[16] R. White, *Porous Carbon Materials from Sustainable Precursors*. Royal Society of Chemistry, 2015.

[17] G. Centi, E. A. Quadrelli, and S. Perathoner, “Catalysis for CO2 conversion: a key technology for rapid introduction of renewable energy in the value chain of chemical industries,” *Energy Environ. Sci.*, vol. 6, no. 6, pp. 1711–1731, 2013.

[18] Y. Park, S. Baek, and S. Ihm, “CO 2 hydrogenation over copper-based hybrid catalysts,” 2002.

[19] O. S. Joo, K. D. Jung, I. Moon, a Y. Rozovskii, G. I. Lin, S. H. Han, and S. J. Uhm, “Carbon dioxide hydrogenation to form methanol via a reverse-water-gas-shift reaction (the CAMERE process),” *Ind. Eng. Chem. Res.*, vol. 38, no. 5, pp. 1808–1812, 1999.

[20] B. Anicic, P. Trop, and D. Goricanec, “Comparison between two methods of methanol production from carbon dioxide,” *Energy*, vol. 77, pp. 279–289, 2014.

[21] Y. Yang, J. Evans, J. a Rodriguez, M. G. White, and P. Liu, “Fundamental studies of methanol synthesis from CO(2) hydrogenation on Cu(111), Cu clusters, and Cu/ZnO(0001).,” *Phys. Chem. Chem. Phys.*, vol. 12, no. 111, pp. 9909–9917, 2010.

[22] G. a. Olah, A. Goeppert, and G. K. S. Prakash, “Chemical recycling of carbon dioxide to methanol and dimethyl ether: From greenhouse gas to renewable, environmentally carbon neutral fuels and synthetic hydrocarbons,” *J. Org. Chem.*, vol. 74, no. 2, pp. 487–498, 2009.

[23] A. Bill, “Carbon Dioxide Hydrogenation to Methanol at low pressure and Temperature,” EPFL, 1997.

[24] F. Arena, G. Mezzatesta, L. Spadaro, and G. Trunfio, “Latest advances in the catalytic hydrogenation of carbon dioxide to methanol/dimethylether,” in *Transformation and Utilization of Carbon Dioxide*, Springer, 2014, pp. 103–130.

[25] J. Kothandaraman, A. Goeppert, M. Czaun, G. K. S. Prakash, and G. A. Olah, “Conversion of CO2 from Air into Methanol Using a Polyamine and a Homogeneous Ruthenium Catalyst,” *J. Am. Chem. Soc.*, p. jacs.5b12354, 2015.

[26] G. Centi and S. Perathoner, “Catalytic Transformation of CO 2 to Fuels and Chemicals , with Reference to Biorefineries,” in *The Role of Catalysis for the Sustainable Production of Bio-fuels and Bio-chemicals*, Elsevier, 2013, pp. 529–555.

[27] J. Ma, N. Sun, X. Zhang, N. Zhao, F. Xiao, W. Wei, and Y. Sun, “A short review of catalysis for CO2 conversion,” *Catal. Today*, vol. 148, no. 3–4, pp. 221–231, 2009.

[28] M. V Twigg and M. S. Spencer, “Deactivation of copper metal catalysts for methanol decomposition, methanol steam reforming and methanol synthesis,” *Top. Catal.*, vol. 22, no. 3–4, pp. 191–203, 2003.

[29] P. Gao, F. Li, N. Zhao, F. Xiao, W. Wei, L. Zhong, and Y. Sun, “Influence of modifier (Mn, La, Ce, Zr and Y) on the performance of Cu/Zn/Al catalysts via hydrotalcite-like precursors for CO2 hydrogenation to methanol,” *Appl. Catal. A Gen.*, vol. 468, no. August, pp. 442–452, 2013.

[30] H. Scott Fogler, *Elements of Chemical Reaction Engineering (4th Edition)*, 4th ed. Prentice Hall, 2005.

[31] R. Raudaskoski, M. V. Niemela, and R. L. Keiski, “The effect of ageing time on co-precipitated Cu/ZnO/ZrO2 catalysts used in methanol synthesis from CO2 and H2,” *Top. Catal.*, vol. 45, no. 1–4, pp. 57–60, 2007.

[32] X. Guo, D. Mao, S. Wang, G. Wu, and G. Lu, “Combustion synthesis of CuO-ZnO-ZrO2 catalysts for the hydrogenation of carbon dioxide to methanol,” *Catal. Commun.*, vol. 10, no. 13, pp. 1661–1664, 2009.

[33] J. Słoczyński, R. Grabowski, a. Kozłowska, P. Olszewski, J. Stoch, J. Skrzypek, and M. Lachowska, “Catalytic activity of the M/(3ZnO·ZrO2) system (M = Cu, Ag, Au) in the hydrogenation of CO2 to methanol,” *Appl. Catal. A Gen.*, vol. 278, no. 1, pp. 11–23, 2004.

[34] X. An, Y. Zuo, Q. Zhang, and J. Wang, “Methanol Synthesis from CO2 Hydrogenation with a Cu/Zn/Al/Zr Fibrous Catalyst,” *Chinese J. Chem. Eng.*, vol. 17, no. 1, pp. 88–94, 2009.

[35] X. An, J. Li, Y. Zuo, Q. Zhang, D. Wang, and J. Wang, “A Cu/Zn/Al/Zr fibrous catalyst that is an improved CO2 hydrogenation to methanol catalyst,” *Catal. Letters*, vol. 118, no. 3–4, pp. 264–269, 2007.

[36] M. Saito, T. Fujitani, M. Takeuchi, and T. Watanabe, “Development of copper/zinc oxide-based multicomponent catalysts for methanol synthesis from carbon dioxide and hydrogen,” *Appl. Catal. A Gen.*, vol. 138, no. 2, pp. 311–318, 1996.

[37] J. Liu, J. Shi, D. He, Q. Zhang, X. Wu, Y. Liang, and Q. Zhu, “Surface active structure of ultra-fine Cu / ZrO2 catalysts used for the CO2 + H2 to methanol reaction,” *Appl. Catal. A Gen.*, vol. 218, pp. 113–119, 2001.

[38] X. M. Liu, G. Q. Lu, and Z. F. Yan, “Nanocrystalline zirconia as catalyst support in methanol synthesis,” *Appl. Catal. A Gen.*, vol. 279, no. 1–2, pp. 241–245, 2005.

[39] J. Toyir, P. Ramírez De La Piscina, J. L. G. Fierro, and N. Homs, “Highly effective conversion of CO2 to methanol over supported and promoted copper-based catalysts: Influence of support and promoter,” *Appl. Catal. B Environ.*, vol. 29, no. 3, pp. 207–215, 2001.

[40] J. Toyir, P. Ramírez de la Piscina, J. L. G. Fierro, and N. Homs, “Catalytic performance for CO2 conversion to methanol of gallium-promoted copper-based catalysts: Influence of metallic precursors,” *Appl. Catal. B Environ.*, vol. 34, no. 4, pp. 255–266, 2001.

[41] X. Guo, D. Mao, G. Lu, S. Wang, and G. Wu, “Glycine-nitrate combustion synthesis of CuO-ZnO-ZrO2 catalysts for methanol synthesis from CO2 hydrogenation,” *J. Catal.*, vol. 271, no. 2, pp. 178–185, 2010.

[42] X. Guo, D. Mao, G. Lu, S. Wang, and G. Wu, “CO2 hydrogenation to methanol over Cu/ZnO/ZrO2 catalysts prepared via a route of solid-state reaction,” *Catal.*

Commun., vol. 12, no. 12, pp. 1095–1098, 2011.

[43] W. Cai, P. R. de la Piscina, J. Toyir, and N. Homs, "CO2 hydrogenation to methanol over CuZnGa catalysts prepared using microwave-assisted methods," *Catal. Today*, vol. 242, pp. 193–199, 2014.

[44] E. Frei, A. Schaadt, T. Ludwig, H. Hillebrecht, and I. Krossing, "The influence of the precipitation/ageing temperature on a Cu/ZnO/ZrO 2 catalyst for methanol synthesis from H2 and CO 2," *ChemCatChem*, vol. 6, no. 6, pp. 1721–1730, 2014.

[45] M. Madej-Lachowska, A. Kasprzyk-Mrzyk, H. Moroz, a I. Lachowski, and H. Wyzgol, "Methanol Synthesis from Carbon Dioxide and Hydrogen over CuO / ZnO / ZrO 2 promoted catalysts," *Chemik*, vol. 68, no. 1, pp. 61–68, 2014.

[46] J. Słoczyński, R. Grabowski, P. Olszewski, a. Kozłowska, J. Stoch, M. Lachowska, and J. Skrzypek, "Effect of metal oxide additives on the activity and stability of Cu/ZnO/ZrO2 catalysts in the synthesis of methanol from CO2 and H2," *Appl. Catal. A Gen.*, vol. 310, no. 1–2, pp. 127–137, 2006.

[47] B. Tidona, C. Koppold, A. Bansode, A. Urakawa, and P. Rudolf Von Rohr, "CO2 hydrogenation to methanol at pressures up to 950 bar," *J. Supercrit. Fluids*, vol. 78, pp. 70–77, 2013.

[48] Q. Sun, "A Novel Process for the Preparation of Cu/ZnO and Cu/ZnO/Al2O3Ultrafine Catalyst: Structure, Surface Properties, and Activity for Methanol Synthesis from CO2+H2," *J. Catal.*, vol. 167, no. 1, pp. 92–105, 1997.

[49] R. Koeppel, A. Baiker, and A. Wokaun, "Copper/zirconia catalysts for the synthesis of methanool from carbon dioxide: Influence of preparation variables on structural and catalytic properties of catalysts," *Appl. Catal. A Gen.*, vol. 84, no. 1, pp. 77–102, 1992.

[50] M. D. Rhodes and A. T. Bell, "The effects of zirconia morphology on methanol synthesis from CO and H 2 over Cu/ZrO2 catalysts: Part I. Steady-state studies," *J. Catal.*, vol. 233, no. 1, pp. 198–209, 2005.

[51] F. Arena, G. Italiano, K. Barbera, S. Bordiga, G. Bonura, L. Spadaro, and F. Frusteri, "Solid-state interactions, adsorption sites and functionality of Cu-ZnO/ZrO2 catalysts in the CO2 hydrogenation to CH3OH," *Appl. Catal. A Gen.*, vol. 350, no. 1, pp. 16–23, 2008.

[52] L. C. Grabow and M. Mavrikakis, "Mechanism of methanol synthesis on cu through CO2 and CO hydrogenation," *ACS Catal.*, vol. 1, no. 4, pp. 365–384, 2011.

[53] F. Studt, I. Sharafutdinov, F. Abild-Pedersen, C. F. Elkjær, J. S. Hummelshøj, S. Dahl, I. Chorkendorff, and J. K. Nørskov, "Discovery of a Ni-Ga catalyst for carbon dioxide reduction to methanol.," *Nat. Chem.*, vol. 6, no. 4, pp. 320–4, 2014.

[54] M. Behrens, F. Studt, I. Kasatkin, S. Kuhl, M. Havecker, F. Abild-Pedersen, S. Zander, F. Girgsdies, P. Kurr, B.-L. Kniep, M. Tovar, R. W. Fischer, J. K. Norskov, and R. Schlogl, "The Active Site of Methanol Synthesis over Cu/ZnO/Al2O3 Industrial Catalysts," *Science (80-.).*, vol. 336, no. 6083, pp. 893–897, 2012.

[55] Y. Yang, C. a. Mims, R. S. Disselkamp, J. H. Kwak, C. H. F. Peden, and C. T. Campbell, "(Non)formation of methanol by direct hydrogenation of formate on copper catalysts," *J. Phys. Chem. C*, vol. 114, no. 40, pp. 17205–17211, 2010.

[56] Y. Yang, C. a. Mims, D. H. Mei, C. H. F. Peden, and C. T. Campbell, “Mechanistic studies of methanol synthesis over Cu from CO/CO 2/H2/H2O mixtures: The source of C in methanol and the role of water,” *J. Catal.*, vol. 298, pp. 10–17, 2013.

[57] Y.-F. Zhao, Y. Yang, C. Mims, C. H. F. Peden, J. Li, and D. Mei, “Insight into methanol synthesis from CO2 hydrogenation on Cu(111): Complex reaction network and the effects of H2O,” *J. Catal.*, vol. 281, no. 2, pp. 199–211, 2011.

[58] K. Klier, V. Chatikavanij, R. Herman, and G. W. Simmons, “Catalytic synthesis of methanol from COH2 IV. The effects of carbon dioxide,” *J. Catal.*, vol. 74, no. 2, pp. 343–360, 1982.

[59] G. H. Graaf, E. J. Stamhuis, and A. A. C. M. Beenackers, “Kinetics of low-pressure methanol synthesis,” *Chem. Eng. Sci.*, vol. 43, no. 12, pp. 3185–3195, 1988.

[60] G. H. Graaf, H. Scholtens, E. J. Stamhuis, and B. A. A. C. M, “Intra-particle diffusion limitations in low-pressure methanol synthesis,” *Chem. Eng. Sci.*, vol. 45, pp. 773–783, 1990.

[61] B. J. Lommerts, G. H. Graaf, and a. a C. M. Beenackers, “Mathematical modeling of internal mass transport limitations in methanol synthesis,” *Chem. Eng. Sci.*, vol. 55, no. 23, pp. 5589–5598, 2000.

[62] M. Peter, “Mechanistic modeling of reaction kinetics and dynamic changes in catalyst morphology on a mesoscopic scale,” 2012.

[63] O. Mäyrä and K. Leiviskä, “Report - Modelling in methanol synthesis,” 2008.

[64] P. Parvasi, M. R. Rahimpour, and A. Jahanmiri, “Incorporation of Dynamic Flexibility in the Design of a Methanol Synthesis Loop in the Presence of Catalyst Deactivation,” *Chem. Eng. Technol.*, vol. 31, no. 1, pp. 116–132, 2008.

[65] G. H. Graaf, P. J. J. M. Sijtsema, E. J. Stamhuis, and G. E. H. Joosten, “Chemical equilibria in methanol synthesis,” *Chem. Eng. Sci.*, vol. 41, no. 11, pp. 2883–2890, 1986.

[66] J. Skrzypek, M. Lachowska, M. Grzesik, J. Słoczyński, and P. Nowak, “Thermodynamics and kinetics of low pressure methanol synthesis,” *Chem. Eng. J. Biochem. Eng. J.*, vol. 58, no. 2, pp. 101–108, 1995.

[67] K. M. Vanden Bussche and G. F. Froment, “A Steady-State Kinetic Model for Methanol Synthesis and the Water Gas Shift Reaction on a Commercial Cu / ZnO / Al 2 O 3 Catalyst,” *J. Catal.*, vol. 10, no. 0156, pp. 1–10, 1996.

[68] É. S. Van-Dal and C. Bouallou, “Design and simulation of a methanol production plant from CO2 hydrogenation,” *J. Clean. Prod.*, vol. 57, pp. 38–45, 2013.

[69] H.-W. Lim, M.-J. Park, S.-H. Kang, H.-J. Chae, J. W. Bae, and K.-W. Jun, “Modeling of the Kinetics for Methanol Synthesis using Cu/ZnO/Al 2 O 3 /ZrO 2 Catalyst: Influence of Carbon Dioxide during Hydrogenation,” *Ind. Eng. Chem. Res.*, vol. 48, no. 23, pp. 10448–10455, 2009.

[70] A. Riaz, G. Zahedi, and J. J. Klemeš, “A review of cleaner production methods for the manufacture of methanol,” *J. Clean. Prod.*, vol. 57, pp. 19–37, 2013.

[71] J. Ladebeck, “Improve Methanol Synthesis,” *Hydrocarb. Process.*, vol. 72.3, 1993.

[72] M. Sahibzada, D. Chadwick, and M. I.S, “Methanol synthesis from CO2/H2 over Pd-promoted Cu/ZnO/Al2O3 catalysts: kinetics and deactivation,” *Stud. Surf. Sci. Catal.*, vol. 107, pp. 29–34, 1997.

[73] I. Lovik, “Modelling, Estimation and Optimization of the Methanol Synthesis with Catalyst Deactivation,” NTNU, 2001.

[74] Y. Song, X. Liu, L. Xiao, W. Wu, J. Zhang, and X. Song, “Pd-Promoter/MCM-41: A Highly Effective Bifunctional Catalyst for Conversion of Carbon Dioxide,” *Catal. Letters*, pp. 1–9, 2015.

[75] T. Fujitani, M. Saito, Y. Kanai, T. Watanabe, J. Nakamura, and T. Uchijima, “Development of an active Ga203 supported palladium catalyst for the synthesis of methanol from carbon dioxide and hydrogen,” *Appl. Catal. A Gen.*, vol. 125, pp. L199–L202, 1995.

[76] X. L. Liang, X. Dong, G. D. Lin, and H. Bin Zhang, “Carbon nanotube-supported Pd-ZnO catalyst for hydrogenation of CO2 to methanol,” *Appl. Catal. B Environ.*, vol. 88, no. 3–4, pp. 315–322, 2009.

[77] X.-L. Liang, J.-R. Xie, and Z.-M. Liu, “A Novel Pd-decorated Carbon Nanotubes-promoted Pd-ZnO Catalyst for CO2 Hydrogenation to Methanol,” *Catal. Letters*, pp. 1138–1147, 2015.

[78] S. E. Collins, D. L. Chiavassa, A. L. Bonivardi, and M. a. Baltanás, “Hydrogen spillover in Ga2O3-Pd/SiO2 catalysts for methanol synthesis from CO2/H2,” *Catal. Letters*, vol. 103, no. 1–2, pp. 83–88, 2005.

[79] Y. Hartadi, D. Widmann, and R. J. Behm, “CO2 Hydrogenation to Methanol on Supported Au Catalysts under Moderate Reaction Conditions: Support and Particle Size Effects,” *ChemSusChem*, vol. 8, no. 3, pp. 456–465, 2015.

[80] W. J. Shen, Y. Ichihashi, H. Ando, Y. Matsumura, M. Okumura, and M. Haruta, “Effect of reduction temperature on structural properties and CO/CO2 hydrogenation characteristics of a Pd-CeO2 catalyst,” *Appl. Catal. A Gen.*, vol. 217, no. 1–2, pp. 231–239, 2001.

[81] J. Qu, X. Zhou, F. Xu, S. Chi, and E. Tsang, “Shape Effect of Pd Promoted Ga2O3 Nanocatalysts for Methanol Synthesis from CO2 Hydrogenation,” *J. Phys. Chem*, vol. 118, pp. 24452–24466, 2014.

[82] H. Kong, H. Y. Li, G. D. Lin, and H. Bin Zhang, “Pd-decorated CNT-promoted Pd-Ga2O3 catalyst for hydrogenation of CO2 to methanol,” *Catal. Letters*, vol. 141, no. 6, pp. 886–894, 2011.

[83] N. Tsubaki and K. Fujimoto, “Promotional SMSI effect on supported palladium catalysts for methanol synthesis,” *Top. Catal.*, vol. 22, no. 3–4, pp. 325–335, 2003.

[84] O. Sanz, F. J. Echave, F. Romero-Sarria, J. A. Odriozola, and M. Montes, “Advances in Structured and Microstructured Catalytic Reactors for Hydrogen Production,” in *Renewable Hydrogen Technologies: Production, Purification, Storage, Applications and Safety*, 2013, pp. 201–224.

[85] P. Avila, M. Montes, and E. E. Miró, “Monolithic reactors for environmental applications: A review on preparation technologies,” *Chem. Eng. J.*, vol. 109, no.

1, pp. 11–36, 2005.

[86] A. Montebelli, C. G. Visconti, G. Groppi, E. Tronconi, C. Ferreira, and S. Kohler, “Enabling small-scale methanol synthesis reactors through the adoption of highly conductive structured catalysts,” *Catal. Today*, vol. 215, pp. 176–185, 2013.

[87] R. J. Farrauto, Y. Liu, W. Ruettinger, O. Ilinich, L. Shore, and T. Giroux, “Precious Metal Catalysts Supported on Ceramic and Metal Monolithic Structures for the Hydrogen Economy,” *Catal. Rev.*, vol. 49, no. 2, pp. 141–196, 2007.

[88] S. Roy, T. Bauer, M. Al-Dahhan, P. Lehner, and T. Turek, “Monoliths as multiphase reactors: A review,” *AIChE J.*, vol. 50, no. 11, pp. 2918–2938, 2004.

[89] M. M. Manfe, “Review Article Industrial Application of Monolith Catalysts,” *Int. J. Adv. Eng. Res. Stud.*, pp. 5–7, 2011.

[90] A. Montebelli, C. G. Visconti, G. Groppi, E. Tronconi, C. Cristiani, C. Ferreira, and S. Kohler, “Methods for the catalytic activation of metallic structured substrates,” *Catal. Sci. Technol.*, vol. 4, no. 9, p. 2846, 2014.

[91] T. Nijhuis, T. Nijhuis, A. Beers, A. Beers, T. Vergunst, T. Vergunst, I. Hoek, I. Hoek, F. Kapteijn, F. Kapteijn, J. Moulijn, and J. Moulijn, “Preparation of monolithic catalysts,” *Catal. Rev.*, vol. 43, no. 4, pp. 345–380, 2001.

[92] L. C. Almeida, F. J. Echave, O. Sanz, M. a. Centeno, J. a. Odriozola, and M. Montes, “Washcoating of metallic monoliths and microchannel reactors,” in *Studies in Surface Science and Catalysis*, 2010, vol. 175, no. August 2015, pp. 25–33.

[93] J. D. Holladay, Y. Wang, and E. Jones, “Review of developments in portable hydrogen production using microreactor technology,” *Chem. Rev.*, vol. 104, no. 10, pp. 4767–4789, 2004.

[94] J. Bravo, A. Karim, T. Conant, G. P. Lopez, and A. Datye, “Wall coating of a CuO/ZnO/Al2O3 methanol steam reforming catalyst for micro-channel reformers,” *Chem. Eng. J.*, vol. 101, no. 1–3, pp. 113–121, 2004.

[95] A. Montebelli, C. G. Visconti, G. Groppi, E. Tronconi, S. Kohler, H. J. Venvik, and R. Myrstad, “Washcoating and chemical testing of a commercial Cu/ZnO/Al2O3 catalyst for the methanol synthesis over copper open-cell foams,” *Appl. Catal. A Gen.*, vol. 481, pp. 96–103, 2014.

[96] A. Montebelli, C. G. Visconti, G. Groppi, E. Tronconi, and S. Kohler, “Optimization of compact multitubular fixed-bed reactors for the methanol synthesis loaded with highly conductive structured catalysts,” *Chem. Eng. J.*, vol. 255, pp. 257–265, 2014.

[97] J. R. Couper, W. R. Penney, J. R. Fair, and S. M. Walas, *Chemical Process Equipment - Selection and Design (Revised 2nd Edition)*, 2nd ed. Elsevier, 2010.

[98] M. Peter, “Mechanistic modeling of reaction kinetics and dynamic changes in catalyst morphology on a mesoscopic scale,” TUM, 2012.

[99] N. Rezaie, A. Jahanmiri, B. Moghtaderi, and M. R. Rahimpour, “A comparison of homogeneous and heterogeneous dynamic models for industrial methanol reactors in the presence of catalyst deactivation,” *Chem. Eng. Process. Process Intensif.*, vol. 44, no. 8, pp. 911–921, 2005.

[100] S. Yusup, N. Phuong Anh, and H. Zabiri, “A simulation study of an industrial methanol reactor based on simplified steady-state model,” *Int. J. Res. Rev. Appl. Sci.*, vol. 5, no. 3, pp. 213–222, 2010.

[101] M. Shahrokhi and G. R. Baghmisheh, “Modeling, simulation and control of a methanol synthesis fixed-bed reactor,” *Chem. Eng. Sci.*, vol. 60, pp. 4275–4286, 2005.

[102] A. Cybulski and J. A. Moulijn, *Structured catalysts and reactors, 2nd edn*, 2nd ed., vol. 2006, no. 4. CRC press, 2006.

[103] Z. Ilsen Önsan and A. K. Avci, *Reactor Design for Fuel Processing*. 2011.

[104] D. Y. Murzin, *Engineering Catalysis*. De Gruyter, 2013.

[105] E. H. Stitt, “Alternative multiphase reactors for fine chemicals: A world beyond stirred tanks?,” *Chem. Eng. J.*, vol. 90, no. 1–2, pp. 47–60, 2002.

[106] B. S. Choi, B. Wan, S. Philyaw, K. Dhanasekharan, and T. a. Ring, “Residence Time Distributions in a Stirred Tank: Comparison of CFD Predictions with Experiment,” *Ind. Eng. Chem. Res.*, vol. 43, no. 20, pp. 6548–6556, 2004.

[107] J. A. Moulijn and A. Stankiewicz, “The Potential of Structured Reactors in Process Intensification,” *Chem. Sustain. Dev.*, vol. 11, pp. 3–9, 2003.

[108] AutoclaveEngineers, “Autoclave Engineers - Laboratory stirrer reactors.” [Online]. Available: www.temflow.se/pdf/temflow_reaktorer_omrorare.pdf. [Accessed: 10-Nov-2015].

[109] W. von Wedel, S. Ledakowicz, and W.-D. Deckwer, “Kinetics of methanol synthesis in the slurry phase,” *Chem. Eng. Sci.*, vol. 43, no. 8, pp. 2169–2174, 1988.

[110] S. Arab, J. M. Commenge, J. F. Portha, and L. Falk, “Methanol synthesis from CO2 and H2 in multi-tubular fixed-bed reactor and multi-tubular reactor filled with monoliths,” *Chem. Eng. Res. Des.*, vol. 2, no. March, pp. 2598–2608, 2014.

[111] X. K. Phan, H. Bakhtiary-Davijany, R. Myrstad, P. Pfeifer, H. J. Venvik, and A. Holmen, “Preparation and performance of Cu-based monoliths for methanol synthesis,” *Appl. Catal. A Gen.*, vol. 405, no. 1–2, pp. 1–7, 2011.

[112] L. Kiwi-Minsker and A. Renken, “Microstructured reactors for catalytic reactions,” *Catal. Today*, vol. 110, no. 1–2, pp. 2–14, 2005.

[113] A. Kundu, J. E. Ahn, S. S. Park, Y. G. Shul, and H. S. Han, “Process intensification by micro-channel reactor for steam reforming of methanol,” *Chem. Eng. J.*, vol. 135, no. 1–2, pp. 113–119, 2008.

[114] G. Chen, S. Li, and Q. Yuan, “Pd-Zn/Cu-Zn-Al catalysts prepared for methanol oxidation reforming in microchannel reactors,” *Catal. Today*, vol. 120, no. 1, pp. 63–70, 2007.

[115] X. K. Phan, H. D. Bakhtiary, R. Myrstad, J. Thormann, P. Pfeifer, H. J. Venvik, and A. Holmen, “Preparation and performance of a catalyst-coated stacked foil microreactor for the methanol synthesis,” *Ind. Eng. Chem. Res.*, vol. 49, no. 21, pp. 10934–10941, 2010.

[116] A. Dinse and R. Schomäcker, “Chapter 16 Reaction Engineering of Oxidation Reactions,” *Nanostructured Catal. Sel. Oxidations*, no. 19, pp. 398–426, 2011.

[117] D. Y. Murzin, T. Salmi, and L.-E. Lindfors, *Heterogen katalys*. Turku: Laboratoriet för teknisk kemi och reaktionsteknik, 2010.

[118] F. Vidal, P. Simell, and I. Hannula, “Power-to-Methanol plant of Carbon Recycling International (CRI),” Espoo, 2015.

[119] CRI, “Carbon Recycling International and Perstorp sign offtake agreement for renewable methanol,” 2015. [Online]. Available: http://www.carbonrecycling.is/index.php?option=com_content&view=article&id=76%3Acarbon-recycling-international-and-perstorp-sign-offtake-agreement-for-renewable-methanol&catid=2&Itemid=6&lang=en. [Accessed: 16-Aug-2015].

[120] M. Chemicals, “Mitsui Chemicals to Establish a Pilot Facility to Study a Methanol Synthesis Process from CO 2,” 2008. [Online]. Available: http://www.mitsuichem.com/release/2008/pdf/080825e.pdf. [Accessed: 19-Aug-2015].

[121] L. Barbato, G. Iaguaniello, and A. Mangiapane, “Reuse of CO2 to Make Methanol Using Renewbale Hydrogen,” in *Green Energy and Technology: CO2: A Valuable Source of Carbon*, vol. 137, Springer, 2013, pp. 67–94.

[122] S. Perathoner and G. Centi, “CO2 recycling: A key strategy to introduce green energy in the chemical production chain,” *ChemSusChem*, vol. 7, no. 5, pp. 1274–1282, 2014.

[123] “Carberry Spinning Basket Catalyst Reactor - Parker Autoclave Engineers.” [Online]. Available: http://www.autoclaveengineers.com/products/catalytic_reactors/carberry_spinning_basket/. [Accessed: 20-Nov-2015].

[124] E. Carlson, “Don t Gamble with Physical Properties for Simulations,” *Chemical Engineering Process*. pp. 35–46, 1996.

[125] Aspen Technology, “Aspen Physical Property System,” pp. 2–11, 2010.

[126] U. of M. Duluth, “Quantitative Gas Chromatography - Chem 2223 Lab Prep.” [Online]. Available: https://www.google.fi/url?sa=t&rct=j&q=&esrc=s&source=web&cd=1&cad=rja&uact=8&ved=0ahUKEwib77W35bzJAhVEJnIKHewZD8EQFggkMAA&url=http://www.d.umn.edu/~dpoe/chem2223/labpreplectures/Quantitative%20Gas%20Chromatography.ppt&usg=AFQjCNFBLmm7bC. [Accessed: 15-Nov-2015].

[127] W. a Dietz, “Response Factors for Gas Chromatographic Analyses,” *Journal Of Gas Chromatography*, vol. 5, no. 2. pp. 68–71, 1967.

[128] A. A. Kiss, J. J. Pragt, H. J. Vos, G. Bargeman, and M. T. de Groot, “Novel efficient process for methanol synthesis by CO2 hydrogenation,” *Chem. Eng. J.*, vol. 284, pp. 260–269, 2016.

[129] D. Mignard and C. Pritchard, “On the use of electrolytic hydrogen from variable renewable energies for the enhanced conversion of biomass to fuels,” *Chem. Eng. Res. Des.*, vol. 86, no. 5, pp. 473–487, 2008.

[130] D. Milani, R. Khalilpour, G. Zahedi, and A. Abbas, “A model-based analysis of CO2 utilization in methanol synthesis plant,” *J. CO2 Util.*, vol. 10, pp. 12–22, 2015.

[131] BASF, “Safety data sheet - Catalyst BASF RP-60 tablets 1.5x1.5 mm,” 2011.

Figure 1. Picture of the expeirmental setup with the heating jacket attached to the autoclave, and to the left the temperature control terminal.

There were in total 3 reactant gas bottles consumed during the course of the experiments, each with roughly the same gas compositions. Table 1 displays the exact gas compositions.

Table 1. AGA analyzed and certified calibration gas and reactant gas bottle compositions.

Compound	Calibration gas (vol-%)	Reactant gas 1 (vol-%)	Reactant gas 2 (vol-%)	Reactant gas 3 (vol-%)
H_2	15	71.3	71.3	71.3
N_2	15	0	0	0
CO	15	23.7	23.7	23.7
CH_4	3.03	0	0	0
CO_2	51.97	5.0	4.99	5.01

Table 2 presents the response factor averages that were used in the calculations, as well as the $\frac{FID}{TCD}$ relationship average.

Table 2. Response factor averages.

	Calibration gas	Reactant gas 1	Reactant gas 2	Reactant gas 3
RF_{H_2}	-	11.257	11.255	11.330
RF_{CO_2}	-	1.155	1.154	1.156
RF_{CO}	0.944	-	-	-
$\frac{FID}{TCD}$	20.779			

Table 3 presents the mass flow meter properties.

Table 3. Mass flow meters used in the experimental setup.

Name	Gas	Max flow rate ($\frac{dm^3}{min}$ at STP)	Model	Manufacturer
MS-FC-102	CO_2	2	F-201CV-5K0-ABD-11-V	Bronkhorst
MS-FC-112	H_2	0.150	F201C-RAA-11-V	
MS-FC-122	H_2	0.050	F-201C-FBC-33V	
MS-FC-132	CO	0.050	F-201CV-RAA-11-V	

Table 4 shows the commercial catalyst properties.

Table 4. Commercial catalyst properties. [131]

Properties	Süd Chemie G-66MR	BASF RP-60
Density (g/cm^3)	1.1	1.8
Pellet size (mm)	6x4	1.5x1.5
BET surface area (m^2/g)	70	64.8
Components		
Al_2O_3 (wt-%)	11	Unknown
CuO (wt-%)	66	50<wt-%<75
ZnO (wt-%)	24	15<wt-%<20
ZrO_2 (wt-%)	0	Unknown

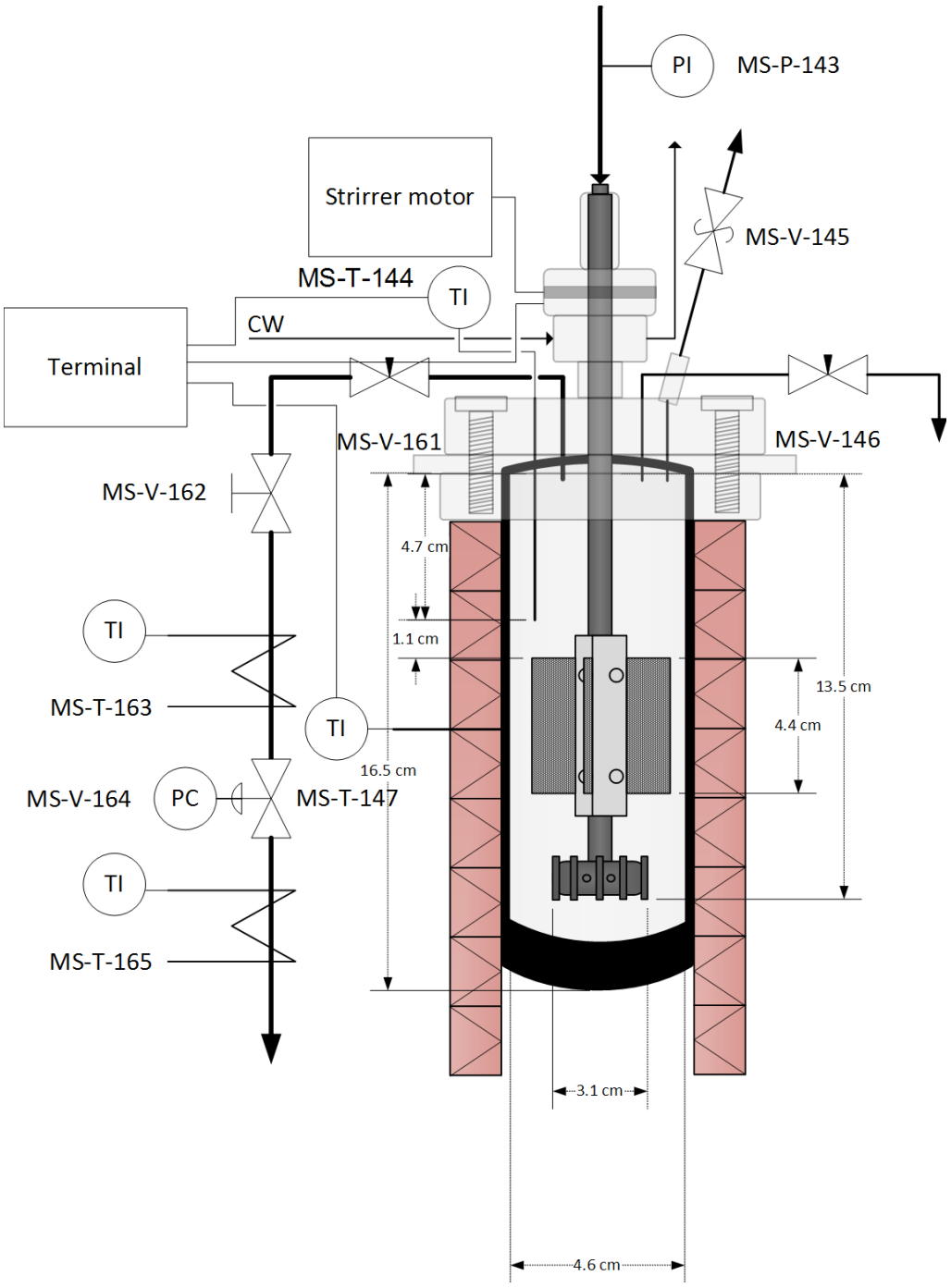

Figure 1. Detailed scetch of the autoclave reactor.

Table 1. Experimental run conditions for all catalysts.

Catalyst	Pelletized	m_{cat} (g)	T_{meas} (°C)	P_{meas} (bar(g))	Stirrer measured ()	Flow rate ($\frac{dm^3}{min}$ at STP)	T.o.S. (min)
Particulate catalysts							
Blank	-	0.00	239	50.0	394	0.186	223
BASF Run 1	no	2.09	240	49.8	394	0.093	174
BASF Run 2	no	2.09	239	49.3	398	0.186	224
BASF Run 3	no	2.09	240	50.0	394	0.370	171
BASF Run 4	no	2.09	199	49.8	395	0.186	194
BASF Run 5	no	2.09	219	49.8	400	0.186	152
BASF Run 6	no	2.08	248	49.1	428	0.186	198
BASF Run 7	no	2.09	240	30.2	408	0.186	191
BASF NC1	no	2.08	240	50.0	420	0.186	223
BASF NC2	no	2.08	239	50.0	398	0.186	214
BASF NC3	no	2.08	240	49.8	405	0.186	175
BASF NC4	no	2.09	240	50.0	424	0.186	221
BASF NC5	no	2.08	239	49.6	427	0.186	241
BASF NC6	no	2.08	240	50.0	427	0.186	224
BASF NC7	no	2.09	240	49.2	427	0.186	270
S-C	no	2.08	240	49.6	427	0.186	237
S-C NC2	no	2.08	240	49.8	404	0.186	217
49	yes	2.09	240	49.5	402	0.186	231
61*	yes	1.60	241	49.8	402	0.186	210
75	yes	2.09	239	49.8	416	0.186	215
49 NC2	yes	1.72	240	49.9	410	0.186	262
61 NC2	yes	1.37	240	49.7	400	0.186	222
75 NC2	yes	1.88	240	49.9	425	0.186	221
FEUP Run1	yes	2.09	200	50.0	402	0.186	190
FEUP Run 2	yes	2.09	220	50.0	401	0.186	155
FEUP Run 3	yes	2.09	239	49.4	401	0.186	231
FEUP Cu1	yes	2.08	239	49.7	432	0.186	245
FEUP Cu2	yes	2.08	240	49.2	431	0.186	247
FEUP Cu3	yes	2.08	239	49.0	428	0.186	215
FEUP 44c	yes	2.07	240	49.6	428	0.186	231
Coated catalysts							
Mesh 1 Blank	-	0.00	240	49.9	430	0.186	204
Mesh 2 Blank	-	0.19	240	49.9	427	0.186	202
Mesh 2 NC-A	-	0.19	240	49.9	431	0.186	230
Mesh 2 NC-B	-	0.11	241	49.5	431	0.186	211
Mesh 2 NC-C	-	0.14	240	50.0	430	0.186	218
Mesh 3 NC-A	-	0.34	240	49.9	430	0.186	240

The heat of reaction for CO_2 hydrogenation is calculated by the following equation:

$$\Delta H_4(T_R) = \left(\Delta H_{f,MeOH}(T_R) + \Delta H_{f,H_2O}(T_R)\right) - \left(3\Delta H_{f,H_2}(T_R) + \Delta H_{f,CO_2}(T_R)\right) \quad (1)$$

And similarly for the rWGS reaction:

$$\Delta H_5(T_R) = \left(\Delta H_{f,CO}(T_R) + \Delta H_{f,H_2O}(T_R)\right) - \left(\Delta H_{f,H_2}(T_R) + \Delta H_{f,CO_2}(T_R)\right) \quad (2)$$

Table 1 and Table 2 shows the results obtained from Aspen for the heats of formation and the calculated heats of reactions.

Table 1. Heats of formations and reactions at different reaction temperatures and constant pressure of 50 bar(g).

	$\Delta H_{f,i}\left[\frac{kJ}{mol}\right]$					$\Delta H_i\left[\frac{kJ}{mol}\right]$	
T_R (°C)	H_2	CO_2	$MeOH$	CO	H_2O	**Reaction (4)**	**Reaction (5)**
200	5.2	-387.2	-199.6	-105.4	-239.2	-67.2	37.4
220	5.8	-386.2	-196.5	-104.8	-238.1	-65.7	37.6
240	6.3	-385.3	-194.4	-104.2	-237.1	-65.4	37.6
250	6.6	-384.8	-193.5	-103.9	-236.7	-65.3	37.6

Tale 2. Heats of formation and reaction at 240 °C and pressure of 30 bar(g).

	$\Delta H_{f,i}\left[\frac{kJ}{mol}\right]$					$\Delta H_i\left[\frac{kJ}{mol}\right]$	
P_R (bar(g))	H_2	CO_2	$MeOH$	CO	H_2O	**Reaction (4)**	**Reaction (5)**
30	6.3	-385.0	-192.3	-104.2	-235.9	-62.2	38.6

Table 1 presents information on the kinetic model studies.

Table 1. Details on the kinetic model studies.

	Graaf model (1988 and 1990) [59] [60]	**vanden Bussche model (1996)** [67]
Reactions considered	CO hydrogenation (3) rWGS (5) CO_2 hydrogenation (4)	CO_2 hydrogenation (4) rWGS (5)
T_R (°C)	207 - 277	180 – 280
P_R (bar)	15 - 50	15-51
Reactant composition	-	$\frac{\dot{n}_{CO_0}}{\dot{n}_{CO_{2_0}}} = 0 - 4.1$
Catalyst	Haldor Topsoe Mk 101 $CuO/ZnO/Al_2O_3$	ICI 51-2 $Cu/ZnO/Al_2O_3$ 150 – 250 µm or 300 – 700 µm particle size
Reactor	Gradientless spinning basket	Packed bed

Table 2 shows information on experimental data used in the calculations of the simulation results both kinetic models.

Table 2. Details on the experimental data used in the kinetic models.

	Graaf model	**vanden Bussche model**
Experimental data	**An et al. (2009)** [34]	**Mignard and Pritchard (2008)** [129] **modified vanden Bussche (1996)** [67]
T_R (°C)	210 - 270	180 – 280
P_R (bar)	20 – 50	15 – 75 (by adjusted *Ea*)
GHSV ($\frac{cm^3}{g_{cat}h}$)	1000 – 10 000	-
Reactant composition	$\frac{CO}{CO_2} = 0$	$\frac{CO}{CO_2} = 0 - 4.1$
Catalyst	Fibrous Cu/Zn/Al/Zr (12:6:1:1). Particle size under 50 µm	ICI 51-2 $Cu/ZnO/Al_2O_3$ 150 – 250 µm or 300 – 700 µm particle size
Reactor	Packed bed	Packed bed

Table 3 presents the kinetic factor parameter values for the Graaf model as implemented in Aspen.

Table 3. Kinetic factors for the Graaf model. [128]

i	k_i	$Ea_i\ (\frac{J}{mol})$
MeOH, 3	$4.0638*10^{-6}$	11695
rWGS, 5	904210000	112860
MeOH, 4	$1.5188*10^{-33}$	266010

Table 4 presents the driving force values for the Graaf model.

Table 4. Constants for driving force expression for the Graaf model. [128]

Reaction	**Expression**	$ln(K_1) = A + \frac{B}{T\ (K)}$		**Expression**	$ln(K_2) = A + \frac{B}{T\ (K)}$	
		A	**B**		**A**	**B**
MeOH,3	K_{CO}	-23.2	14225	$\frac{K_{CO}}{K_{MeOH,3}^{eq}}$	28.895	2385
rWGS,5	K_{CO_2}	-22.48	9777	$\frac{K_{CO_2}}{K_{rWGS,5}^{eq}}$	-28.12	15062
MeOH,4	K_{CO_2}	-22.48	9777	$\frac{K_{CO_2}}{K_{MeOH,4}^{eq}}$	23.974	3222

Table 5 presents the adsorption expression values for the Graaf model.

Table 5. Adsorption expression constants for the Graaf model. [128]

Term	**Expression**	$ln(K_i) = A + \frac{B}{T\ (K)}$		$\prod C_j^{v_j}$
		A	**B**	
1	**1**	0	0	$f_{H_2}^{0.5}$
2	$\frac{K_{H_2O}}{K_H^{0.5}}$	-26.158	13842	f_{H_2O}
3	K_{CO}	-23.2006	14225	$f_{CO}f_{H_2}^{0.5}$
4	$\frac{K_{CO}K_{H_2O}}{K_H^{0.5}}$	-49.3574	38067	$f_{CO}f_{H_2O}$
5	K_{CO_2}	-22.4827	9777	$f_{CO_2}f_{H_2}^{0.5}$
6	$\frac{K_{CO}K_{H_2O}}{K_H^{0.5}}$	-48.6395	23619	$f_{CO_2}f_{H_2O}$

Table 6 presents the values used for implementing the vanden Bussche model in Aspen.

Table 6. Parameters for the vanden Bussche model. [68]

Term	$ln(k_i) = A + \frac{B}{T\ (K)}$	
	A	B
k_1	-29.87	4811.2
k_2	8.147	0
k_3	-6.452	2068.4
k_4	-34.95	14928.9
k_5	4.804	-11797.5
k_6	17.55	-2249.8
k_7	0.131	-7023.5

Table 1. Micro-GC and GC analysis of 3 samples from the catalyst 75 run at 240 °C and 50 bar(g) for the non-condensable gases.

Sample information	**Catalyst 75**		
	Sample 1	**Sample 2**	**Sample 3**
	(vol-%)	(vol-%)	(vol-%)
H_2	69.7	69.7	69.2
O_2+Ar	0.1	0.1	0.1
N_2	5.9	5.9	5.9
CO	2.0	2.0	2.0
CO_2	23.4	23.4	23.9
	(vol-ppm)	(vol-ppm)	(vol-ppm)
Methane (CH_4)	95	80	81
Ethane (C_2H_6)	11	9	9
Ethene (C_2H_4)	0	0	0
Propane (C_3H_8)	7	6	6
Propene (C_3H_6)	0	0	0
Acetylene (C_2H_2)	0	0	0
Dimethyl ether (C_2H_6O)	0	0	0
Iso-Butane (I-C_4H_{10})	0	0	0
Propadiene (C_3H_4)	0	0	0
N-Butane (N-C_4H_{10})	3	3	3
T-2-Butene (T-2-C_4H_8)	0	0	0
Iso-Butene (I-C_4H_8)	0	0	0
1-Butene (1-C_4H_8)	0	0	0
Cis-2-Butene (CIS-2-C_4H_8)	0	0	0
Iso-Pentane (I-C_5H_{12})	0	0	0
N-Pentane (N-C_5H_{12})	0	0	0
1,3-Butadiene (1,3-C_4H_6)	0	0	0
Trans-2-pentene (T-2-C_5H_{10})	0	0	0
2-Methyl-2-Butene(2-M-C_5H_{10})	0	0	0
1-Pentene (1-C_5H_{10})	0	0	0
cis-2-pentene (Cis-2-C_5H_{10})	0	0	0
n-Hexane (N-C_6H_{14})	0	0	0
Benzene	0	0	0
Toluene	0	0	0
	vol-%	vol-%	vol-%
Hydrocarbons total	0	0	0
ESTD	101.1	101.3	101.1

Table 1. Molar balance of BASF catalyst run at 240 °C, 50 bar(g) and WHSV 3.17 1/h.

Component	IN		OUT	
	$V\%_0$ (vol-%)	$\dot{n}_0$ ($\frac{mmol}{min}$)	$V\%$ (vol-%)	$\dot{n}$ ($\frac{mmol}{min}$)
H_2	71.30	5.92	64.03	5.05
CO_2	23.70	1.97	19.47	1.54
MeOH	0.00	0.00	3.15	0.25
CO	0.00	0.00	2.46	0.19
H_2O	0.00	0.00	5.62	0.44
N_2	5.00	0.42	5.27	0.42
Total	**100.00**	**8.31**	**100.00**	**7.89**

Table 2 Elemental balance of BASF catalyst run at 240 °C, 50 bar(g), and WHSV 3.17 1/h.

Element	IN	OUT	$\frac{OUT}{IN}$ (%)
	$\dot{n}_0$ ($\frac{mmol}{min}$)	$\dot{n}$ ($\frac{mmol}{min}$)	
C	1.97	1.98	**100.5**
H	11.84	11.98	**101.1**
O	3.94	3.96	**100.5**
N	0.83	0.83	**100.0**

Table 3. Outlet compositions in mol-% and elemental balances for all runs.

Catalyst	Outlet composition (mol-%)						Elemental balance $\frac{OUT}{IN}$ (%)		
	H_2	CO_2	MeOH	CO	H_2O	N_2	C	H	O
Particulate catalysts									
Blank	71.4	23.6	0.0	0.0	0.0	5.0	98.6	99.2	98.6
BASF Run 1	63.1	19.3	3.6	2.5	6.1	5.4	99.3	99.4	99.3
BASF Run 2	64.0	19.5	3.2	2.5	5.6	5.3	100.5	101.1	100.5
BASF Run 3	64.8	19.8	2.7	2.4	5.1	5.2	101.8	102.2	101.8
BASF Run 4	67.2	21.4	2.0	1.1	3.1	5.2	99.8	100.5	99.8
BASF Run 5	64.7	20.2	3.1	1.8	4.9	5.2	101.2	101.4	101.2
BASF Run 6	63.7	19.2	3.1	2.8	5.9	5.3	99.6	100.3	99.6
BASF Run 7	65.9	19.7	1.5	3.1	4.6	5.1	99.8	100.4	99.8
BASF NC1	63.6	19.3	3.4	2.5	5.9	5.3	100.8	101.3	100.8
BASF NC2	63.6	19.3	3.4	2.5	5.9	5.3	100.8	101.3	100.8
BASF NC3	63.8	19.3	3.3	2.5	5.8	5.3	100.7	101.6	100.7
BASF NC4	64.3	19.6	3.0	2.4	5.4	5.3	99.7	100.3	99.7
BASF NC5	64.6	19.8	2.9	2.3	5.2	5.3	99.9	100.3	99.9
BASF NC6	64.8	19.8	2.7	2.4	5.1	5.3	99.6	99.9	99.6
BASF NC7	63.5	19.4	3.3	2.6	5.9	5.3	101.1	101.3	101.1
S-C	63.5	19.4	3.3	2.5	5.9	5.3	100.3	100.8	100.3
S-C NC2	63.6	19.3	3.4	2.5	5.9	5.3	100.7	101.2	100.7
49	69.1	22.4	1.0	0.8	1.8	5.0	101.6	101.7	101.6
61*	66.7	20.7	1.5	2.2	3.7	5.1	100.8	100.7	100.8
75	66.7	20.8	1.7	2.0	3.7	5.2	99.6	100.0	99.6
49 NC2	68.8	22.1	1.0	1.0	2.0	5.1	99.2	99.5	99.2
61 NC2	66.7	20.7	1.6	2.1	3.7	5.2	99.1	99.5	99.1
75 NC2	66.7	20.7	1.8	2.0	3.7	5.2	99.4	100.0	99.4
FEUP Run 1	67.7	21.5	1.7	1.1	2.8	5.2	99.4	100.3	99.4
FEUP Run 2	65.3	20.5	2.7	1.8	4.5	5.2	100.9	100.9	100.9
FEUP Run 3	64.0	19.6	3.1	2.5	5.6	5.3	100.8	101.1	100.8
FEUP Cu1	63.6	19.5	3.3	2.5	5.8	5.3	100.3	100.8	100.3
FEUP Cu2	63.7	19.6	3.3	2.4	5.7	5.3	100.0	100.4	100.0
FEUP Cu3	63.9	19.5	3.1	2.6	5.7	5.3	100.0	100.6	100.0
FEUP 44c	64.1	19.6	2.9	2.6	5.5	5.3	99.9	100.3	99.9
Coated catalysts									
Mesh 1 Blank	71.4	23.5	0.0	0.0	0.0	5.0	98.2	99.1	98.2
Mesh 2 Blank	71.4	23.5	0.0	0.0	0.0	5.0	98.1	99.1	98.1
Mesh 2 NC-A	71.2	23.6	0.0	0.0	0.0	5.1	98.0	98.7	98.0
Mesh 2 NC-B	71.2	23.6	0.0	0.0	0.0	5.1	98.1	98.8	98.1
Mesh 2 NC-C	71.4	23.5	0.0	0.0	0.0	5.0	98.2	99.1	98.2
Mesh 3 NC-A	70.7	23.1	0.2	0.4	0.6	5.1	98.3	98.8	98.3

Table 1. Relative performance of particulate catalysts in %compared to BASF catalyst at 240 °C, 50 bar(g) and WHSV of 3.17 1/h.

Catalyst *i*	$\frac{X_{CO_2}(i)}{X_{CO_2}(BASF)}$ (%)	$\frac{S_{MeOH}(i)}{S_{MeOH}(BASF)}$ (%)	$\frac{Y_j^{CO_2}(i)}{Y_j^{CO_2}(BASF)}$ (%)		$\frac{STY_j(i)}{STY_j(BASF)}$ $(\frac{mmol}{g_{cat}h})$	
			MeOH	**CO**	**MeOH**	**CO**
BASF	100	100	100	100	100	100
BASF NC1	104.4	102.3	106.8	101.4	107.0	101.6
BASF NC2	104.5	102.6	107.2	101.1	107.7	101.6
BASF NC3	103.1	101.7	104.8	100.9	105.2	101.2
BASF NC4	95.8	97.4	93.4	98.9	93.5	99.1
BASF NC5	91.9	98.4	90.5	93.9	90.7	94.1
BASF NC6	90.2	93.9	84.7	97.2	84.9	97.5
BASF NC7	104.5	99.2	103.6	105.6	104.1	106.1
S-C	103.5	101.3	104.9	101.7	105.7	102.5
S-C NC2	104.5	102.5	107.1	101.2	107.4	101.4
49	33.0	97.7	32.2	34.0	32.2	34.0
61*	87.1	90.5	78.8	97.8	79.0	98.0
75	68.2	70.9	48.4	93.6	63.2	122.3
49 NC2	36.3	92.1	33.4	40.0	40.6	48.6
61 NC2	66.7	78.1	52.1	85.4	79.3	130.1
75 NC2	67.6	84.2	56.9	81.3	63.1	90.1
FEUP	95.8	97.4	93.4	98.9	93.5	99.1
FEUP Cu1	102.0	101.2	103.2	100.4	104.0	101.2
FEUP Cu2	100.0	103.0	103.0	96.2	103.7	96.9
FEUP Cu3	100.2	97.1	97.3	103.9	98.1	104.8
FEUP 44c	97.4	92.6	90.2	106.7	91.4	108.1